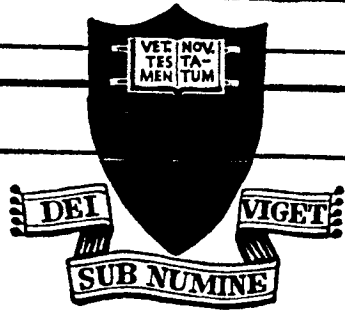


729

1.65190904



[Handwritten scribbles and signatures]

(THRU) *8*
(DATE) *33*
(CATEGORY)

NO 1-39999
(ACCESSION NUMBER)
110
(PAGES)
Ad 59612
(NASA CR OR TMX OR AD NUMBER)

UNIT PRICE \$

CFSTI PRICE(S) \$

Hard copy (HC)

Microfiche (MF)

653 July 85

PRINCETON UNIVERSITY
THOMAS PORTER
INSTITUTE CENTER
LIBRARY

PRINCETON UNIVERSITY

DEPARTMENT OF
AEROSPACE AND MECHANICAL SCIENCES

MIXING AND HEAT TRANSFER OF A PARTIALLY
IONIZED ARGON JET
WITH A COAXIAL FLOW OF COLD HELIUM

by


David B. Fradkin

Thesis, M.S.E.

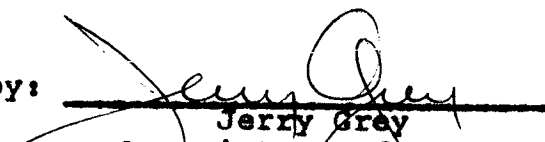
Aeronautical Engineering Laboratory

Report No. 729

Submitted by:


David B. Fradkin

Approved by:


Jerry Gray
Associate Professor
Dept. of Aerospace
and Mechanical Sciences

A thesis submitted to the Department of Aerospace and
Mechanical Sciences of Princeton University in partial
fulfillment of the requirements for the degree of Master
of Science in Engineering.

PRINCETON UNIVERSITY
Princeton, New Jersey

1965

ACKNOWLEDGMENT

The author wishes to thank Professor Jerry Grey for his advice and encouragement during the preparation of this thesis. Mr. Peter M. Williams was also of great assistance.

The experimental research was fortunate in having the able assistance of Mr. T. Peoples, Mr. M. R. Candelori, and Mr. J. Semler. Mention should be made of the assistance of the instrumentation group and of the drafting room of the Guggenheim Laboratories. Mr. D. Ley and Mr. R. Mills were of great help in reducing the experimental data.

Special thanks go to Mrs. M. Griffiths who typed the manuscript.

The author is especially grateful to the Thermomechanics Branch, USAF Aeronautical Research Laboratory, Wright-Patterson Air Force Base, and to the Space Nuclear Propulsion Office, NASA, who assisted in the funding of this research under Contracts AF 33(657)-9962 and NASr-216 respectively.

TABLE OF CONTENTS

	PAGE
TITLE PAGE	1
ACKNOWLEDGEMENTS	2
TABLE OF CONTENTS	3
I. SUMMARY	4
II. INTRODUCTION	6
A. Purpose	6
B. Background	6
C. History	7
III. DESCRIPTION OF TEST PROGRAM	11
A. Apparatus	11
1. Plasma Generator	11
2. Duct and Test Section	13
3. Instrumentation	14
B. Conduct of Tests	17
1. Visual Studies	17
2. Detailed Surveys	19
3. High Coaxial Velocity Surveys	20
IV. THEORETICAL STUDIES	22
V. DISCUSSION OF RESULTS	30
A. Visual Studies	30
B. Detailed Mapping of Flow Field	31
C. Effects of Turbulence	34
D. Variations of Core Jet Mass Flow	37
E. High Coaxial Flows	37
VI. CONCLUSIONS	40
REFERENCES	43
LIST OF ILLUSTRATIONS	45
APPENDIX A: List of Symbols	A-1
B: Data Reduction Procedure	B-1

I. SUMMARY

The mixing of a subsonic, one-centimeter-diameter argon arcjet with a coaxial flow of cold helium in a 3-inch-diameter duct has been studied visually by schlieren photography and quantitatively by use of a 0.075-inch-diameter calorimetric and sampling probe. Measurements of enthalpy, velocity and composition of the mixing field were made at a pressure of 1 atmosphere for a laminar argon jet having a mass flow of 0.32 gm/sec, an exit-plane peak temperature of 20,000°R, and an exit-plane peak velocity of 550 ft/sec. The effects of cold coaxial helium flow velocities of 0, 0.27 and 2.7 ft/sec on jet mixing characteristics were studied, as well as the effect on the flow field of varying the argon jet flow from 0.2 to 1.4 grams per second at a fixed coaxial helium velocity of 0.27 ft/sec.

The data obtained for the coaxial helium flow experiments were correlated with experimental and theoretical investigations for a free argon arcjet at similar initial conditions, mixing with stagnant helium at 1 atmosphere. The results are in excellent agreement over the regime of laminar flow investigated. The principal effect of the controlled ducted flow was to hasten mixing by causing earlier transition of the arcjet to turbulent flow. The dominant mixing process for both the free and ducted jets

was found to be the inflow of the coaxial gas into the hot argon jet, the effects of radiation and recombination being negligible. This results from the high specific heat and high diffusion coefficients of helium at arcjet temperatures. In cases where turbulence is present, the dominant mixing process is still the inflow of the coaxial gas, although the rate of this inflow is substantially enhanced by the turbulence. The centerline jet enthalpy was found to be almost independent of mixing characteristics; that is, it was not affected by the wide extremes of jet centerline temperature, velocity, and composition, or by the variation of the location of the transition point for the various flow conditions. It was also found that in the cases where the coaxial flow was able to supply adequate amounts of helium, the duct had no measurable effect on the flow field.

The experiments with variable argon mass flows showed that at increased argon mass flows the rate of mixing of the jet was retarded, a phenomenon commonly observed in other types of jets.

An extension of existing free-jet laminar-flow theories was made to include coaxial gas velocities up to 1000 ft/sec. The results showed that even at high coaxial flows, (up to 1,000 ft/sec), the dominant mixing process was still the inflow of the coaxial gas. Several runs were made with no duct using a coaxial nitrogen flow of 200 ft/sec to verify the theoretical predictions.

II. INTRODUCTION

A. Purpose

The purpose of the investigation was to determine the mixing and heat transfer characteristics of a hot, high-molecular-weight, partially ionized gas into an annular flow of a surrounding cool, low-molecular-weight gas. Of interest were radial and axial profiles of temperature, velocity and composition, the effect of the coaxial flow on transition, and the effect of heat-release due to radiation and ion recombination in the inner jet.

In addition, the range of applicability of Sherman's free-jet laminar mixing theory¹ was to be determined, and its extension to the coaxial-flow case was to be made.

B. Background

The interaction of a high temperature, partially-ionized gas jet with a low-temperature gaseous environment is of importance in several advanced propulsion concepts. One of the possible applications is the coaxial-flow gaseous-core nuclear rocket^{2,3,4} in which energy must be transferred from a low-velocity, ionized-fuel plasma to a high-velocity, low-molecular-weight propellant gas with little mixing of the two gas streams to minimize fuel losses. Performance of this powerplant is governed by the energy-exchange process between the ionized fuel atoms and the

propellant gas, while the mixing process determines the fuel loss and thus the operating performance and cost of the device.

Another application is that of providing short-term high thrust levels in low thrust, high-specific impulse systems such as thermal arcjets. This can be done by diluting the high-energy jet with cold propellant, thereby reducing the exhaust velocity but increasing the thrust. The performance in such a device depends on the mixing of the cold and hot coaxial gas streams.

A third application is the film cooling of chambers for extreme-energy propulsion systems such as the gaseous core concept discussed previously, or some form of magnetohydrodynamic accelerator using high-temperature ionized gases. Further, the nature of the decay of such jets is a fundamental consideration in high-temperature flow facilities such as hyperthermal wind tunnels, arc tunnels, etc.

C. History

The three principal lines of analytical attack on the coaxial jet mixing problem are:

- (1) Point-source diffusion of momentum, material, and temperature. This method is valid only at distances downstream from the point of initial mixing which are large compared to the initial jet radius. Thus the range of applicability of this approach is greatly limited, and

adequate information about early mixing is not available.

(2) Boundary-layer approximation of the Navier-Stokes equations, into which are inserted various transport theories.

(3) Integral equations of motion.

The case of coaxial, turbulent, low-temperature jets has been treated by Squire and Trouncer.⁵ Jacobs⁶ has extended the Squire and Trouncer solutions to flows at very high temperatures, where partial ionization has occurred. The principal problem in analyzing turbulent flows by use of the Navier-Stokes equations is the determination of the transport properties. Pai⁷ by using simplifying assumptions has solved the isothermal case in which the compositions of both jets are identical. Lakkay, Krause, and Woo⁸ have used an inverse solution of the Navier-Stokes equations to determine turbulent transport properties from experimentally-determined profiles where no chemical, dissociation, or ionization reactions are taking place.

For laminar coaxial flows, solution of the Navier-Stokes equations has been the most fruitful method. Following Pai's treatment of the isothermal case⁷, Squire⁹ solved the Navier-Stokes equations exactly for the hot jet with no chemical or ionization reactions taking place. The problem was extended by Marble and Adamson¹⁹ and Cheng and Kovitz¹¹ to include chemically reacting flows.

The introduction of ionization reactions greatly complicates the problem. Not only is the energy equation modified by the addition of a chemical production term, but the transport properties must be determined for an ionized gas. Using the boundary layer approximation of the Navier-Stokes equations, and an extension of the Chapman-Enskog method for the calculation of transport properties, Sherman¹ analyzed the case of a hot, laminar, partially-ionized jet exhausting into a cool stagnant atmosphere.

With regard to experimental studies between the years 1935 and 1948 several investigations of an axisymmetric jet exhausting into a stagnant atmosphere were made. The most comprehensive of these was by Hinze and Zijnen¹², who investigated material, momentum, and heat transfer. In 1949 Forstall and Shapiro¹³ investigated the case of isothermal coaxial flows in order to verify the theoretical work of Squire and Trouncer. Subsequent experimental investigations of coaxial jet mixing, including some degree of temperature variation between identical coaxial gases, were performed by Pitkin¹⁴, John¹⁵, and Willis¹⁶.

The development of the arc plasma generator provided the ability to obtain high temperature central jets in which ionization, dissociation, and radiation

effects may be important. Jacobs and Grey¹⁷ investigated the turbulent mixing of a partially ionized gas with a cool coaxial flow. At the high jet temperatures available, the density is low and the viscosity is high, and thus the Reynolds number can be quite low. Under certain conditions, it was found possible to obtain laminar flow. Sherman's experiment on a partially-ionized laminar jet exhausting into a cool stagnant atmosphere was used to evaluate his analytical studies with a fair degree of success.

The present work reevaluates some of Sherman's experimental results and extends the work to the case of a partially-ionized initially laminar jet exhausting into a coaxial flow of cool gas.

III. DESCRIPTION OF TEST PROGRAM

A. Apparatus

The entire experimental apparatus is diagrammed in Figure 1. It consists of a plasma generator mounted so as to eject a partly-ionized gas jet horizontally into a test chamber, the test chamber itself forming part of a 1,000-gallon tank. For the purposes of these tests, a series of ducts could be mounted which permitted the injection of a coaxial flow of cool gas concentric with the plasma jet axis. Instrumentation consisted of a schlieren system for visual studies, a calorimetric probe¹⁸ and drive systems suitable for pressure, composition and enthalpy mapping of the entire duct interior, and miscellaneous instrumentation related to the arc generator and duct. Details of each major component are described in the ensuing paragraphs.

1. Plasma Generator

The initial visual studies were made with a Plasmaflame Model F-80 arcjet manufactured by Thermal Dynamics, Inc. (Figure 2). This generator was available at Princeton, and for the purpose of these tests utilized a 3/8"-diameter straight-bore water-cooled nozzle, whose exterior was tapered so as to provide smooth-entry mixing with the annular light-gas flow (Figure 3).

The torch was powered by a marine diesel generator driving four Westinghouse RA-2 rectifiers, one of which was provided with remote current adjustment, having a total DC capacity (after power factor and lead losses) of approximately 75 kw. A water-cooled, copper-tipped prod was used for torch starting, and operation was controlled from a modified Thermal Dynamics console. The torch, nozzle and leads were cooled with 300 psi water from a Pesco gear pump. Calorimetric measurement of the rate of heat extraction from the torch by the coolant was available.

As described below, it was later found visually that the laminar jet obtained with the Thermal Dynamics torch was too unstable for probe profile measurements. Therefore, a new plasma generator was obtained. This new generator (Figure 4), manufactured by Creare, Inc., was adaptable to the existing power supply, ducts, and test chamber. Its principal advantages were (a) micrometer adjustment of radial and axial cathode position, and (b) a sectioned straight-tube nozzle consisting of a series of thin insulated segments, one of which could be grounded so that the anode arc contact point could be preselected and maintained. This generator provided excellent laminar stability under nearly all operating conditions, and was used to collect the probe test data described later.

An adapter and light-gas injection plate compatible with the duct were designed and installed for this generator (Figure 5). The injection plate, which covered the entire duct inlet, was uniformly drilled with small holes to provide approximately uniform flow of the light gas.

The test gases used were argon for the hot gas and helium for the cool gas. Several test runs were also made using nitrogen for the cool gas for reasons to be discussed later.

2. Duct and Test Section

The test section consisted of a rectangular parallelepiped 18" square by 3 feet long, opening into a 1,000-gallon commercial gasoline tank internally braced for vacuum operation (see Figure 6). The test section was equipped with quartz windows for viewing either the open plasmajet exhaust or the duct. The plasma generator and duct were mounted on opposite sides of the test section endplate, as shown in Figure 6, with the duct fully contained within the test section. Two conventional mechanical vacuum pumps connected to the tank could provide test section pressures down to about 1" Hg absolute. The tank pressure was prevented from exceeding one atmosphere (absolute) by a large flapper. A telescope mounted in the far end of the tank, opposite the duct and arcjet, provided capability for viewing the interior of the arc chamber during operation.

Three different ducts were used for this test program. A cylindrical Vycor duct (Figure 7) was first constructed to provide visual indication of the nature of the jet mixing region. Although this was suitable for direct viewing, the curvature of the Vycor precluded the use of schlieren photography. Consequently, a metal duct of square cross-section having approximately the same dimensions (3") and fitted with flat quartz windows (Figure 8) was used for photographic recording of the mixing region, as will be described later. Correlation between flows in the two ducts is also described later.

Detailed flow-parameter surveys were made in a brass calorimetric duct (Figure 9) designed to provide two-dimensional coverage of the entire duct interior by the calorimetric probe. This duct was water-cooled, permitting measurement of the overall heat transfer to the duct walls.

3. Instrumentation

The two unique items of instrumentation required for the subject program were the schlieren system and the calorimetric probe. Other more or less standard items, which included those necessary for measurements of arcjet power, gas flow rates, tank pressures, etc., are not described in detail here.

(a) Schlieren System

In order to establish the general nature

of the flow within the duct (i.e., length of laminar core, location of transition, structure and stability of the laminar core flow, etc.), the schlieren system of Figure 10 was used, together with the flat-sided duct of Figure 3. The system was of standard design, employing parabolic mirrors instead of lenses in order to gain light-path length, and utilizing a BH-6 micro-second spark source with an open-shutter camera in order to obtain sufficient illumination to provide transparency of the intensely luminous arcjet.

The system yielded good schlieren photographs when the hot argon jet issued into cold nitrogen. The quality was barely adequate, however, when the jet was cooled by helium, since the density of the hot argon was sufficiently close to that of the coaxial helium so that the density gradients were at the limits of the systems resolution.

(b) Calorimetric Probe

The calorimetric probe is an instrument which measures enthalpy, stagnation pressure, and composition of gases at temperatures up to at least 25,000°F. It has been used for some time in arcjet diagnosis, and since it has been described in detail elsewhere¹⁸⁻²¹, only its general nature is outlined here.

The probe configuration and its associated instrumentation are diagrammed in Figures 11 and 12,

respectively. The construction of the probe itself is of copper, with a brass base. Cooling water from a high-pressure source (up to 1,000 psi) enters through the mounting block, passes through the outer channel to the tip, and leaves via the inner channel. Sheathed, ungrounded thermocouple junctions are located where the probe cooling water flow enters and leaves the sampling tube. A steady flow of sample gas can be drawn by a vacuum pump from the probe tip through the central tube past a thermocouple junction located in the tube, and then through the support shaft to valving and instrumentation.

The flow of the hot sample gas in the central tube causes the probe cooling water to rise in temperature a greater amount than when the gas sample flow is not permitted to flow through the tube. A flowmeter measures the probe coolant flow and a critical orifice measures the gas flow. These measurements are sufficient to compute the enthalpy of the gas sample at the point where it enters the probe.

The composition of the two-component gas sample is determined by measuring its thermal conductivity in a carefully calibrated commercial cell, and stagnation pressure is measured when the gas sample is not flowing by simply diverting, through appropriate valving, the gas

sample line from the vacuum pump to a water manometer. Enthalpy can be converted to temperature, once the gas composition is known, from an equilibrium theory such as the Saha equation. The measured stagnation pressure is converted to velocity using the Bernoulli equation, since the gas Mach number is less than 0.1 (See Appendix B).

The sensitivity and calibration of the probe under similar experimental conditions have been described elsewhere²⁰. In previous work, energy and mass balances showed that the probe's accuracy (standard deviation from the mean) was about 3 per cent¹⁸.

B. Conduct of Tests

1. Visual Studies

The visual studies were undertaken with the dual objective of (a) establishing the general character of the jet mixing as a guide to the ensuing probe measurements, and (b) establishing that the jet was sufficiently stable and uniform that worthwhile and reproducible probe data could be obtained. Findings in accordance with this latter objective resulted in postponing the probe measurements until the new Creare plasma generator could be installed, as was described previously. The majority of the visual experiments were made with the Thermal Dynamics torch, and although the flame was not sufficiently steady for detailed probing, it was satisfactory from the standpoint of establishing the general nature of the flow.

The first series of visual studies was made in the round Vycor duct, and data were obtained using both helium and nitrogen as the coaxial gas. The conduct of the experiments was generally the same for both gases. The test chamber and the 1000-gallon exhaust tank were evacuated to about $1/5$ atmosphere, since it was found experimentally that longer laminar flames, and thus greater flame length differences, could be obtained at reduced pressure. It was believed that this would not invalidate the visual data, since the purpose of the visual study was only to establish trends to be later verified by probe measurements at one atmosphere.

Once the proper test chamber pressure was established, the plasma generator was started and adjusted to produce as long a laminar flame as possible. Most of these tests were run with an argon flow of about 100 SCFH at a net plasma generator power of about 19 kw.

With the arcjet thus adjusted, observations were made of the character of the jet for different coaxial gas velocities. The typical observation procedure was to first observe the flame with no coaxial gas flow, and record the full length of the laminar portion of the jet. The coaxial flow was then initiated, and the new length of the laminar portion of the jet was observed, together with the flow rate of the coaxial gas. Observations were

continued at increasingly higher coaxial flows until the laminar jet disappeared and turbulence was observed at the nozzle exit plane.

These visual observations were made with the aid of schlieren photography, to define as nearly as possible the exact length of the laminar jet. Figure 13 is a schlieren photograph illustrating a typical laminar arcjet and its transition to turbulence in a free environment. Figure 14 is a schlieren photograph of laminar and turbulent jets taken through the windows of the square three-inch duct. Although the quality of these latter photographs is not as good as for the free jet, the difference between laminar and turbulent flows can be clearly distinguished. Note from Figure 14 that turbulence can exist right at the nozzle exit plane.

As stated previously, schlieren photographs could not be taken through the round duct. The photographs taken in the square duct were therefore used to confirm the round-duct visual observations. Data were taken with both helium and nitrogen coaxial flows, in both round and square ducts, and also with a free jet in nitrogen.

2. Detailed Surveys

The probe measurements were conducted in the calorimetric duct of Figure 9. Radial profile measurements were taken, beginning at the exit plane and then

moving downstream at quarter-inch intervals to the point at which the jet had become fully turbulent and mixing of the arcjet with the coaxial gas flow had been completed.

Profile data were taken under the following initial conditions for the argon jet:

Plasma generator power	14 kw
Argon Mass Flow Rate	0.323 gm/sec
Jet Temperature at Nozzle Exit*	20,000°R
Initial Jet Velocity*	550 ft/sec
Coaxial Helium Velocity	0,0.27 and 2.7 ft/sec

A second series of runs was taken at an axial station 1 inch downstream from the nozzle with a coaxial helium flow of 0.27 ft/sec and a variable argon flow between 0.24 and 1.34 gm/sec.

3. High Coaxial Velocity Surveys

The high velocity surveys were defined as those cases in which the velocity of the coaxial gas was of the same magnitude as the peak core gas velocity. For economic reasons nitrogen was employed as the coaxial gas for these tests. Due to the high nitrogen flow rates that were required, a modified version of the Plasmaflame Model F-80 torch using a segmented anode (Figures 15 and 16) was used in conjunction with a newly-designed injection plate (Figure 17). These tests were conducted without a

*Typical centerline values. Profile data given later provide exact initial condition.

duct using the calorimetric probe configuration shown in Figure 18. Conduct of the tests was otherwise as described previously.

Profile data were taken under the following conditions:

Plasma generator power	9 kw
Argon Mass Flow Rate	.83 gm/sec
Average Coaxial Nitrogen Velocity	200 ft/sec

Radial surveys were taken $1/2"$, $3/4"$, $1"$ and $1\ 1/2"$ downstream from the nozzle exit plane. In addition, cold-flow profiles were taken $1/32"$, $3/8"$, $3/4"$, $1\ 1/8"$ and $1\ 1/2"$ downstream of the nozzle.

IV. THEORETICAL STUDIES

The purpose of the theoretical study was to determine if Sherman's laminar boundary layer theory was applicable to the laminar region of the coaxial flow problem. The immediate problem was to introduce the experimental exit profiles of temperature, velocity and composition into the theory.

Sherman's procedure was to take the fluid dynamic equations of motion and nondimensionalize them using the following dimensionless groups:

$$\text{Reynolds Number} = \frac{\rho_0 u_0 r_0}{\mu_0} = \text{Re}$$

$$\text{Prandtl Number} = \frac{c_{p0} \mu_0}{k_0} = \text{Pr}$$

$$\text{Schmidt Number} = \frac{\mu_0}{D_0 \rho_0} = \text{Sc}$$

$$\text{Radiative to Conductive Parameter} = \frac{P_{\text{ref}} r_0^2}{\lambda_0 T_0} = R_{\text{rad}}$$

The Von Mises transformation, which transforms the spatial coordinate r to the stream function ψ , is then performed, and the equations are put into finite difference form. The resulting equations are:

Momentum:

$$u_N^{M+1} = u_N^M + \frac{\Delta z}{\Delta Y^2} \left[g u r^2 u \right]_N^M \delta^2 u + 2 \frac{\Delta z}{\Delta Y} u_N^M \delta u + \frac{\Delta z}{\Delta Y^2} g r^2 u \left[(u_N^M)^2 + \frac{\Delta z}{\Delta Y^2} \left[g u r^2 u \right]_N^M \left[\frac{\delta u}{\delta} + \frac{\delta u}{\lambda} \right] \delta u \right]$$

Helium Continuity:

$$\left\{ \bar{X} - \frac{1}{2} X_A \left[1 - 2R - \frac{\partial X_A}{\partial X_H} \right] \right\} (X_{H,N}^{M+1} - X_{H,N}^M) \\ - \frac{1}{2} X_H \frac{\partial X_A}{\partial T} (T_{N}^{M+1} - T_N^M) = - \frac{\Delta Z}{\Delta Y^2} \frac{\rho u r^2}{Sc} \left\{ (R D_{HH} - D_{HA}) \delta^2 X_H \right. \\ + (2[D_{HI} - D_{HA}] \delta^2 X_E + (R \delta D_{HH} - \delta D_{HA}) \delta X_H \\ + 2(\delta D_{HI} - \delta D_{HA}) \delta X_E \left. \right\} - \frac{\Delta Z}{\Delta Y^2} \frac{\rho^2 u r^2}{Sc} \left[\frac{2}{3} \delta \beta \right. \\ + \frac{\delta u}{\lambda} - \frac{2}{\bar{X}} \delta \bar{X} \left. \right] \left[(R D_{HH} - D_{HA}) \delta X_H \right. \\ + 2(D_{HI} - D_{HA}) \delta X_E \left. \right] \\ - \frac{\Delta Z}{\Delta Y^2} \frac{\rho \delta}{Sc} \left[(R D_{HH} - D_{HA}) \delta X_H + (D_{HI} - D_{HA}) \delta X_E \right]$$

Energy:

$$\left[\frac{1}{T} - \frac{\left(1 + \frac{T}{T} \right) \frac{\partial X_A}{\partial T}}{1 + X_A - X_H \frac{\partial X_A}{\partial X_H}} \right] [T_N^{M+1} - T_N^M] = - \frac{\Delta Z}{Pr} \frac{R_{rad} P_{rad}}{Pr} \\ + \frac{\Delta Z}{\Delta Y^2} \left\{ \frac{\rho u r^2}{Pr} \left[\delta^2 T + \delta T \left(\frac{\delta \beta}{\beta} + \frac{\delta u}{u} + \frac{\delta \lambda}{\lambda} \right) \right] \right\} \\ + \frac{\Delta Z}{\Delta Y^2} \frac{2 \rho \lambda}{Pr} \delta T + \frac{\Delta Z}{\Delta Y^2} \frac{\rho^2 u r^2}{Sc T X} \delta T \\ \left\{ (R D_{HH} - D_{HA}) \delta X_H + 2(D_{HI} - D_{HA}) \delta X_E \right. \\ \left. - (1 - 2R) \left[(R D_{HH} - D_{HA}) \delta X_H + 2(D_{HI} - D_{HA}) \delta X_E \right] \right\}$$

Energy (Contd):

$$\begin{aligned}
 & + \frac{\Delta Z}{\Delta Y} \left(1 + \frac{2}{R}\right) \frac{\delta}{S_C} \frac{\partial Y_A}{\partial X_H} \left\{ (RD_{HH} - D_{HA}) \delta^2 X_H \right. \\
 & + 2(D_{AI} - D_{AH}) \delta^2 X_E + \delta(RD_{HH} - D_{HA}) \delta X_H \\
 & + \delta[2(D_{AI} - D_{AA})] \delta X_E + \left[\frac{(1-2R)(X_H \frac{\partial Y_A}{\partial X_H} - X_A) - \frac{\partial Y_A}{\partial X_H}}{1 + X_A - X_H \frac{\partial X_A}{\partial X_H}} \right] \\
 & \left. \left[(RD_{HH} - D_{HA}) \delta^2 X_H + 2(D_{AI} - D_{HA}) \delta^2 X_E \right. \right. \\
 & \left. \left. + \delta(RD_{HH} - D_{HA}) \delta X_H + 2\delta(D_{AI} - D_{HA}) \delta X_E \right] \right\} \\
 & + \frac{\Delta Z}{\Delta Y} \frac{2R}{S_C X} \left\{ (RD_{HH} - D_{HA}) \delta X_H \right. \\
 & + 2(D_{AI} - D_{AA}) \delta X_E \\
 & + \left[\frac{(1-2R)(X_H \frac{\partial Y_A}{\partial X_H} - X_A) - \frac{\partial Y_A}{\partial X_H}}{1 + X_A - X_H \frac{\partial X_A}{\partial X_H}} \right] \\
 & \left. \left[(RD_{HH} - D_{HA}) \delta X_H + 2(D_{AI} - D_{HA}) \delta X_E \right] \right\}
 \end{aligned}$$

where the differences are:

$$\frac{\partial A}{\partial \Psi} = \frac{A_{N+1}^M - A_{N-1}^M}{2 \Delta \Psi} = \frac{\delta A}{\Delta \Psi}$$

$$\frac{\partial^2 A}{\partial \Psi^2} = \frac{A_{N+1}^M - 2A_N^M + A_{N-1}^M}{\Delta \Psi^2} = \frac{\delta^2 A}{\Delta \Psi^2}$$

$$\frac{\partial A}{\partial Z} = \frac{A_{M+1}^N - A_{M-1}^N}{\Delta Z} = \frac{\delta A}{\Delta Z}$$

These equations can be solved numerically by choosing $\Delta \Psi$ and ΔZ for a given set of initial profiles of $T(\Psi)$, $u(\Psi)$ and $X(\Psi)$.

Sherman has shown that for a stable solution,

$$\Delta Z < \frac{\Delta \Psi^2}{2g\mu r^2} \left[\frac{Sc_m}{\beta D_{OA}} \right]$$

or

$$\Delta Z < \frac{\Delta \Psi^2}{2g\mu r^2} \left[\frac{C_p \mu P_r}{\lambda} \right]$$

whichever is more restrictive.

In the above equations the properties T , u , X , β , μ , D , and λ are all functions of the stream function Ψ . Thus, by choosing a Ψ which puts an upper limit on the chosen value of ΔZ , the equations can be solved if the above-mentioned properties are known as functions of Ψ . The experimentally determined exit profiles yield the properties as a function of radius, r . Ψ is defined by the

Von Mises transform as:

$$\left(\frac{\partial \Psi}{\partial r}\right)_x = g u r$$

$$\left(\frac{\partial \Psi}{\partial x}\right)_r = -g v r$$

$$\Psi = 0 \quad \text{at} \quad r = 0$$

Thus:

$$\Psi = \int_0^r g(r') u(r') r' dr'$$

The integral was evaluated using a three point Weddle approximation on an I.B.M. 7094 digital computer. The truncation error was not evaluated; instead, comparison of the exit-plane theoretical profiles with the exit-plane experimental profiles was used as a measure of accuracy. The difference was at most 2%, and in most cases much less. Evaluation of the integral gives Ψ as a function of r . Thus the desired quantities $T(\Psi)$, $u(\Psi)$ and $X(\Psi)$ are known, and $g(\Psi)$, $\mu(\Psi)$, $D(\Psi)$ and $\lambda(\Psi)$ can be computed.

The equations of motion were then integrated numerically on the 7094 computer. The results gave profiles

of temperature, composition and velocity at chosen downstream positions. These profiles, along with experimental profiles for the case of the jet exhausting into a stagnant helium atmosphere, are shown in Figures 19 through 25.

For purposes of the theoretical computations the experimental profiles 1/32" downstream of the nozzle exit plane were used as the initial profiles required by the computation technique. The agreement between theory and experiment is discussed later.

The introduction of coaxial helium flows into the analysis was accomplished by using the experimental exit-plane profiles for no coaxial flow, but setting the velocity equal to a predetermined value when $r > \text{nozzle radius}$. Repeating the above-described analytical procedure yielded the desired downstream theoretical profiles. Figures 26 through 31 show theoretical profiles of temperature, velocity, and composition for coaxial helium flows of 550 ft/sec and 1000 ft/sec.

It is conceivable that the experimentally-observed domination of the mixing process by the helium inflow (see later discussion) may have resulted from the very low helium-to-argon velocity ratio; that is, from the comparatively long "stay time" of the helium in the neighborhood of the jet. The rate of argon dispersion under conditions of high coaxial velocities is therefore of special interest.

For these high coaxial gas velocities, the rate of argon dispersion was determined by computing the argon mass flow within the original jet area at downstream positions and comparing it with the mass flow into the plasma generator. The argon mass flow was computed by the following procedure:

Using the perfect gas law:

$$\rho = \frac{P}{RT}$$

where

$$\bar{R} = \frac{1545.4}{X_A M_A + X_H M_H}$$

$$X_A = (1 - X_H)$$

thus

$$\bar{R} = 386.1/9.98 - 8.98 X_H$$

The total mass flow at a radial point is:

$$dm = \rho u dA$$

The weight fraction of argon is:

$$W_A = \frac{X_A M_A}{X_H M_H + X_A M_A}$$

$$W_A = \frac{1 - X_H}{1 + 8.98 X_H}$$

The argon mass flow is then

$$d\dot{m}_A = \rho u w_A dA$$

The argon mass flow within the original jet area at an axial distance x becomes:

$$\dot{m}_A = \int_0^{r_{\text{NOZZLE}}} 2\pi r \rho(r, x) u(r, x) w_A(r, x) dr$$

where $T(r, x)$, $u(r, x)$ and $X_H(r, x)$ for the theoretical cases are given by the theoretical profiles. The integral was evaluated numerically by hand, and results are discussed later.

V. DISCUSSION OF RESULTS

A. Visual Studies

The quantitative results of the visual studies are summarized in Figures 32 and 33, in which the length of the laminar jet is plotted against Reynolds number and velocity, respectively. The region of interest in these figures was originally concentrated on axial locations greater than six inches, because transition to turbulence was not expected to occur much upstream of this location, and the calorimetric probe, which was used to diagnose the jet in the region near the nozzle exit, is a more reliable measurement. This was particularly true in the case of coaxial helium flow, since the high luminosity of the first few inches of the jet precludes precise visual observations.

It is quite apparent from the visual results that the laminar arcjet is very easily disturbed by the coaxial flow, with the laminar jet being shortened to less than six inches at coaxial velocities of only one foot per second. Although some disturbance of the jet by the coaxial flow had been anticipated, it had not been expected that such small velocities would be so significant. This led to closer investigation of the coaxial gas character, and it was observed that the coaxial gas was introduced with considerable initial turbulence, as shown in schlieren photograph of Figure 34. The quantitative effect of this

initial turbulence on producing transition in the laminar jet is discussed later in connection with results of the calorimetric probe measurements.

B. Detailed Mapping of Flow Field

Verification of the general nature of the visual study results, as well as quantitative mixing characteristics, were established with the calorimetric probe, covering the region from the nozzle exit plane to the downstream point at which the initial jet had become fully turbulent. Results are summarized in Figures 35 through 38, which show jet centerline values of temperature, velocity, composition, and enthalpy respectively, and in Figures 39 through 44, illustrating radial temperature, velocity, and composition profiles at various axial stations. Also shown on certain of these figures are both theoretical and experimental data on the mixing of a free jet.

From the centerline data of Figures 35, 36 and 37, it can be seen that the rapidity of mixing, as evidenced by the rate of decay of the centerline values of temperature, velocity and composition, is strongly influenced by the velocity of the coaxial gas flow, as was indicated by the visual studies discussed above. When the coaxial gas flow was 2.7 ft/sec, mixing was fully accomplished at one inch, or about three jet diameters downstream. At a velocity of 0.27 ft/sec, complete mixing was not accomplished for three

inches, or eight diameters downstream. In the case of no coaxial flow in the duct, as well as in the unbounded jet, mixing was still not completed six inches (about 20 diameters) downstream.

In the case of the free jet, as well as in that for the ducted jet with no coaxial flow (except for Figure 37, which is discussed below), not only did the data indicate confirmation of the visual observations, (i.e., that the jets remained laminar in the region surveyed by the probe) but there was also rather close agreement with laminar mixing theory. With the free laminar jet it was found that the flow of helium into the jet was the dominant mechanism for jet cooling and mixing, and that the effects of radiation and ionization were negligible. This experimental result, accurately predicted by the laminar mixing theory, is attributed to helium's high specific heat and high diffusion coefficients at arcjet temperatures. This mechanism was also experimentally indicated in the coaxial studies, and accounts for the similarity between the free and ducted cases at 0.27 ft/sec coaxial flow in the laminar flow region within one or two diameters ($1/2$ to 1 inch) of the nozzle exit plane.

Direct similarities in this region between the free jet (or the no-coaxial-flow ducted case) and the high-coaxial-flow case (2.7 ft/sec) were, on the other hand,

not observed, obviously because of the early transition to turbulence indicated by Figures 32, 35, 36, and 37.

The large difference in helium concentration data between the no-coaxial-flow ducted case and the others, as shown in Figures 37, 39, 40, etc., also has a simple explanation. In this case, the equilibrium concentration of cold helium in the duct is less than 20 per cent (see Figures 39, 40, 41) because most of the helium originally present is very swiftly swept out with the argon jet, and the ambient conditions are therefore substantially different than for the free jet or the higher coaxial-flow ducted cases. On the other hand, helium concentration data for the 0.27 ft/sec ducted coaxial flow, before turbulence is initiated, were found to be essentially similar to those of the free jet case because an ample supply of cold helium was always available at the jet boundary.

Considerable insight into the mechanism of mixing is obtained by consideration of enthalpy rather than temperature decay. Although the various cases differ widely in terms of temperature, velocity and species concentration, a plot of centerline enthalpy (Figure 38) indicates that the basic mixing process is the same in all cases. In this figure, it is shown that the centerline enthalpy decay coincides closely for all coaxial gas flows. Thus it is necessary to conclude that radiation and ionization effects are negligible, since reference to Figure 35 shows that at

even small distances from the nozzle, the jet temperatures differ by many thousands of degrees. For example, at one inch from the nozzle, the temperatures of the jets which were still laminar were about $11,000^{\circ}\text{R}$, while that of the turbulent jet, in which mixing was substantially complete, was only $1,000^{\circ}\text{R}$; still, the enthalpies at the centerline were nearly equal. Clearly, if radiation and ion recombination effects were important mechanisms for jet power loss, the higher-temperature jets should show lower enthalpies. Furthermore, if there were substantial dispersion of the argon jet, the centerline enthalpy of the well-mixed case should be substantially less.

The results of Figure 38 therefore indicate that the principal mechanism for energy transfer (jet cooling) is the inflow of coaxial helium rather than either the direct loss of energy (by radiation or recombination) or the outflow of argon from the core jet.

It may be concluded that while turbulence (of the degree present in these experiments) substantially increases the rate of jet mixing, the effect of the turbulence is to aid the inflow of coaxial helium and not to disperse the argon jet itself.

C. Effects of Turbulence

The very large effect of turbulence on the rate of mixing, in that an apparently small disturbance can cause the jet to lose its initially laminar characteristics, is a prominent result of the experimental program.

Unfortunately, understanding of turbulent jet mixing and the factors causing arcjet turbulence, like all turbulent phenomena, suffers from the fact that present theories of turbulence are inadequate, and most information on turbulence is empirical. The general character of the observed behavior is consistent with other forms of turbulent-flow experience, however, as is indicated by the summary of results (observed from both the visual and probe studies) in Table I. In this table, Reynolds numbers more than one diameter downstream are based on the length of the jet at the point of observation rather than on the jet diameter. The initial Reynolds number (at the nozzle exit) is based on jet diameter, and is 450 for all cases.

Table I shows that transition of turbulent flow did not occur in the free jet until a Reynolds number of 10,000 was reached, while very small disturbances, such as convective currents resulting from the simple presence of the duct^{*} or from very small coaxial flows, caused transition at Reynolds numbers of 4,000 and 3,000 respectively. Furthermore, a coaxial flow of only 2.7 feet per second of helium produced transition in less than one jet diameter from the exit plane at a Reynolds number of only 450.

^{*}The convective turbulence caused simply by the presence of the duct was evidenced by visually-observed motion of dust particles, and has also been observed in combustion experiments where the flow conditions were similar.²²

TABLE I

Effect of Test Conditions on Reynolds Number at Transition

<u>Test Conditions</u>	<u>Approximate Laminar Jet Length, Inches</u>	<u>Approximate Reynolds Number At Transition</u>
Free jet, 1 atm, no coaxial flow	18	10,000
Ducted jet, 1 atm, no coaxial flow	5	4,000
Ducted jet, 1/5 atm, no coaxial flow	18	4,000
Ducted jet, 1 atm, 0.27 ft/sec coaxial He	2	3,000
Ducted jet, 1 atm, 2.7 ft/sec coaxial He	1/2	450

It should be remarked that only by basing the Reynolds number on a linear dimensional quantity can transition data be obtained which are consistent with the general range in which it is usually observed. Reynolds numbers based on the jet diameter remained nearly constant at about 500 for all types of flow observed, and therefore are not useful as a guide to transition predictions.

On the basis of the above results, it is believed that in any practical propulsion device it would be impossible to maintain laminar flow for more than a few nozzle diameters. These devices should therefore be designed to operate in the turbulent mode.

D. Variation of Mass Flow in Core Jet

Figures 45 through 47 are profiles of temperature, velocity, and composition respectively at one inch downstream from the nozzle exit plane when the argon jet mass flow was varied from 0.24 to 1.34 g/sec while the coaxial helium flow was maintained at 0.27 ft/sec. It can be concluded from the general shape of the profiles that spreading and mixing were little affected, although a wide variation of mass flow was experienced. The plasma generator efficiency is significantly augmented by increased mass flows, and this results in the higher temperatures and velocities observed at the high mass flows. The plots do not indicate which profiles represent laminar flows and which represent turbulent flows, but based on visual observations the profiles at the higher mass flows are likely to be turbulent. It is a tentative conclusion that high mass flow rates tend to reduce jet mixing over a given distance, even though turbulence may be present. This is, of course, similar to the phenomena observed in more familiar types of jets.

E. High Coaxial Flows

Figures 19 through 25, which show profiles of temperature, velocity, and composition at the exit plane, and at 5/16", 1/2", 1", 2", 3", and 4" downstream respectively for the free argon jet exhausting into stagnant helium,

exhibit good agreement between theory and experiment. The lack of consistency in the concentration data results from the unavoidable buildup of argon during the performance of the tests. A composition curve which has been normalized to the tank reference value of helium concentration is shown on the composition plots, and agreement between this curve and the data is good.

The curves of Figure 19 were used as the initial profiles for the determination of the theoretical high-coaxial-flow profiles of Figures 26 through 31. The results of these figures were used to compute the curves of Figure 48. Figure 48 shows that according to laminar mixing theory there is essentially no dispersion of the argon jet. Therefore, the "stay time" of the helium in the neighborhood of the jet is unimportant, and the dominant mixing mechanism for high coaxial flows is still the inflow of helium.

Figures 49 through 51 are experimental profiles of temperature, velocity, and composition respectively at an argon flow of .81 g/sec with average coaxial nitrogen velocity of 200 ft/sec. The decay pattern of these curves is qualitatively predicted by the theory. The data obtained from Figures 49 through 51 were used to compute the fraction of argon within the original jet area at the downstream positions as shown in Figure 52. This figure indicates that

while turbulence does enhance the dispersion of the argon jet, substantial amounts of argon remain within the original jet area at sizeable distances downstream (approximately 0.80 at 3 diameters downstream). This result confirms the theoretical prediction of Figure 48 in that even with high turbulent coaxial flows, the dominant mixing mechanism is still the inflow of the coaxial gas.

The mixing process was much slower for coaxial flows of nitrogen than for coaxial flows of helium, even when the coaxial nitrogen velocities were two orders of magnitude greater than the coaxial helium velocities. This behavior results principally from the lower specific heat (about 1/4) and lower diffusion coefficient of the nitrogen at arcjet temperatures, and partly from the higher argon mass flow used for the high velocity nitrogen experiments.

VI. CONCLUSIONS

1. Up to about three jet diameters downstream from the nozzle exit plane there is little difference between the experimental laminar mixing characteristics of a free jet and a bounded jet when the coaxial flow of helium in the duct is sufficient to provide similar ambient helium concentrations, but not so large as to disturb the laminar character of the jet. In this region a theoretical analysis for a laminar free jet is also applicable to a similar ducted jet.
2. Very low velocities of an initially turbulent coaxial flow were sufficient to cause transition in an initially laminar core jet, and increases in coaxial gas velocities produced earlier transition to turbulence.
3. Mixing of the jet was very rapid once turbulence was initiated, and in one case (the highest coaxial helium velocity tested) complete mixing of the jet was accomplished in less than three jet diameters from the nozzle exit.
4. With increased core-jet mass flow, mixing of the jet at three diameters downstream was diminished, even though the jet may have become turbulent. This is, of course, similar to the phenomena observed in more familiar types of jets.
5. The most significant process in the mixing of either a free or a ducted laminar argon arcjet was found to

be the flow of helium into the jet, the effects of radiation and recombination being negligible. This behavior results from helium's high specific heat and high diffusion coefficient at arcjet temperatures.

Similar behavior was noted when the coaxial gas was nitrogen, except that the effect was not nearly as pronounced as when the coaxial gas was helium, due to nitrogen's lower specific heat and diffusion coefficient.

6. The principal effect of turbulence, in the scale studied, was to cause augmentation of the coaxial gas inflow rather than dispersion of the jet.

7. An arcjet Reynolds number based on length rather than diameter was most useful in correlating the onset of turbulence, in accordance with conventional laminar free-jet practice.

8. Owing to the difficulty of obtaining and maintaining stable laminar jets, turbulent models should be used in the design of practical propulsion devices.

9. Laminar mixing theory due to Sherman agreed well with experiment for the jet exhausting into stagnant helium, and predicted reasonable results for cases of coaxial helium flows.

10. The results indicate potential feasibility of the coaxial flow, gaseous-core nuclear rocket concept, since it was found that the argon arcjet decayed as a result

of inflow of cool coaxial helium rather than dispersion of the argon core, even at high coaxial gas velocities and under conditions when turbulent mixing was significant.

REFERENCES

1. Sherman, M. P., "Interactions Between a Partly-Ionized Laminar Subsonic Jet and a Cool Stagnant Gas," Princeton University Aeronautical Engineering Laboratory Report No. 710, 1964.
2. Bussard, R. W., "Concepts for Future Nuclear Rocket Propulsion," Jet Propulsion 28, April 1958, p. 223.
3. Grey, J., "A Gaseous-Core Nuclear Rocket Utilizing Hydrodynamic Containment of Fissionable Material," Paper No. 848-59, American Rocket Society, June 8, 1959.
4. Weinstein, H., and Ragsdale, R. G., "A Coaxial Flow Reactor - A Gaseous Nuclear Rocket Concept," Paper No. 1518-60, American Rocket Society, December 6, 1960.
5. Squire, H. B., and Trouncer, J., "Round Jets in a General Stream," ARC Technical Report R & M No. 1974, 1944.
6. Jacobs, P. F., "Turbulent Mixing in a Partially Ionized Gas," Princeton University Aeronautical Engineering Laboratory Report No. 625, 1962.
7. Pai, S. I., "Fluid Dynamics of Jets," D. van Nostrand Company, Princeton, N. J., 1954.
8. Zakkay, V., Krause, E., Woo, S., "Turbulent Transport Properties for Axisymmetric Heterogeneous Mixing," AIAA Journal Vol. 2, 11, November 1964.
9. Squire, H. B., "The Round Laminar Jet," Quarterly Journal of Mechanical and Applied Math, Vol. 4, September 1951.
10. Adamson, Jr., T. C., "Ignition and Combustion in a Laminar Mixing Zone," Jet Propulsion Laboratory, C.I.T. Report No. 20-79, 1954.
11. Kovits, A. A., "Ignition in the Laminar Wake of a Flat Plate," PhD Dissertation, Princeton University, 1956.
12. Hinze, J. O., and vander Hegge Zijnen, B. G., "Heat and Mass Transfer in the Turbulent Mixing Zone of an Axially Symmetrical Jet," Seventh International Congress for Applied Mechanics, London (1948).

13. Forstall, W. Jr., and Shapiro, A. H., "Momentum and Mass Transfer in Coaxial Gas Jets," M.I.T. Meteor Report 39, July 1949.
14. Pitkin, E. T., "An Experimental Investigation of an Axially Symmetric Supersonic Jet Mixing with Free Air," Princeton University Aeronautical Engineering Laboratory Report No. 243, August 1953.
15. John, J. E. A., "An Experimental Investigation of the Bounded Mixing of Two Compressible Axially Symmetric Jet Streams," Princeton University Aeronautical Engineering Laboratory Report No. 399, 1957.
16. Willis, D. R., "The Mixing of Unbounded Axially Symmetric Turbulent Compressible Jets," Princeton University Aeronautical Engineering Laboratory Report No. 352, 1956.
17. Grey, J., Jacobs, P. F., "Experiments on Turbulent Mixing in a Partially Ionized Gas," AIAA Journal 2, March 1964, p. 433.
18. Grey, J., Jacobs, P. F., and Sherman, M. P., "Calorimetric Probe for the Measurement of Extremely High Temperature," Rev. Sci. Instr. 33, July 1962, pp. 738-741.
19. Grey, J., Sherman, M. P., and Jacobs, P. F., "Measurements of Arcjet Radiation with a Cooled Collimated Probe," IEEE Transactions on Nuclear Science, Vol. NS-11, January 1964, p. 176.
20. Grey, J., Williams, P. M., Sherman, M. P., and Jacobs, P. F., "Laminar Mixing and Heat Transfer Phenomena Between a Partially-Ionized Gas and a Gaseous Coolant," Report No. ARL 63-237, OAR, USAF, December 1963.
21. Sherman, M. P., and Grey, J., "Interactions Between a Partly-Ionized Laminar Subsonic Jet and a Cool Stagnant Gas," Princeton University Aeronautical Engineering Laboratory Report No. 707, September 1964.
22. Becker, H. A., Hottel, H. C., and Williams, G. C., Ninth Symposium (International) on Combustion, p. 7, Academic Press 1963.

LIST OF ILLUSTRATIONS

FIGURE

- 1 Diagram of Apparatus
- 2 Thermal Dynamics F-80 Arcjet Torch with Swirl Plate and Cathode
- 3 Nozzle-Anode Used with F-80 Arcjet Torch
- 4 Creare Plasma Generator
- 5 Adaptor and Light-Gas Injection Plate
- 6 Creare Generator Installed in Test Apparatus
- 7 View of Round Vycor Duct Used for Visual Coaxial-Flow Transition Studies
- 8 View of Square Duct Used for Coaxial-Flow Transition Studies by Schlieren Photography
- 9 View of Calorimetric Duct Used for Detailed Coaxial-Flow Mixing and Heat Transfer Experiment
- 10 Traveling Schlieren System
- 11 Diagram of Calorimetric Probe
- 12 Diagram of Instrumentation Used with Tare-Measurement Calorimetric Probe to Measure Enthalpy, Velocity, and Gas Composition
- 13 Schlieren Photographs of a Free Argon Arcjet in Nitrogen
- 14 Schlieren Photographs of Argon Arcjet in Nitrogen in 3-Inch Square Duct
- 15 Modified Thermal Dynamics F-80 Arcjet Torch for High Coaxial Flows
- 16 Segmented Anode of Modified F-80 Arcjet Torch
- 17 Injection Plate and Nozzle for Modified F-80 Arcjet Torch for High Coaxial Flows
- 18 Calorimetric Probe

FIGURE

- 19 Temperature, Velocity, and Composition Profiles at 1/32 Inch Downstream from Nozzle Exit Plane for Free Jet
- 20 Temperature, Velocity, and Composition Profiles at 5/16 Inch Downstream from Nozzle Exit Plane for Free Jet
- 21 Temperature, Velocity, and Composition Profiles at 1/2 Inch Downstream from Nozzle Exit Plane for Free Jet
- 22 Temperature, Velocity, and Composition Profiles at 1 Inch Downstream from Nozzle Exit Plane for Free Jet
- 23 Temperature, Velocity, and Composition Profiles at 2 Inches Downstream from Nozzle Exit Plane for Free Jet
- 24 Temperature, Velocity, and Composition Profiles at 3 Inches Downstream from Nozzle Exit Plane for Free Jet
- 25 Temperature, Velocity, and Composition Profiles of 4 Inches Downstream from Nozzle Exit Plane for Free Jet
- 26 Theoretical Temperature Field for Coaxial Helium Velocity = 550 ft/sec
- 27 Theoretical Velocity Field for Coaxial Helium Velocity = 550 ft/sec
- 28 Theoretical Composition Field for Coaxial Helium Velocity = 550 ft/sec
- 29 Theoretical Temperature Field for Coaxial Helium Velocity = 1000 ft/sec
- 30 Theoretical Velocity Field for Coaxial Helium Velocity = 1000 ft/sec
- 31 Theoretical Composition Field for Coaxial Helium Velocity = 1000 ft/sec
- 32 Visual Length of Laminar Arcjet versus Reynolds Number of Coaxial Gas

FIGURE

- 33 Visual Length of Laminar Arcjet versus Velocity of Coaxial Gas
- 34 Schlieren Photographs Showing Scale of Turbulence in Coaxial Helium Flow
- 35 Centerline Temperature Versus Axial Position
- 36 Centerline Velocity Versus Axial Position
- 37 Centerline Helium Concentration Versus Axial Position
- 38 Centerline Enthalpy Versus Axial Position
- 39 Temperature, Velocity and Composition Profiles at Nozzle Exit Plane
- 40 Temperature, Velocity and Composition Profiles at 1/2 Inch Downstream from Nozzle Exit Plane
- 41 Temperature, Velocity and Composition Profiles at 1 Inch Downstream from Nozzle Exit Plane
- 42 Temperature, Velocity and Composition Profiles at 2 Inches Downstream from Nozzle Exit Plane
- 43 Temperature, Velocity and Composition Profiles at 3 Inches Downstream from Nozzle Exit Plane
- 44 Temperature, Velocity and Composition Profiles at 5 Inches Downstream from Nozzle Exit Plane
- 45 Temperature Profile at 1 Inch Downstream from Nozzle Exit Plane for Variable Argon Flow Rate
- 46 Velocity Profile at 1 Inch Downstream from Nozzle Exit Plane for Variable Argon Flow Rate
- 47 Composition Profile at 1 Inch Downstream from Nozzle Exit Plane for Variable Argon Flow Rate
- 48 Theoretical Argon Mass Within Original Jet Area
- 49 Experimental Temperature Profiles for Coaxial Nitrogen Velocity = 200 ft/sec

FIGURE

- 50 Experimental Velocity Profiles for Coaxial
 Nitrogen Velocity = 200 ft/sec
- 51 Experimental Nitrogen Mole Fraction for Co-
 axial Nitrogen Velocity = 200 ft/sec
- 52 Experimental Argon Mass Within Original Jet
 Area for Coaxial Nitrogen Velocity = 200 ft/sec

APPENDIX A

LIST OF SYMBOLS

C_p	Specific heat (BTU/lb-°F)
\bar{C}_p	Effective specific heat (BTU/lb-°F)
C^*	Cold helium mole fraction
D_{ij}	Diffusion coefficient (cm ² /sec)
h	Total enthalpy (BTU/lb)
I	Ionization energy per ionization (erg)
k	Boltzmann constant (1.38×10^{-16} erg/°K)
K	Equilibrium constant
\dot{m}	Mass flow (g/sec)
n	Number density (cm ⁻³)
P_{rad}	Radiant power emitted per unit volume
p	Pressure (dynes/cm ²)
r	radial distance = r^*/r nozzle
R	Ratio of helium to argon atom mass (also universal gas constant)
R_{rad}	Radiative to conductive parameter
T	Temperature (°K)
U	Axial velocity component (cm/sec)
V	Radial velocity component (cm/sec)
X_i	Mole fraction of species i
\bar{X}	$X_A + RX_u + X_E$
x	Axial distance (cm)
z	Finite difference axial distance (x/Re)

GREEK LETTERS

λ	Thermal conductivity (erg -°K/cm-sec)
μ	Viscosity (gm/cm-sec)
ρ	Density (g/cm ³)
ψ	Stream function

SUBSCRIPTS

a	Atmosphere
A	Argon atoms
AI	Argon atoms and ions
E	Electrons
g	Sample gas flow through probe
go	Sample gas out
H	Helium
I	Ions
W	Probe water

APPENDIX B

DATA REDUCTION

The necessary input data for the computerized data reduction program are the output from the thermal conductivity cell, probe water thermocouples, gas sample exit temperature thermocouple, radial position potentiometer, probe water flow, and critical orifice stagnation pressure. These data were obtained in the following manner:

The probe was aligned optically with the left and right edges of the nozzle to calibrate the radial potentiometer position indicator. The thermal conductivity cell readings for pure argon and pure helium (nitrogen for certain tests) were used to set zero and range on the recording potentiometer. The 1,000-gallon test tank was evacuated and filled with the desired atmosphere.

The probe was then placed at the desired axial position and moved radially through a series of positions, each of which constituted a data "point". After passing through the region of interest the probe was moved to another axial location and the procedure repeated. During the time the gas sample was flowing, recordings were taken of the thermal conductivity cell reading, the gas sample flow rate manometer levels, the probe water differential temperature, and the probe exit gas temperature. When the gas sample was shut off for the "tare" reading, the stagnation pressure manometer indication was also recorded.

The torch readings, consisting of coolant flow rate and temperature rise, torch current and voltage, and argon flow rate, all of which remained constant during the taking of a "point", were recorded while waiting for the probe instrumentation to stabilize. The outputs from the thermal conductivity cell, probe water thermocouples, gas sample exit temperature thermocouple, and radial position potentiometer were recorded on Leeds and Northrop recording potentiometers in the Guggenheim Laboratories central recording room. All other data were noted visually from the control panel in the test cell.

The abovementioned data, along with the barometric pressure, were listed on a data sheet from which I.B.M. punched cards were made. The information was then processed on an I.B.M. 1620 digital computer. The computer output gave values of temperature, velocity, gas composition, degree of ionization, mass flow, and jet power at each data point.

The computer program contained all the necessary calibrations to convert the probe output into useful information. From this information the enthalpy at the probe tip was given by

$$h = \Delta T_w \frac{\dot{m}_w}{\dot{m}_g} + \bar{C}_{p,g} T_{g^0}$$

where $\Delta^2 T_w$ was the change in temperature rise of the probe water for the gas "flow" and "no flow" conditions. In a plasma with any degree of ionization the enthalpy is a complex function of temperature and helium mole fraction (nitrogen will be discussed later). It is impossible to compute the temperature directly since the true helium mole fraction in the plasma is not the same as the value measured in the thermal conductivity cell. The two values are related by

$$C^* = (1 - X_E) C$$

The value of X_E is determined, assuming thermal equilibrium and low ionization fractions, by use of the Saha equation

$$K_n = \frac{n_E^2}{n_A} = \frac{X_E^2}{X_A} n = C T^{3/2} e^{-E_{ion}/kT}$$

Define

$$K_x = \frac{X_E^2}{X_A} = \frac{K_n}{n}$$

Assuming a perfect gas,

$$p = n k T$$

and

$$K_x = \frac{X_E^2}{X_A} = \frac{K_n hT}{P}$$

Putting in the values for argon gives:

$$K_x = 2.309 \times 10^{-6} T^{2.851} e^{-1.8282 \times 10^5 / T}$$

From continuity

$$X_A + 2 X_E = 1 - C^*$$

Thus

$$X_E = -K_x + \sqrt{K_x^2 + K_x(1 - C^*)}$$

By assuming initial values of T and C^* , the composition and enthalpy are computed. The computed values of enthalpy and "cold" (cell reading) helium mole fraction are compared to the known experimental values. Using a Newton-Raphson technique, the actual temperature and composition are obtained by iterating until computed and experimental values agree. A flow diagram for the temperature determination loop is given at the end of this Appendix.

The procedure for determining the temperature when the secondary gas was nitrogen was essentially the

same; however, several added problems arise. The secondary gas can now dissociate and ionize, and the specific heat is now a function of temperature. In order to simplify the calculations it was assumed that the nitrogen would not ionize, since only very small amounts of nitrogen would be found in the regions of the jet hot enough to cause any measurable degree of ionization. This assumption was verified experimentally.

The amount of dissociated nitrogen was determined from the relations:

$$\frac{[n_N]^2}{[n_{N_2}]} = \frac{k_s}{k_r} = K_n$$

$$K_x = \frac{K_n}{n} = \frac{kT}{p} K_n$$

Putting in the values for nitrogen gives:

$$K_x = \frac{[X_N]^2}{[X_{N_2}]} = 1.57 \times 10^3 \frac{T}{p_0} e^{-113,200/T}$$

From continuity

$$\frac{[X_N]^2}{K_x} + X_{N_2} = X_{N_2}^*$$

where

$X_{N_2}^*$ is the mole fraction of nitrogen as read by the thermal conductivity cell.

Thus:

$$X_N = -\frac{K_x}{2} + \frac{1}{2} \sqrt{K_x^2 + 4K_x X_{N_2}^*}$$

Since the enthalpy of the sample gas must be computed theoretically, the enthalpy of the nitrogen was calculated as follows:

$$C_V = C_V \text{ translation} + C_V \text{ rotation} + C_V \text{ vibration} + C_V \text{ excitation}$$

$$C_V \text{ translation} = \frac{3}{2} R$$

$$C_V \text{ rotation} = R$$

$$C_V \text{ vibration} = \sum_i \frac{R \left(\frac{\Theta_i}{T} \right)^2 e^{\Theta_i/T}}{(e^{\Theta_i/T} - 1)^2}$$

where for nitrogen $\Theta_i = 3400^\circ K$

$$C_p = C_V + R$$

Thus

$$C_p = \frac{7}{2} R + \sum_i \frac{R (3400/T)^2 e^{3400/T}}{(e^{3400/T} - 1)^2} + C_V \text{ excitation}$$

where $C_V \text{ excitation}$ was determined from tabulated data.

By definition:

$$H = \int_0^T C_p(T) dT$$

Defining an effective specific heat

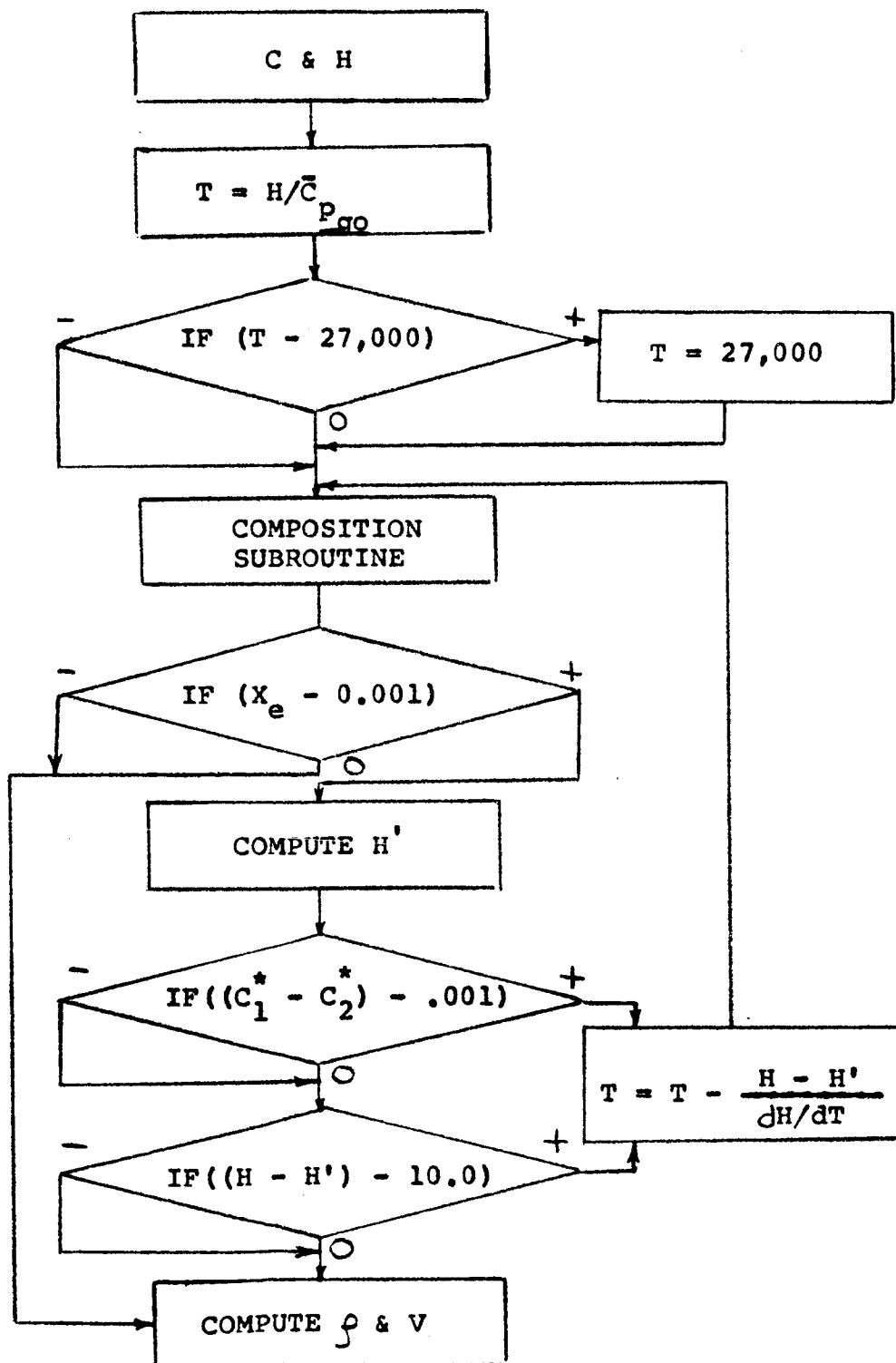
$$\bar{C}_p = \int_0^T C_p(T) dT/T$$

$$H = \bar{C}_p T$$

\bar{C}_p was computed by numerical integration of the above definitions.

Knowing the temperature and composition, the density was computed using the perfect gas law. Velocity could then be computed using the Bernoulli equation, since Mach numbers were on the order of 0.1.

TEMPERATURE LOOP
FLOW DIAGRAM



KEY

- T• TEMPERATURE
- P• PRESSURE
- m• MASS FLOW RATE
- k• THERMAL CONDUCTIVITY
- V• VOLTAGE
- A• CURRENT

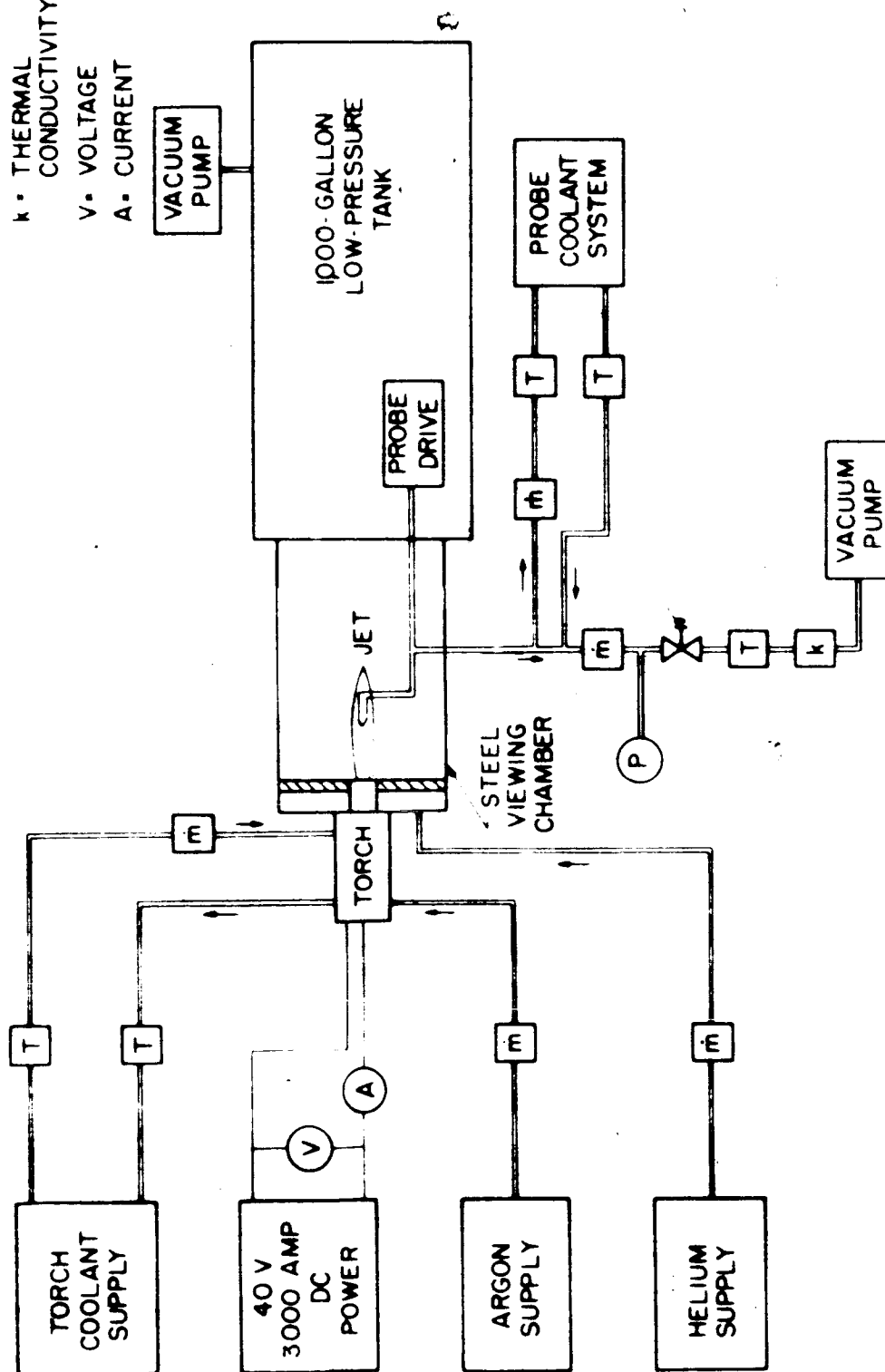
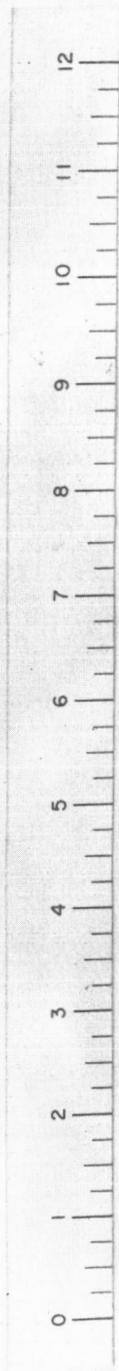
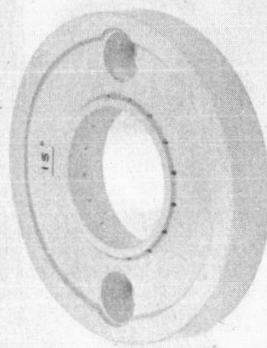
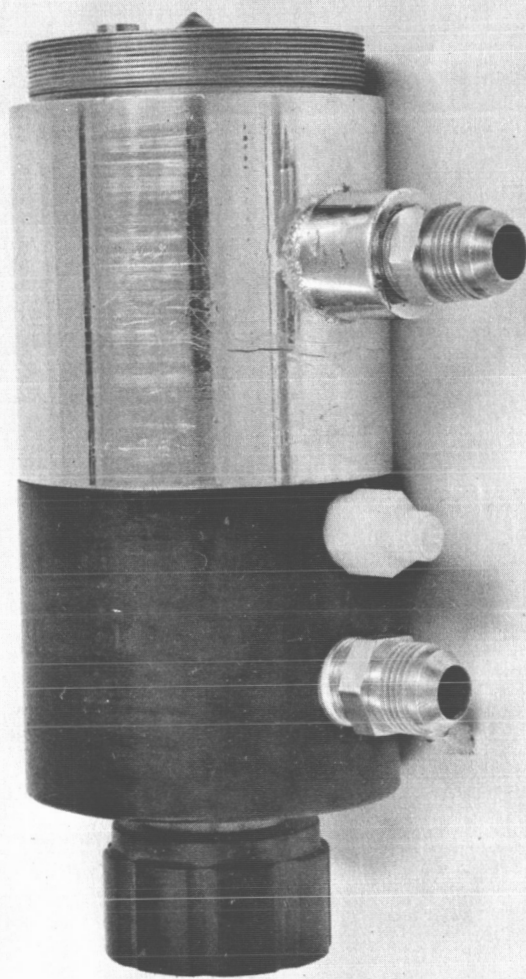


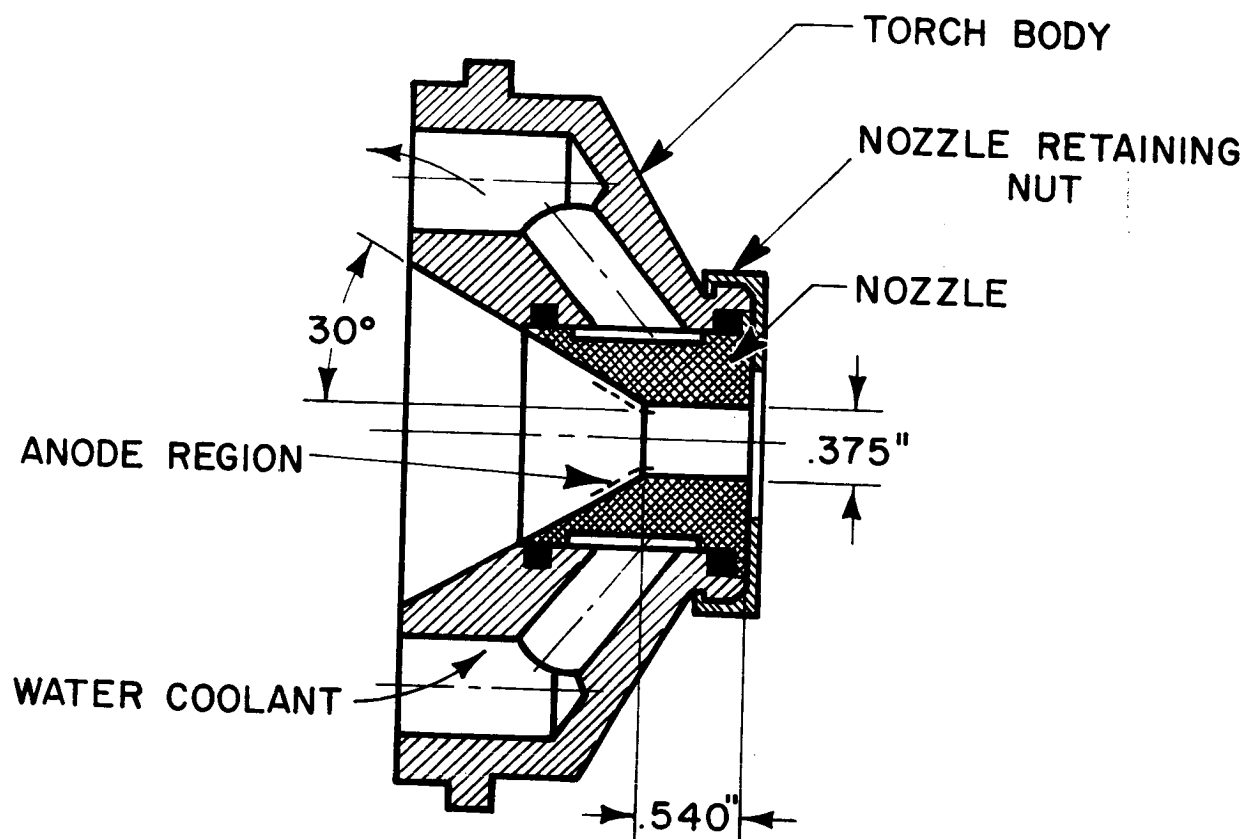
DIAGRAM OF APPARATUS

FIGURE 1

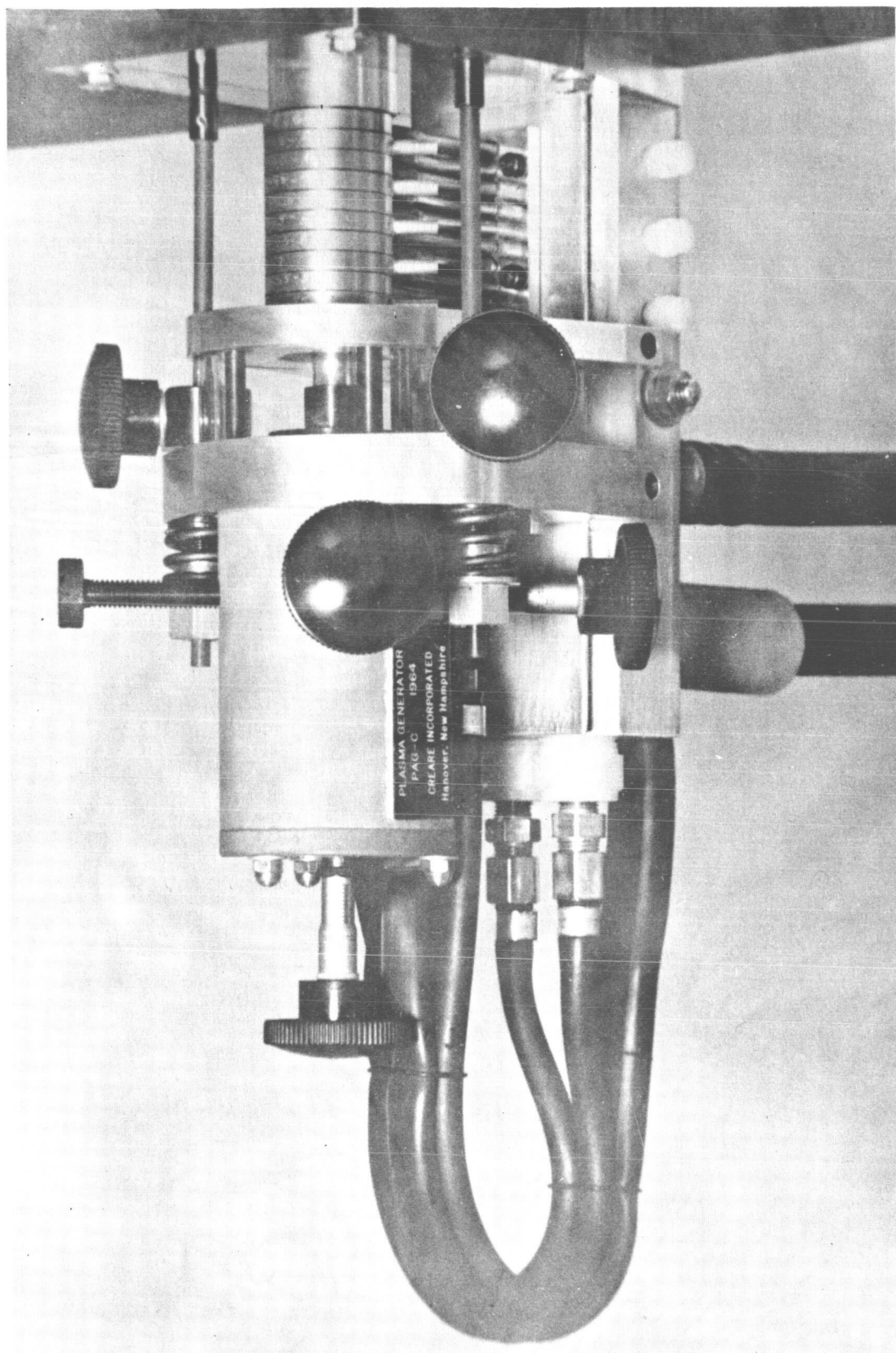


THERMAL DYNAMICS F-80 ARCJET TORCH WITH SWIRL PLATE AND CATHODE

FIGURE 2

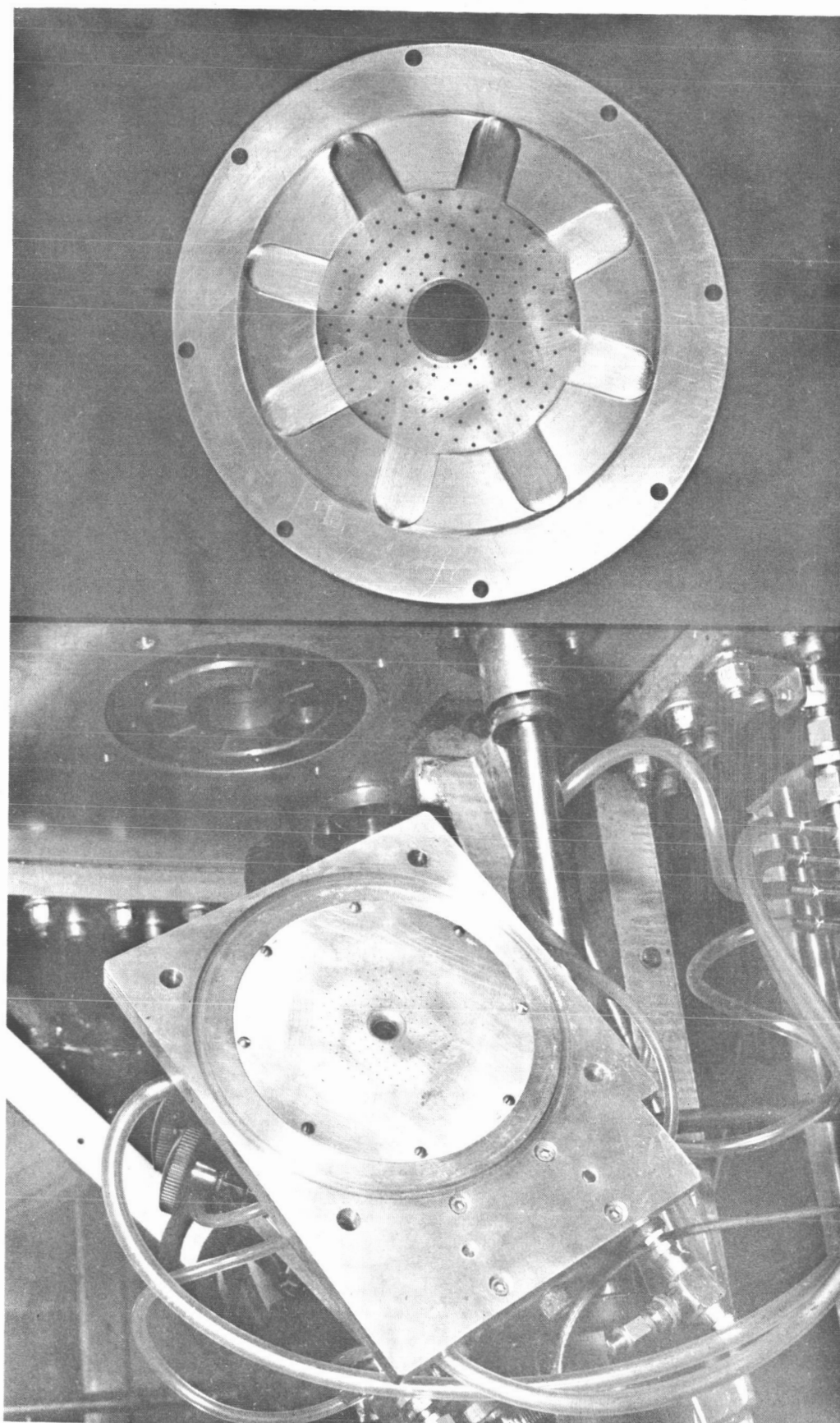


NOZZLE - ANODE USED WITH F-80
ARCJET TORCH

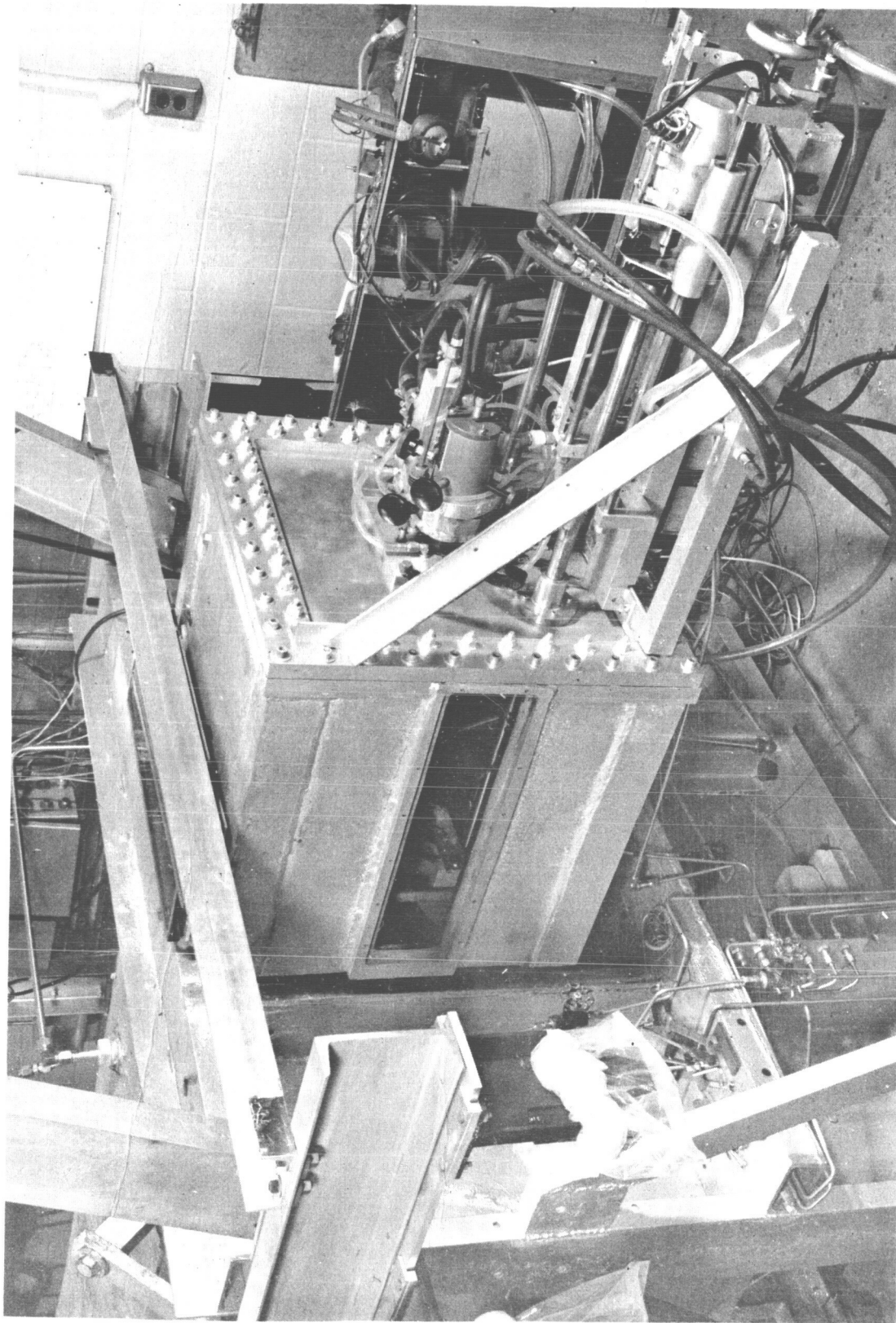


CREAME PLASMA GENERATOR

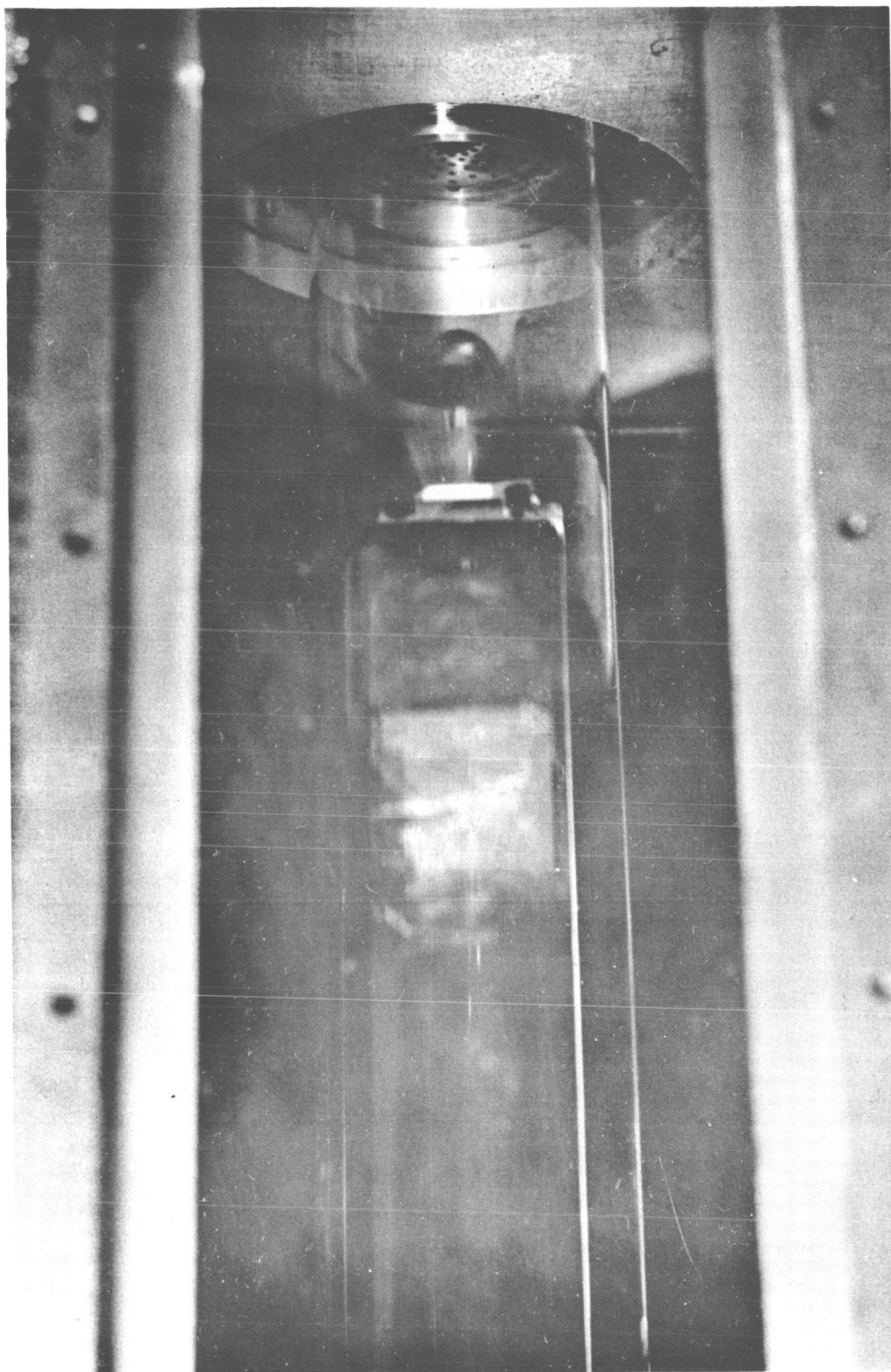
FIGURE 4



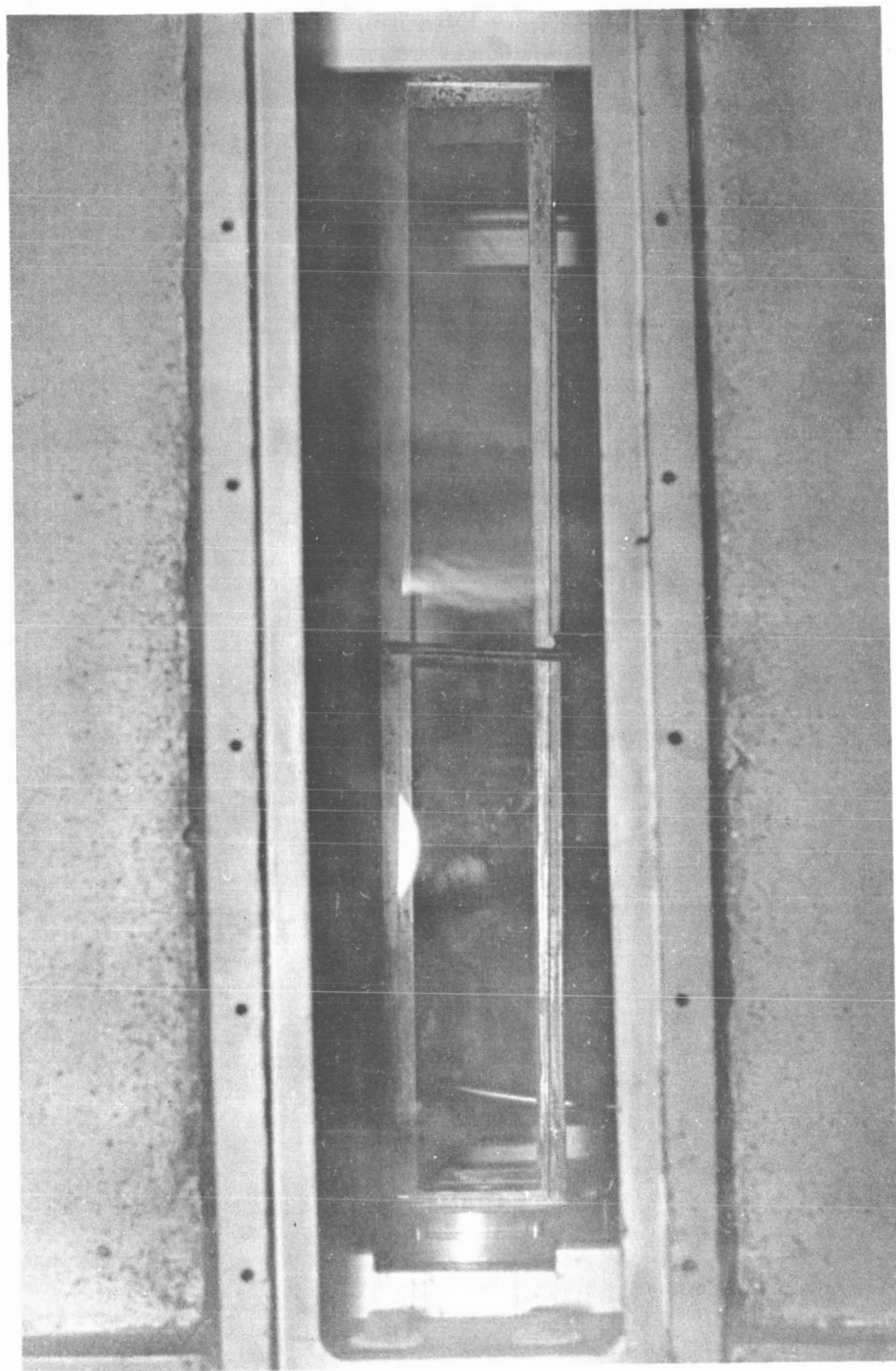
ADAPTER AND LIGHT GAS INJECTION PLATE



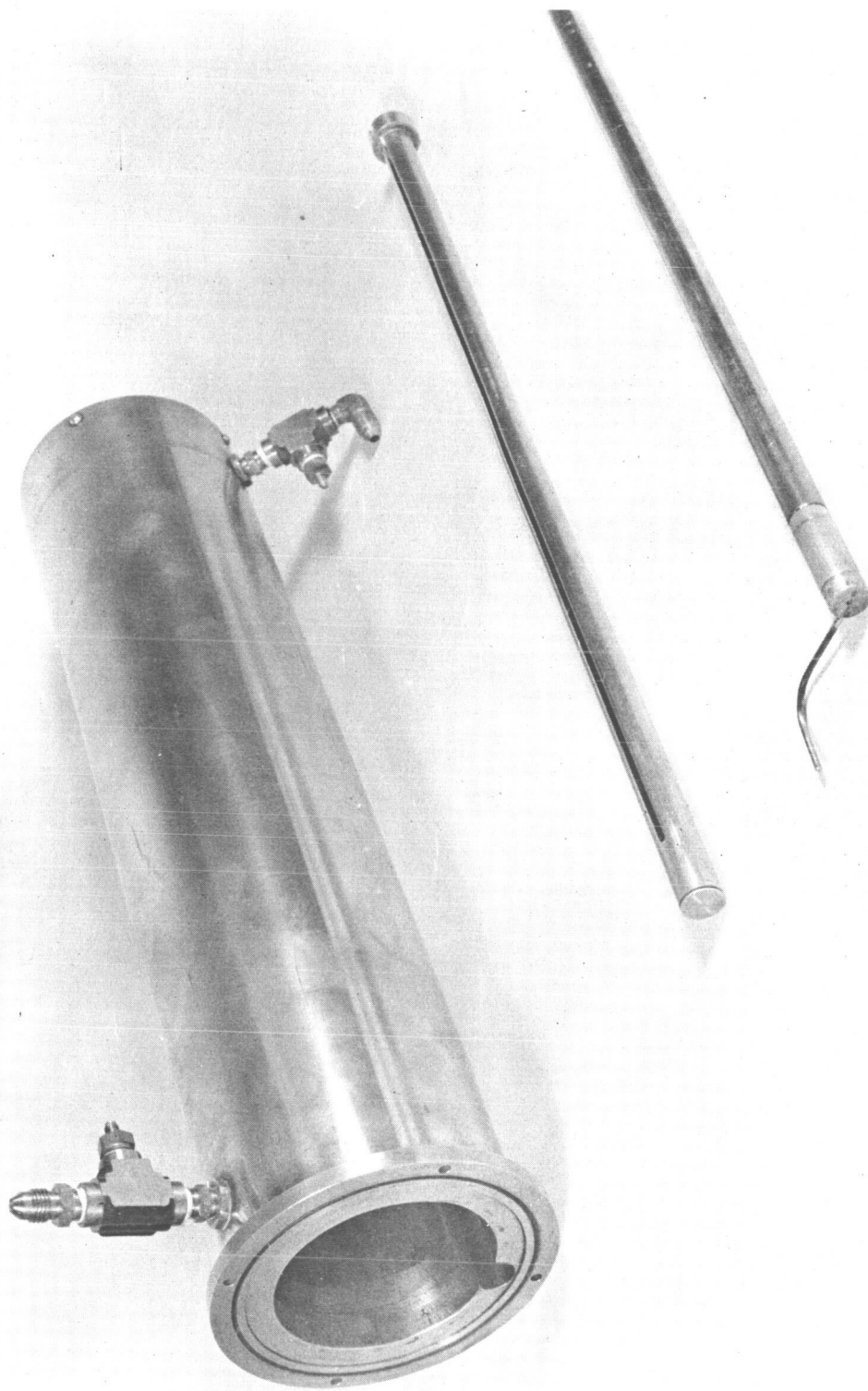
CREATE GENERATOR INSTALLED IN TEST APPARATUS



VIEW OF ROUND VYCOR DUCT USED FOR VISUAL
COAXIAL -FLOW TRANSITION STUDIES

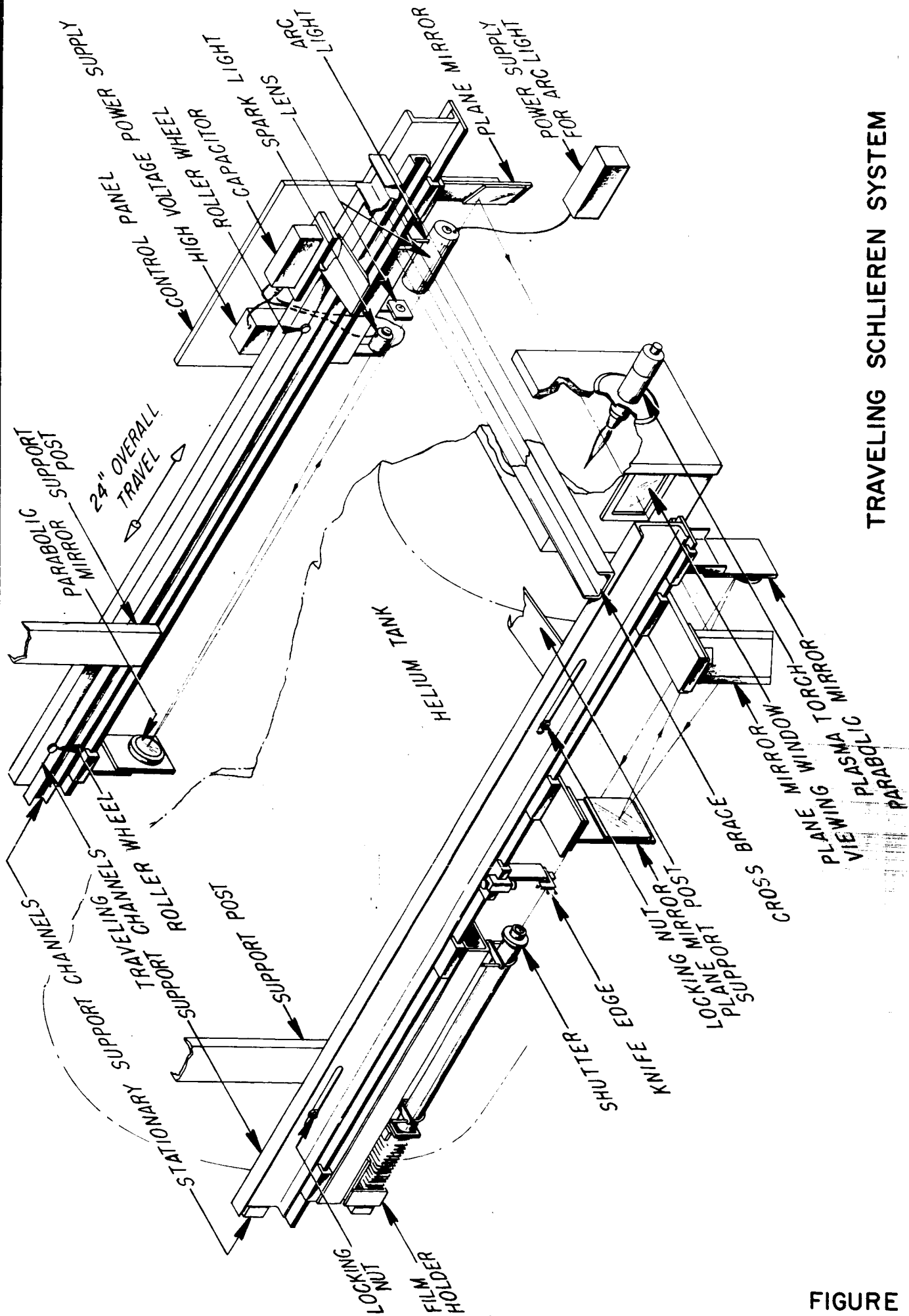


VIEW OF SQUARE DUCT USED FOR COAXIAL-FLOW
TRANSITION STUDIES BY SCHLIEREN PHOTOGRAPHY



VIEW OF CALORIMETRIC DUCT USED FOR DETAILED
COAXIAL - FLOW MIXING AND HEAT TRANSFER MEASUREMENTS

FIGURE 9



TRAVELING SCHLIEREN SYSTEM

FIGURE 10

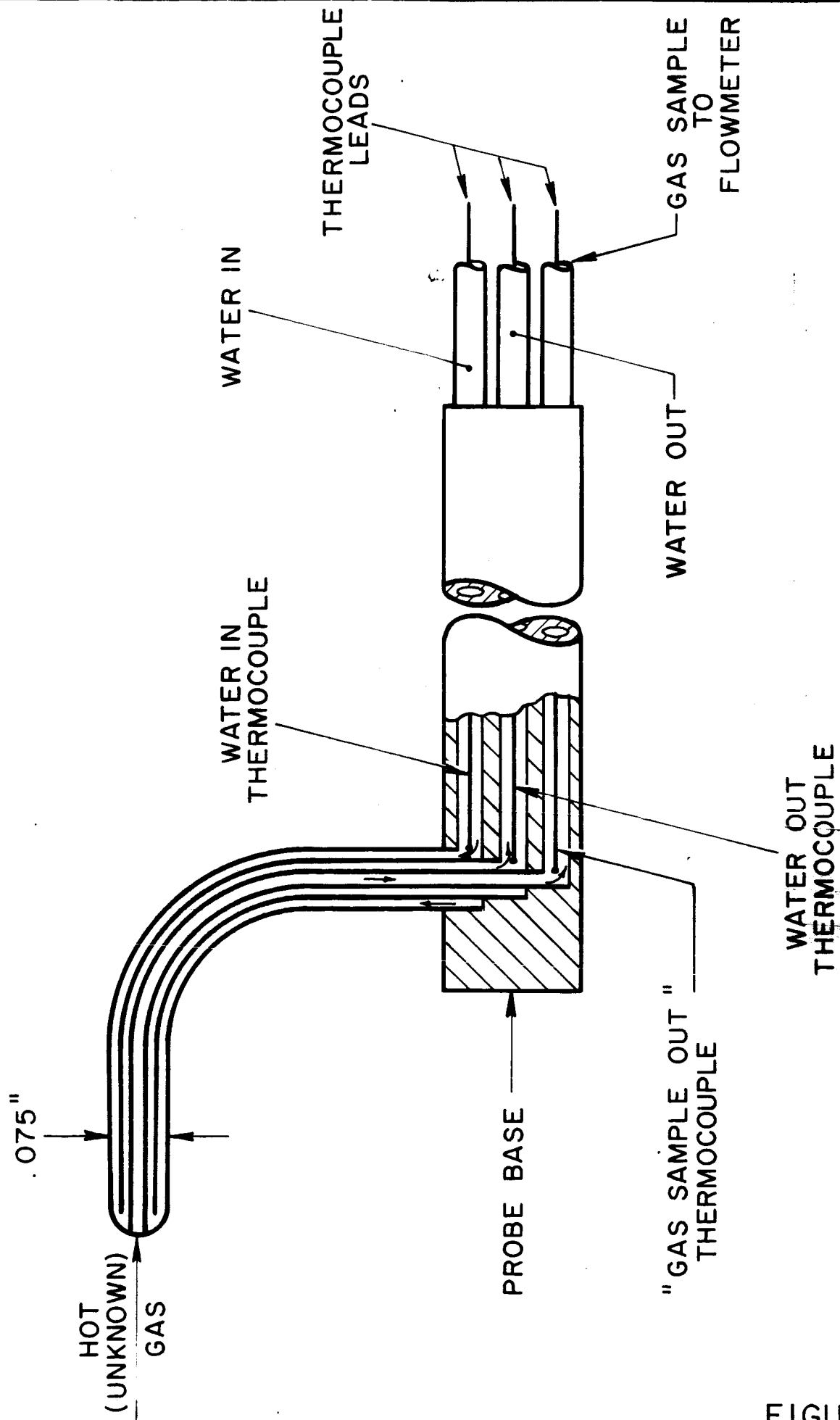
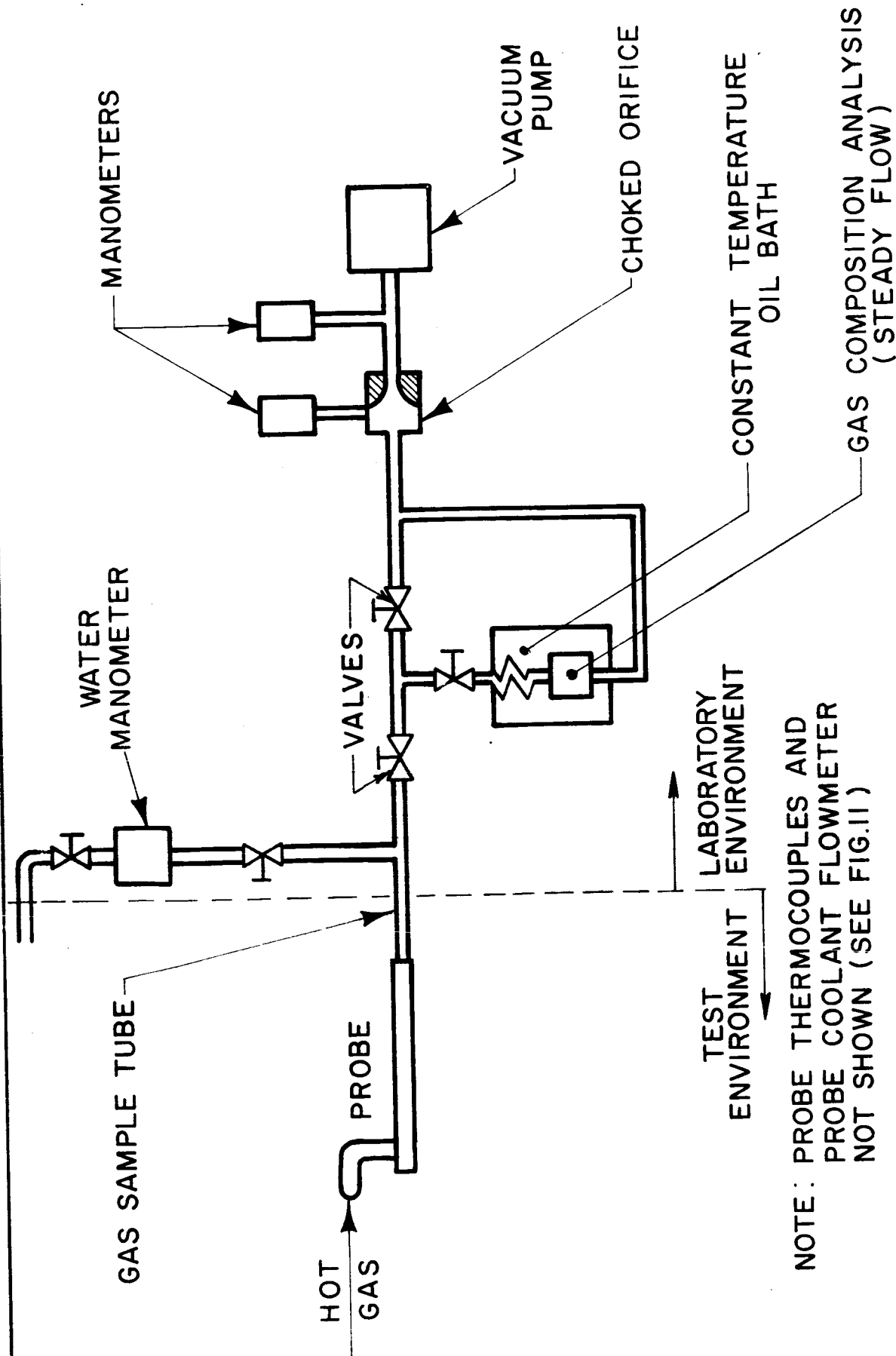


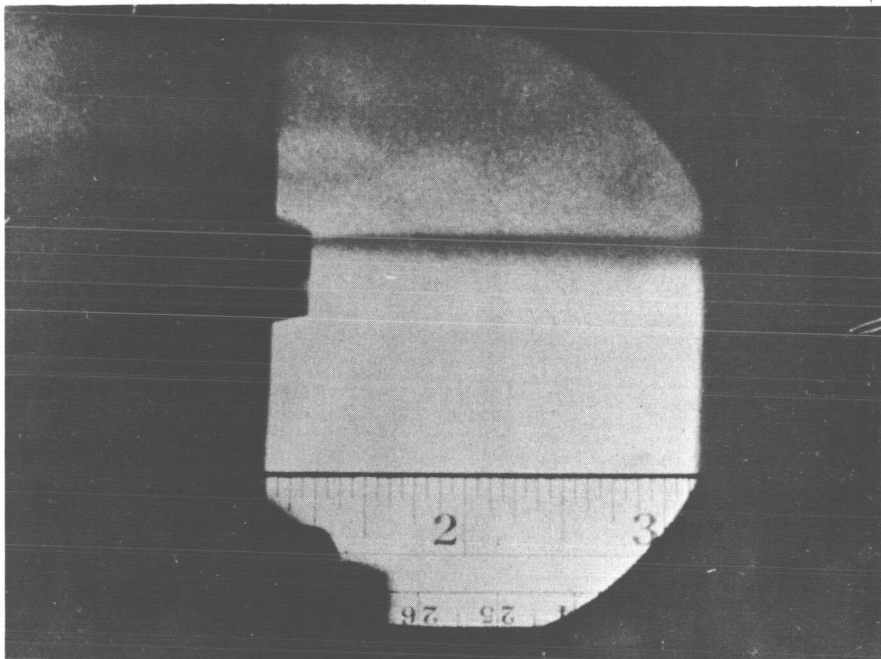
DIAGRAM OF CALORIMETRIC PROBE

FIGURE II

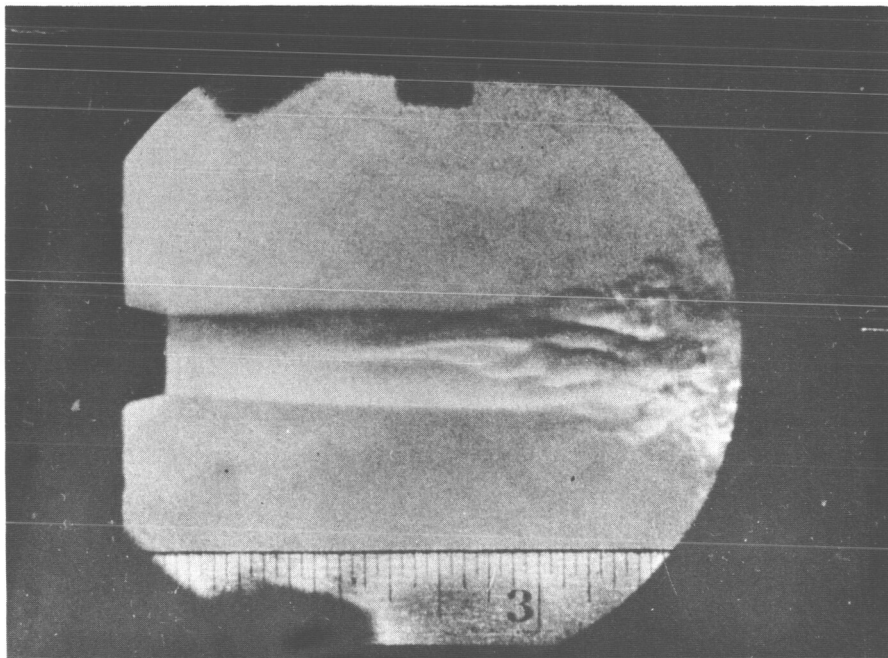


NOTE: PROBE THERMOCOUPLES AND
PROBE COOLANT FLOWMETER
NOT SHOWN (SEE FIG.11)

DIAGRAM OF INSTRUMENTATION USED WITH TARE-MEASUREMENT
CALORIMETRIC PROBE TO MEASURE ENTHALPY, VELOCITY
AND GAS COMPOSITION



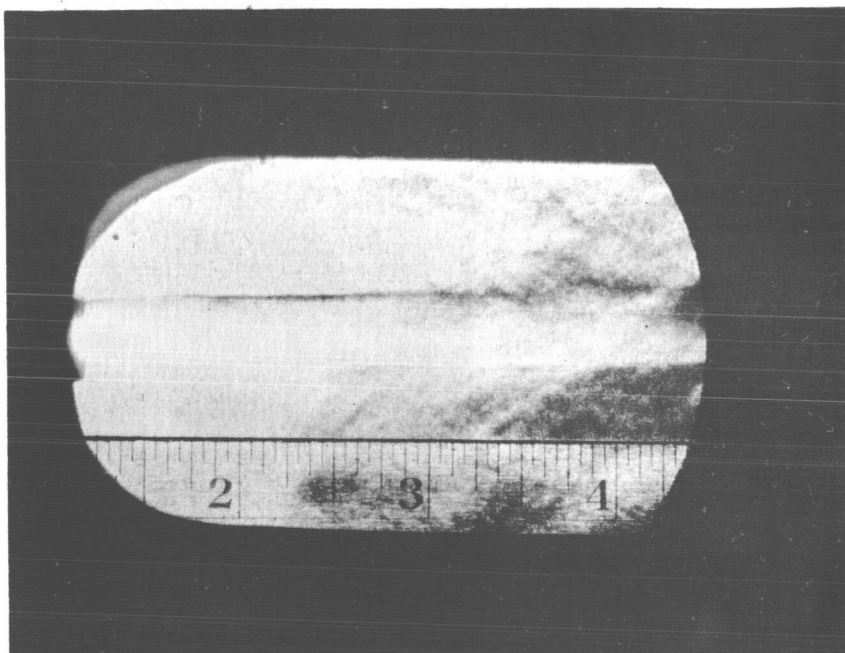
LAMINAR



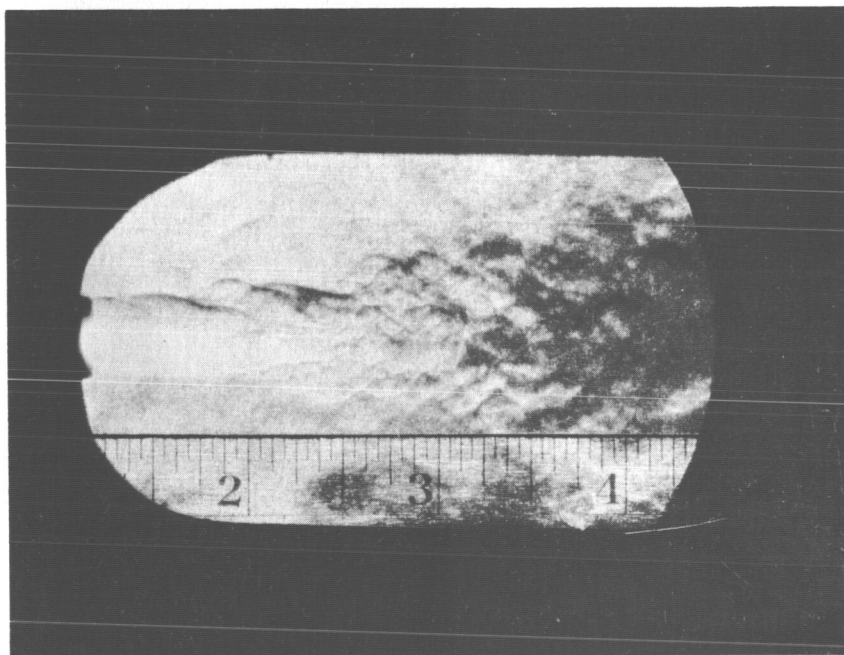
LAMINAR AND TRANSITION

SCHLIEREN PHOTOGRAPHS OF A FREE ARGON
ARCJET IN NITROGEN

FIGURE 13

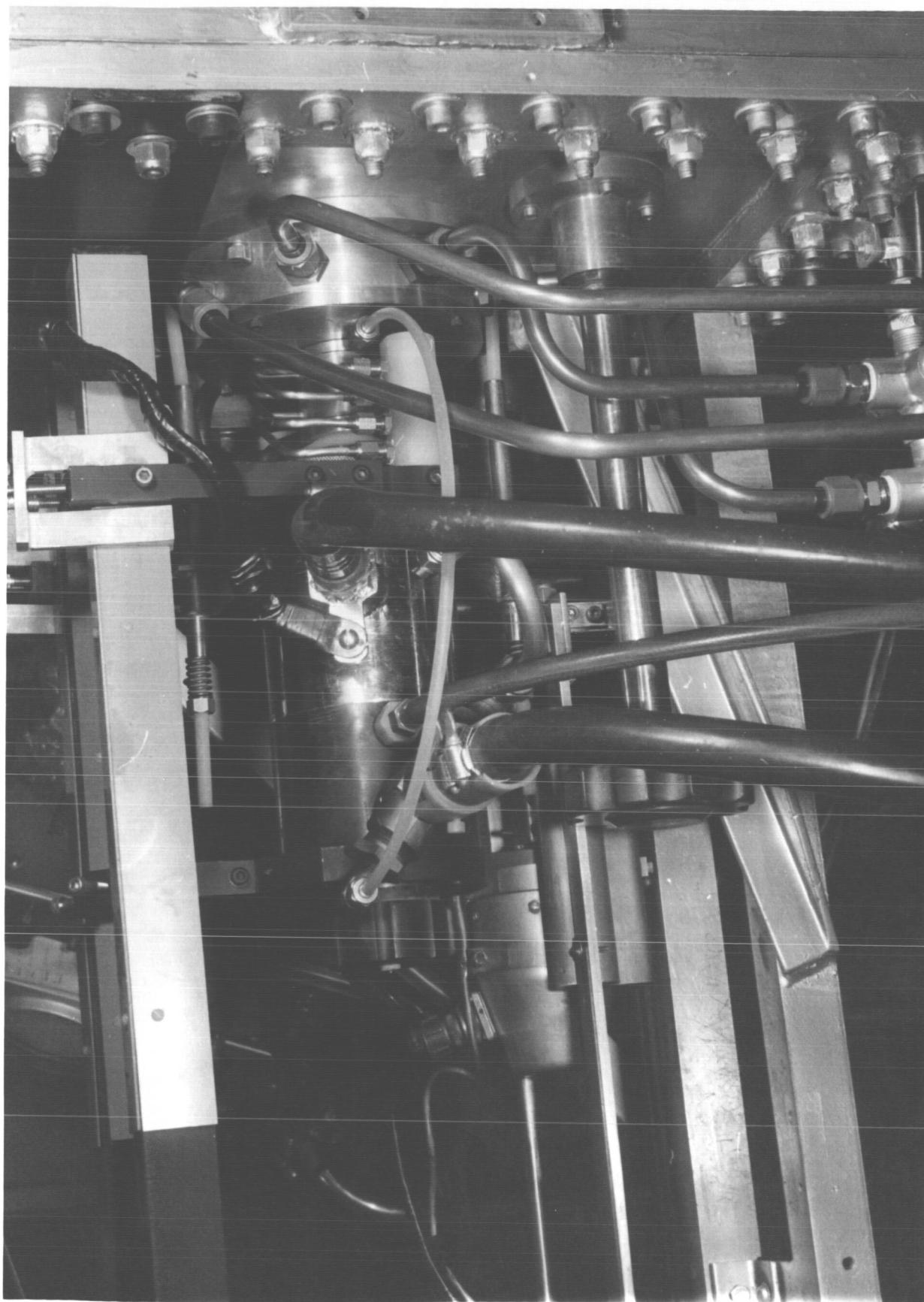


LAMINAR



TURBULENT

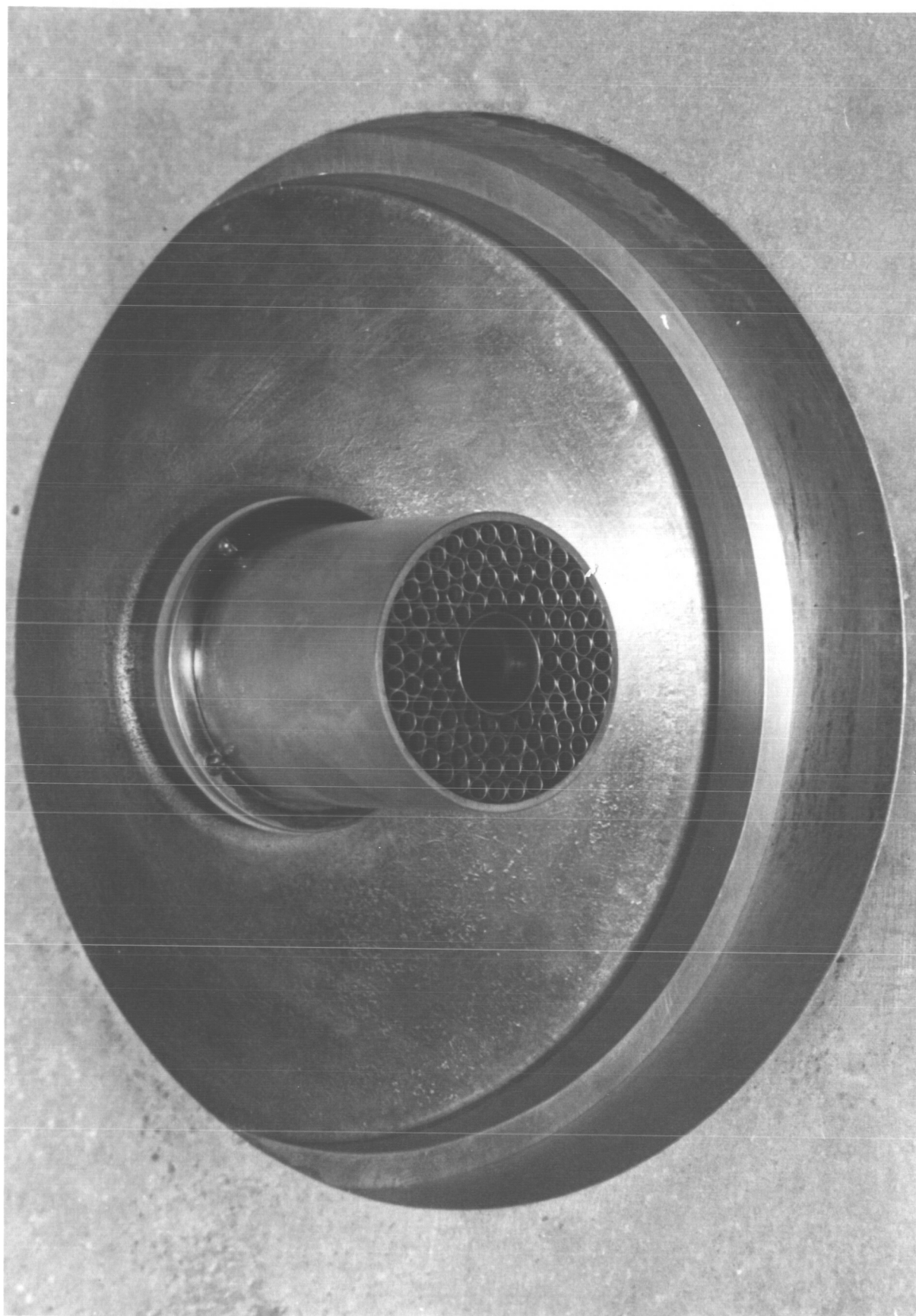
SCHLIEREN PHOTOGRAPHS OF ARGON ARCJET
IN NITROGEN IN 3 INCH SQUARE DUCT
($3/8$ " DIAMETER NOZZLE - 1 ATMOSPHERE)



MODIFIED THERMAL DYNAMICS F-80 ARCJET TORCH
FOR HIGH COAXIAL FLOWS

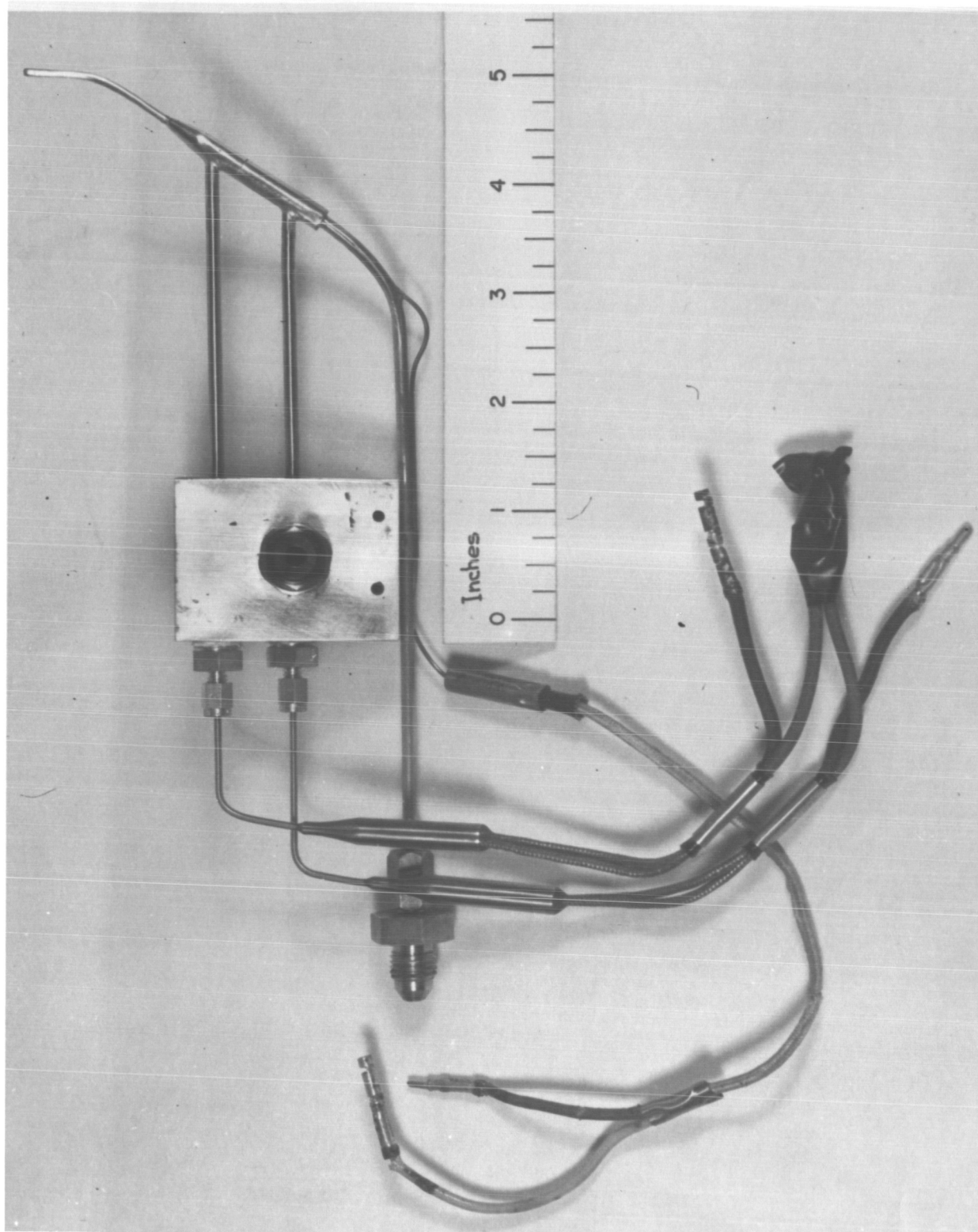


SEGMENTED ANODE OF MODIFIED F-80 ARCJET TORCH

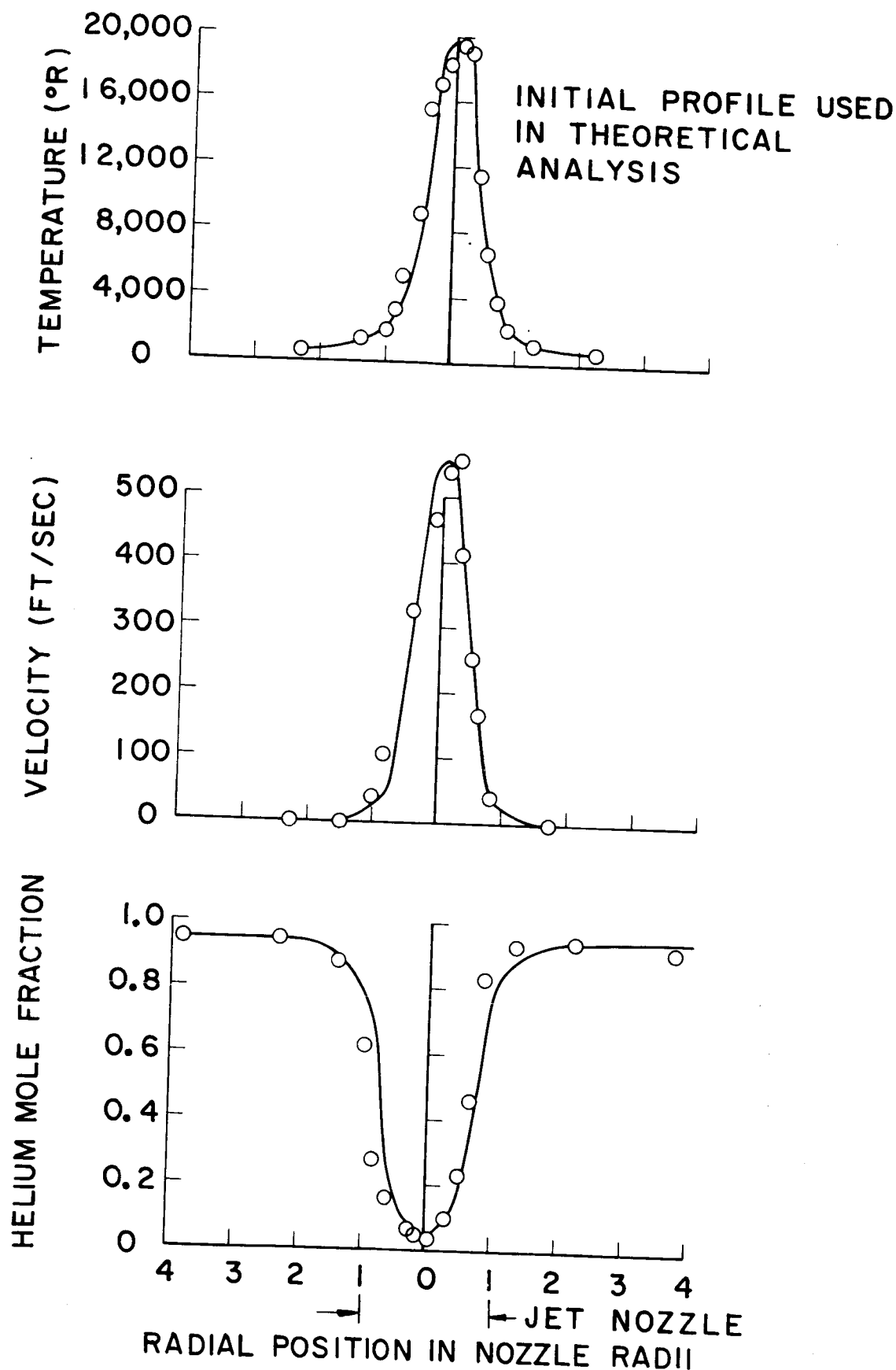


INJECTION PLATE AND NOZZLE FOR MODIFIED F-80 ARCJET TORCH FOR USE
WITH HIGH COAXIAL FLOWS

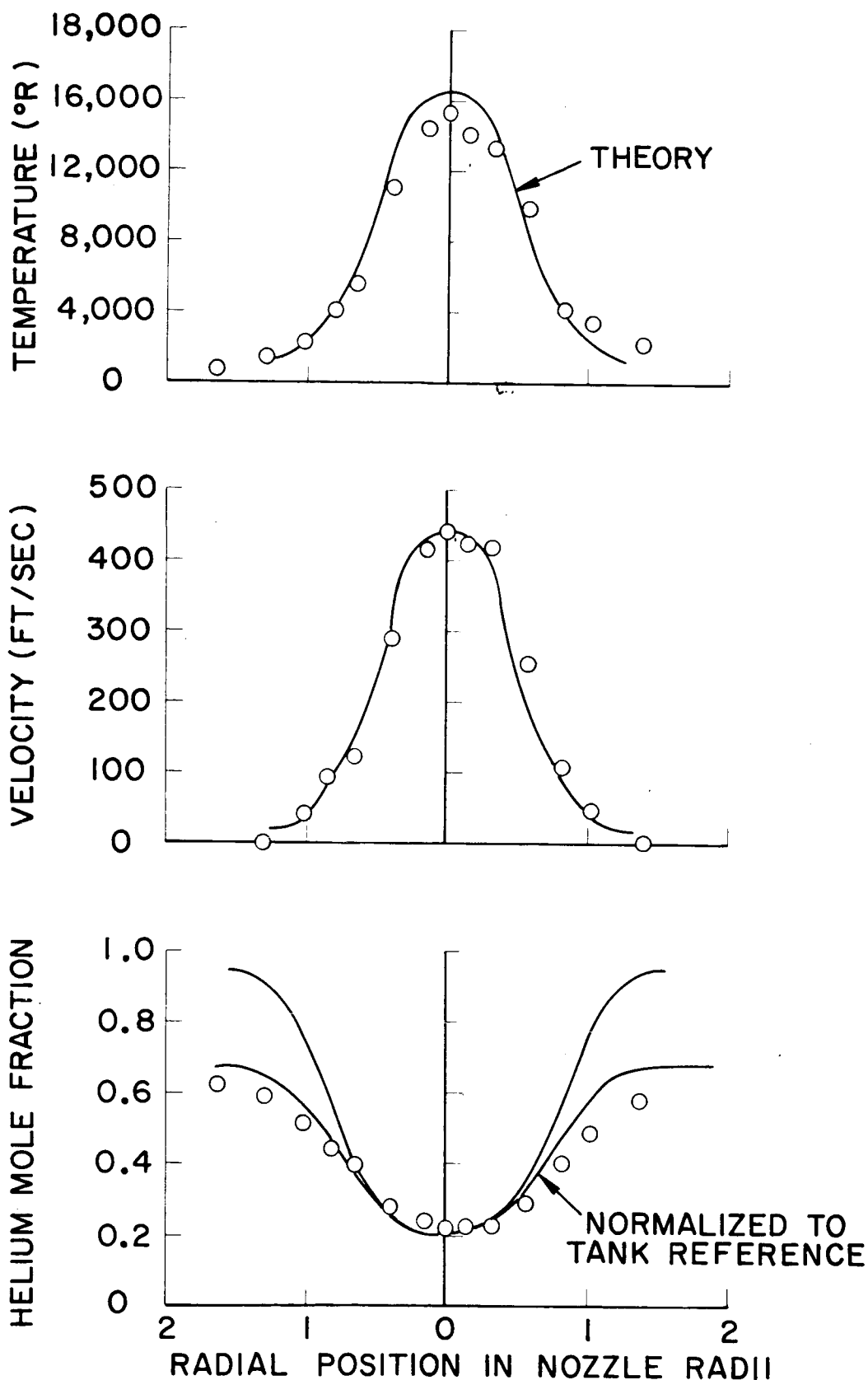
FIGURE 17



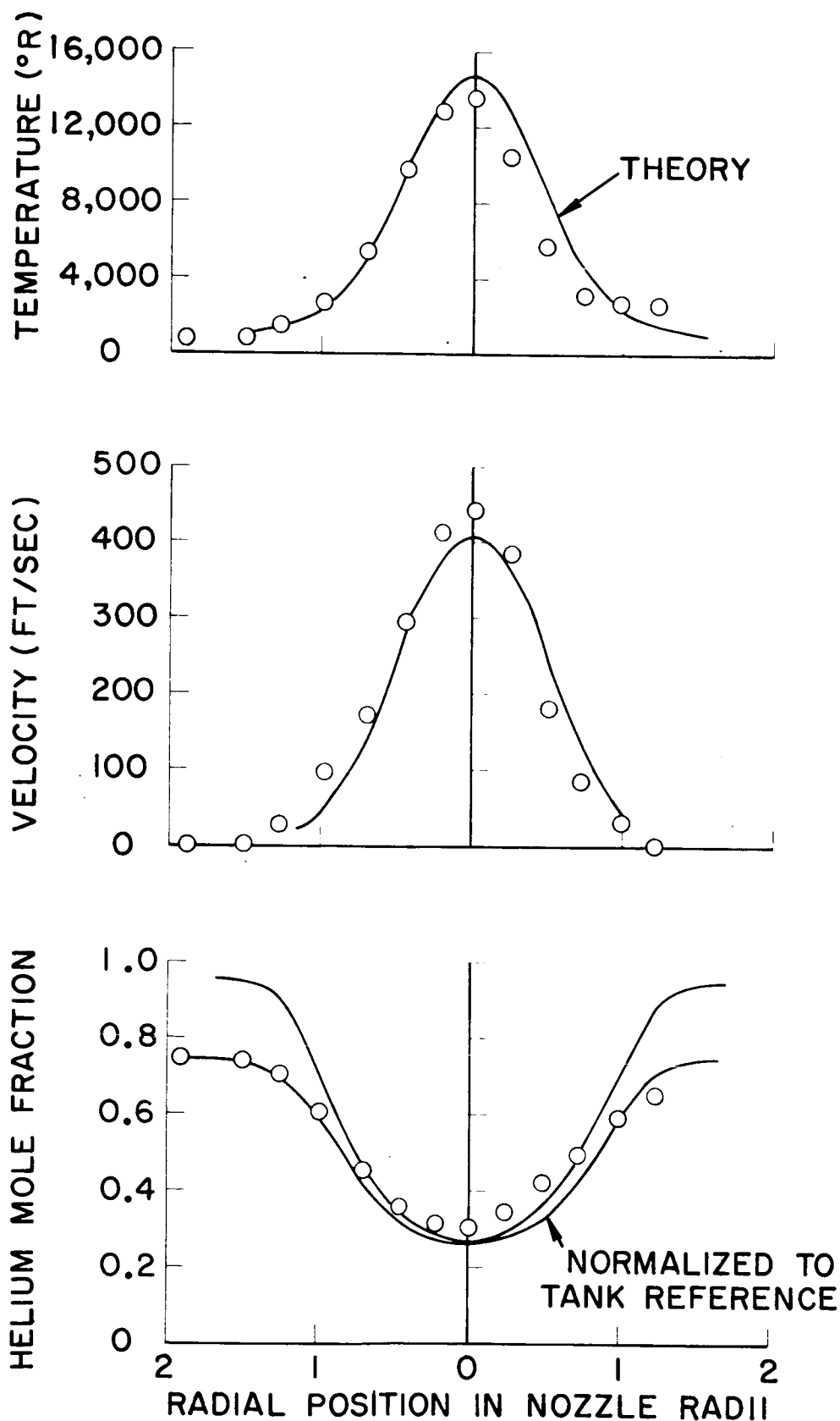
CALORIMETRIC PROBE



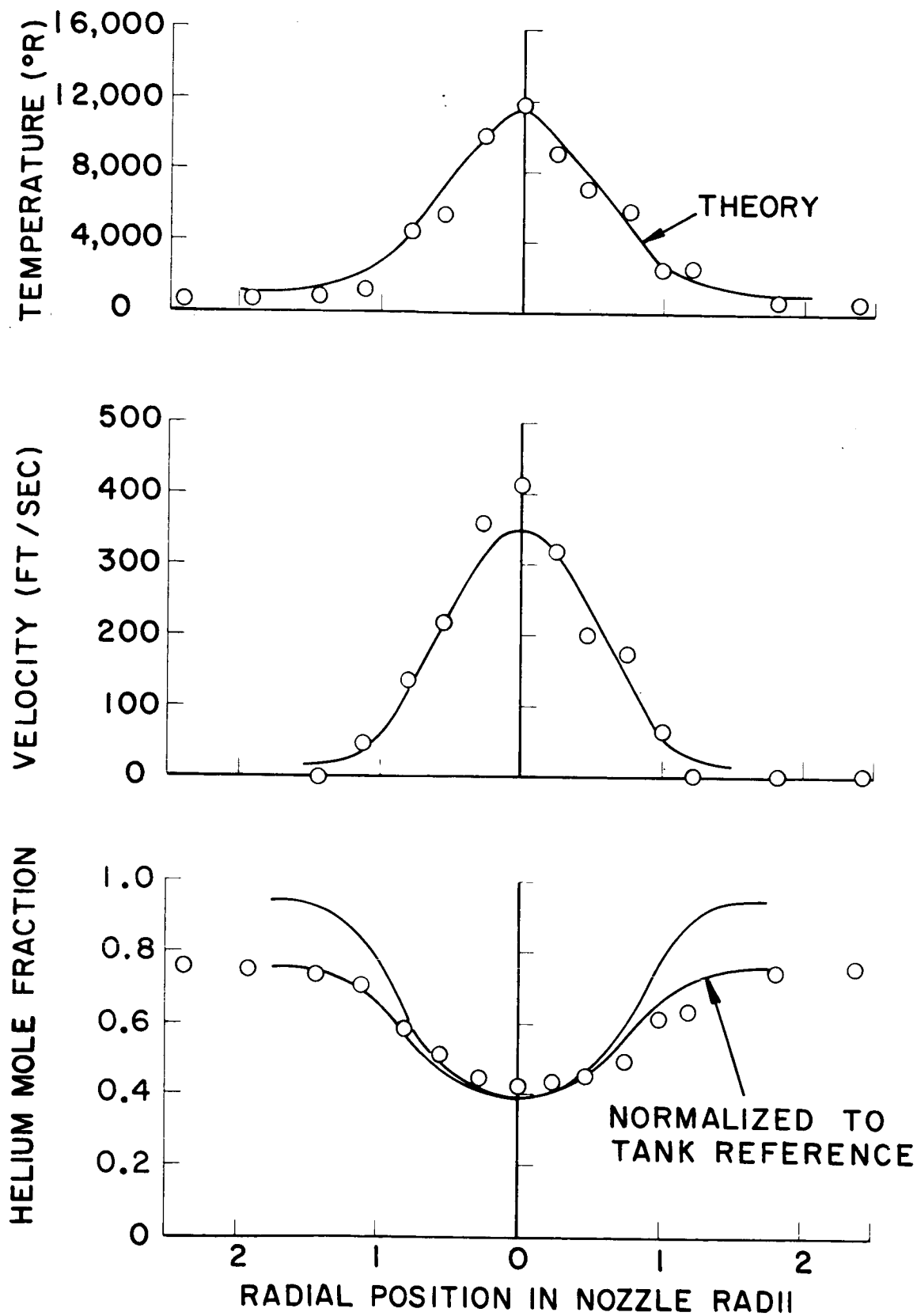
TEMPERATURE, VELOCITY, AND COMPOSITION PROFILES
AT $\frac{1}{32}$ INCH DOWNSTREAM FROM NOZZLE EXIT PLANE



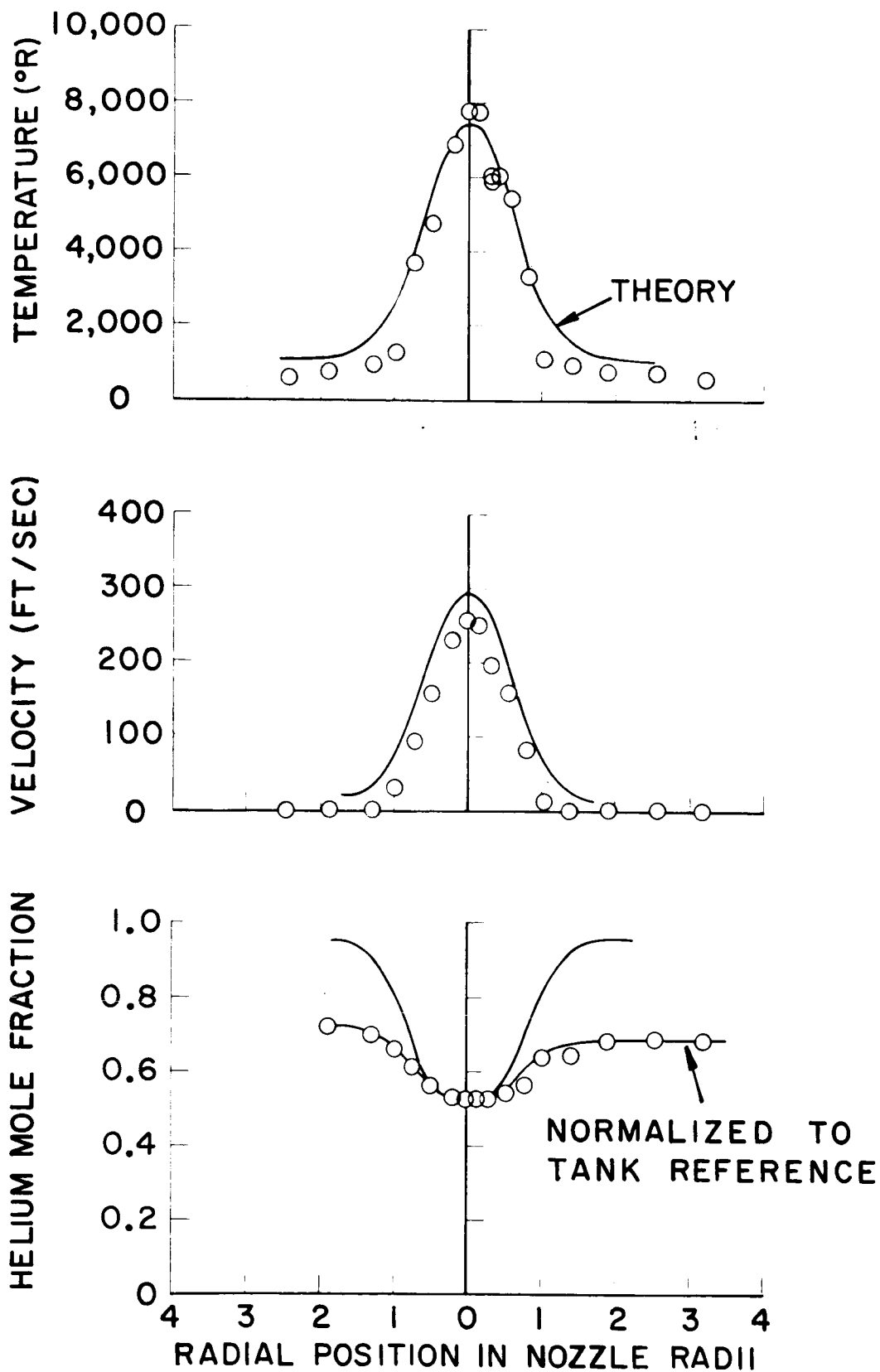
TEMPERATURE, VELOCITY, AND COMPOSITION PROFILES
AT 5/16 INCH DOWNSTREAM FROM NOZZLE EXIT PLANE



TEMPERATURE, VELOCITY, AND COMPOSITION PROFILES
AT 1/2 INCH DOWNSTREAM FROM NOZZLE EXIT PLANE

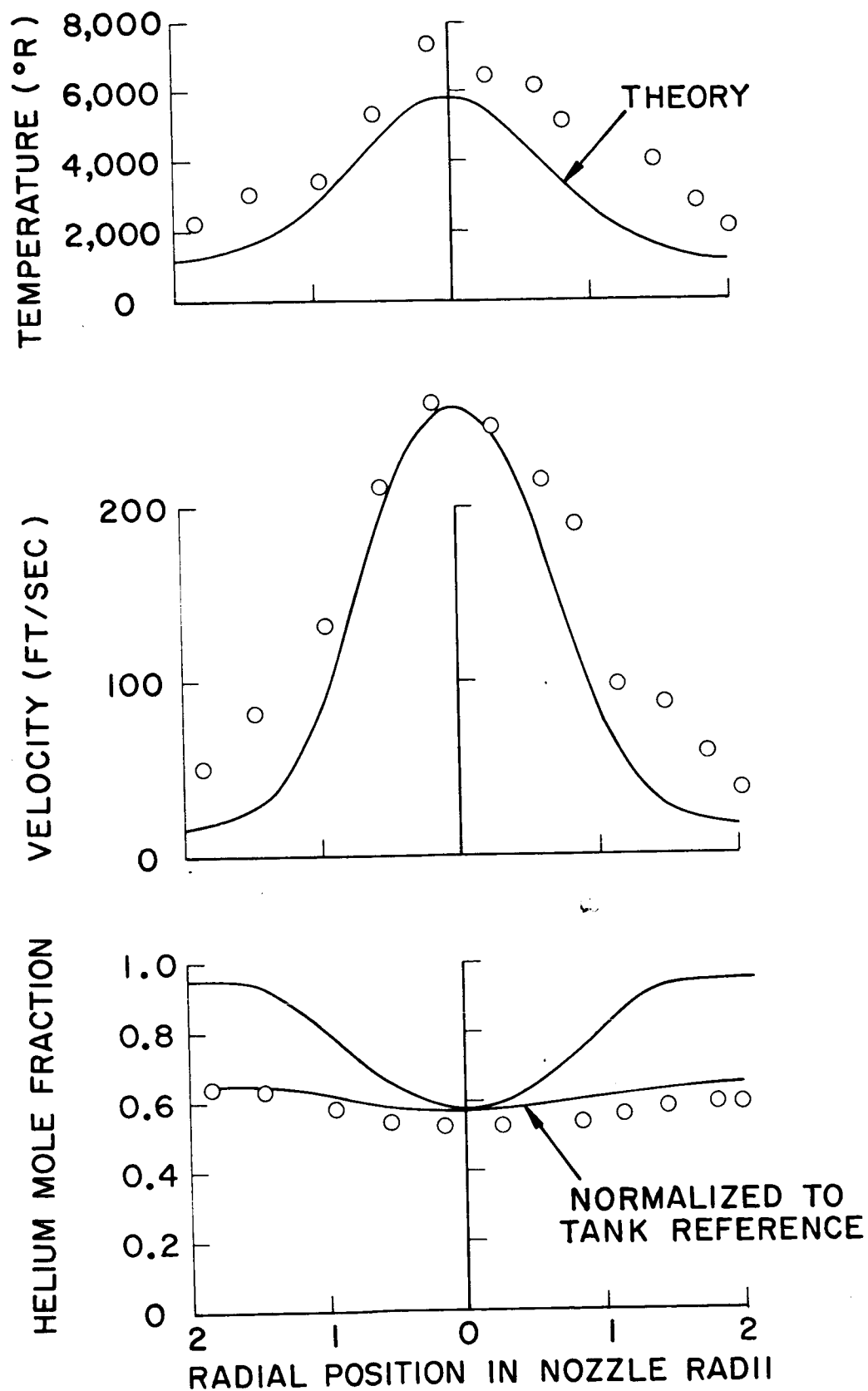


TEMPERATURE, VELOCITY, AND COMPOSITION PROFILES
AT 1 INCH DOWNSTREAM FROM NOZZLE EXIT PLANE

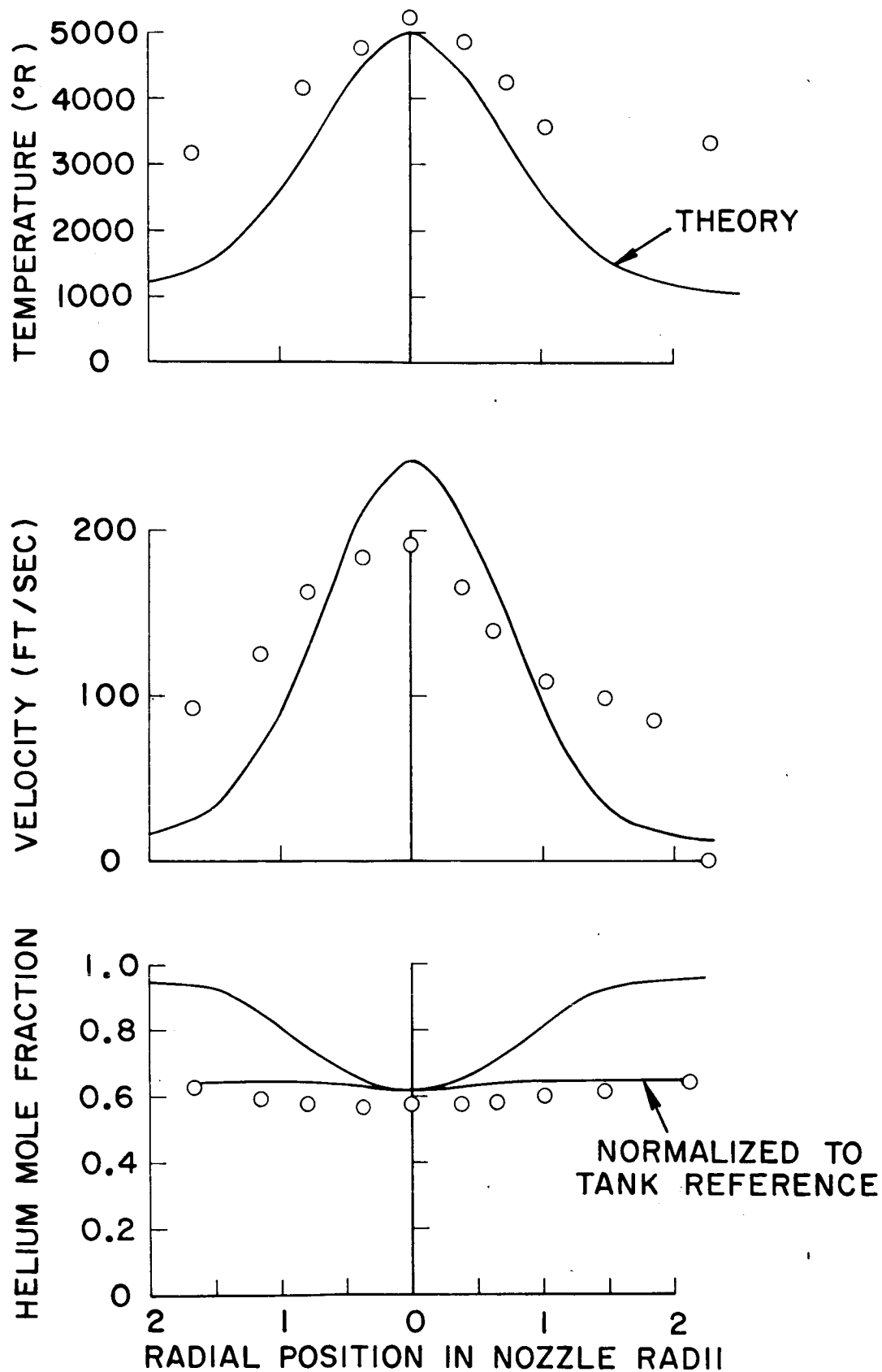


TEMPERATURE, VELOCITY, AND COMPOSITION PROFILES
AT 2 INCHES DOWNSTREAM FROM NOZZLE EXIT PLANE

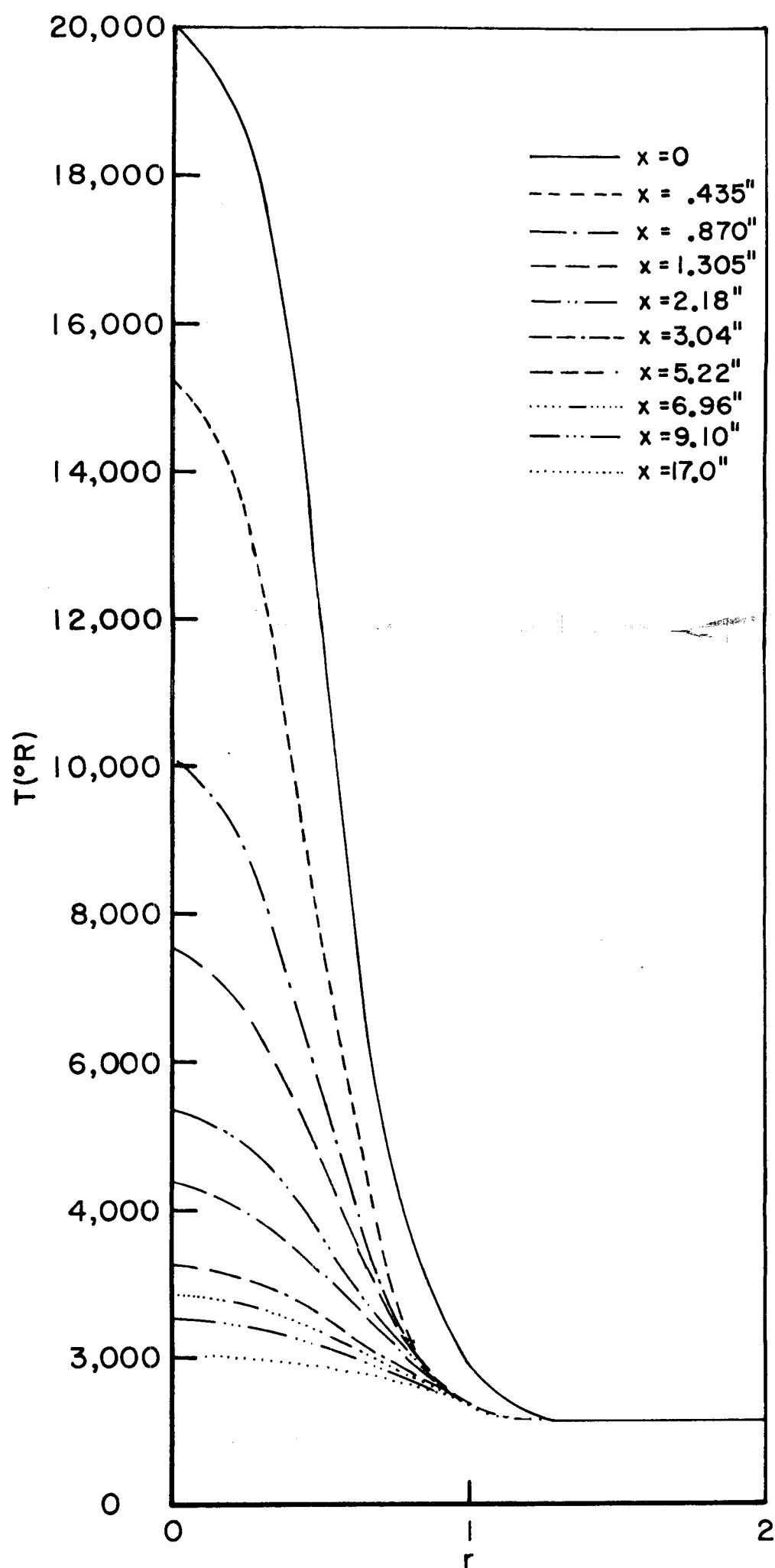
FIGURE 23



TEMPERATURE, VELOCITY, AND COMPOSITION PROFILES
AT 3 INCHES DOWNSTREAM FROM NOZZLE EXIT PLANE

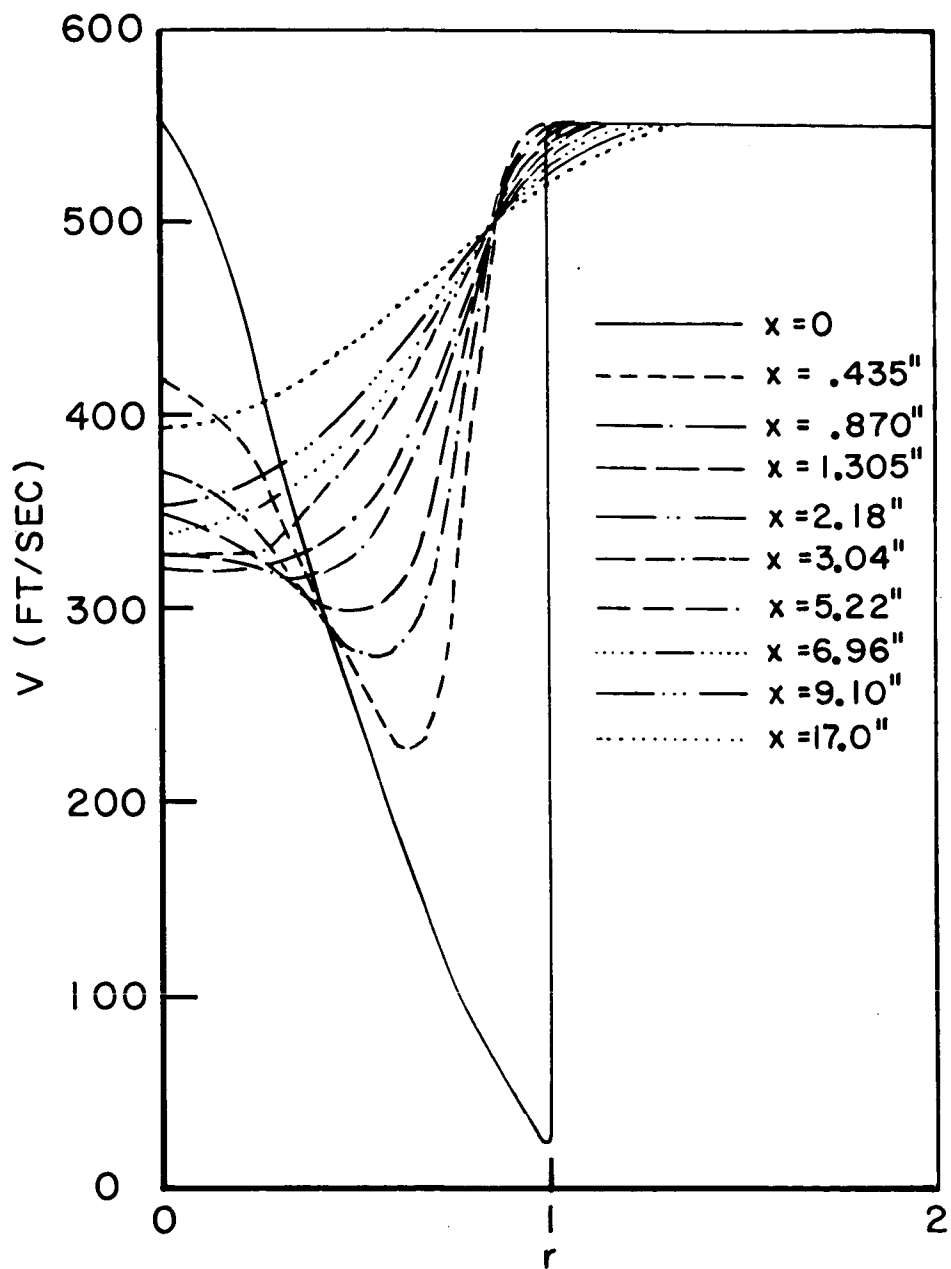


TEMPERATURE, VELOCITY, AND COMPOSITION PROFILES
AT 4 INCHES DOWNSTREAM FROM NOZZLE EXIT PLANE

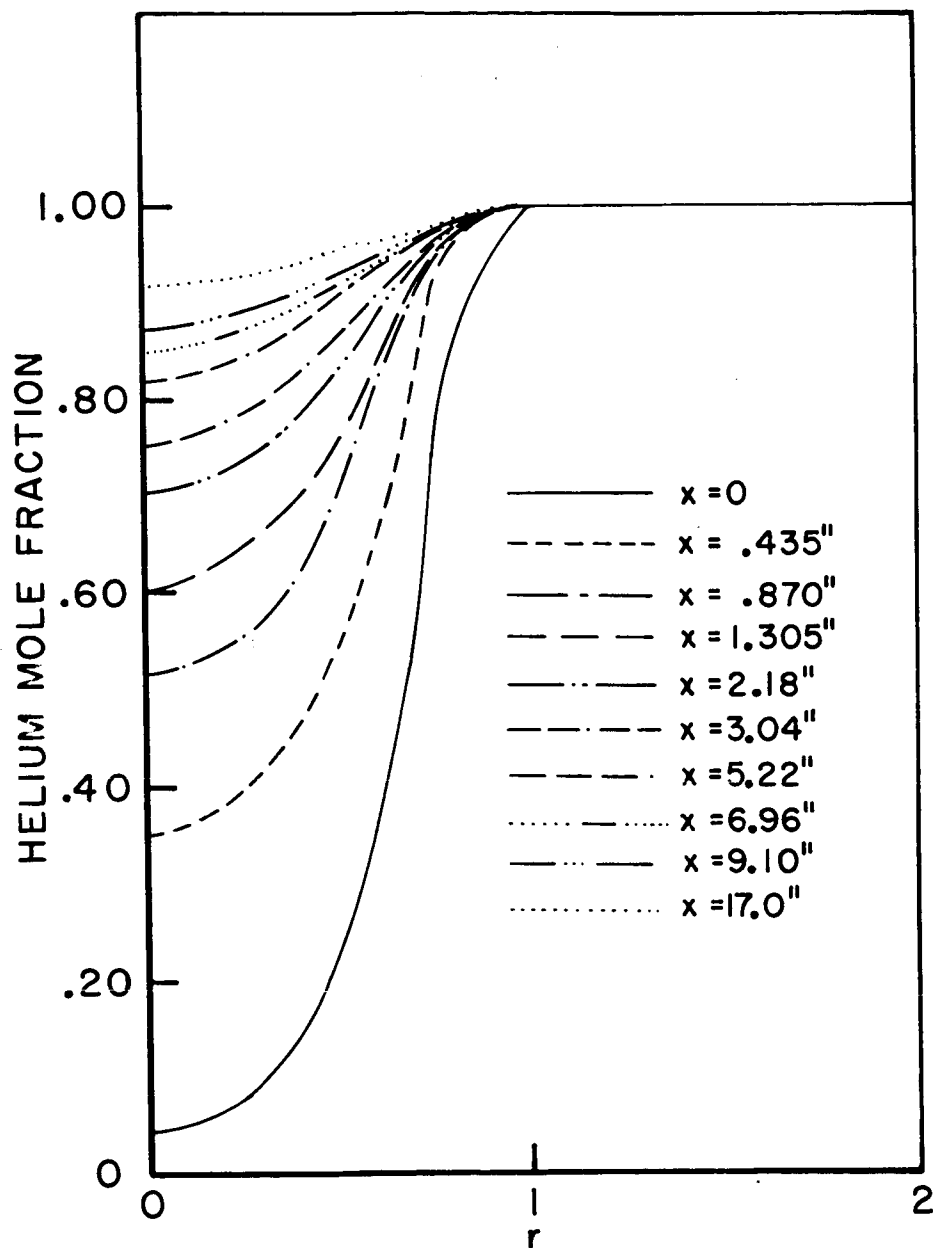


THEORETICAL TEMPERATURE FIELD FOR
COAXIAL NITROGEN VELOCITY = 550 FT/SEC

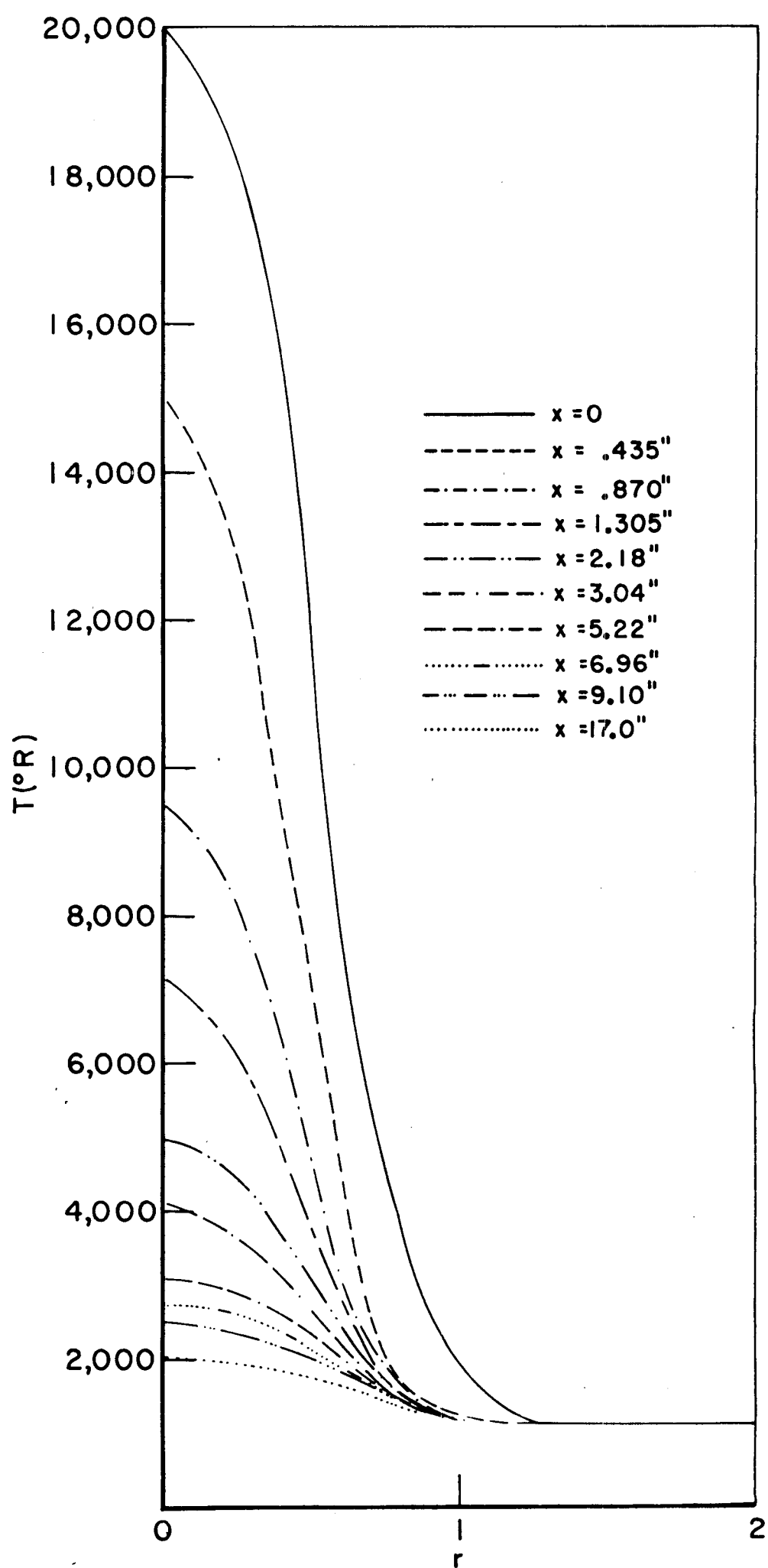
FIGURE 26



THEORETICAL VELOCITY FIELD FOR
COAXIAL HELIUM VELOCITY = 550 FT/SEC

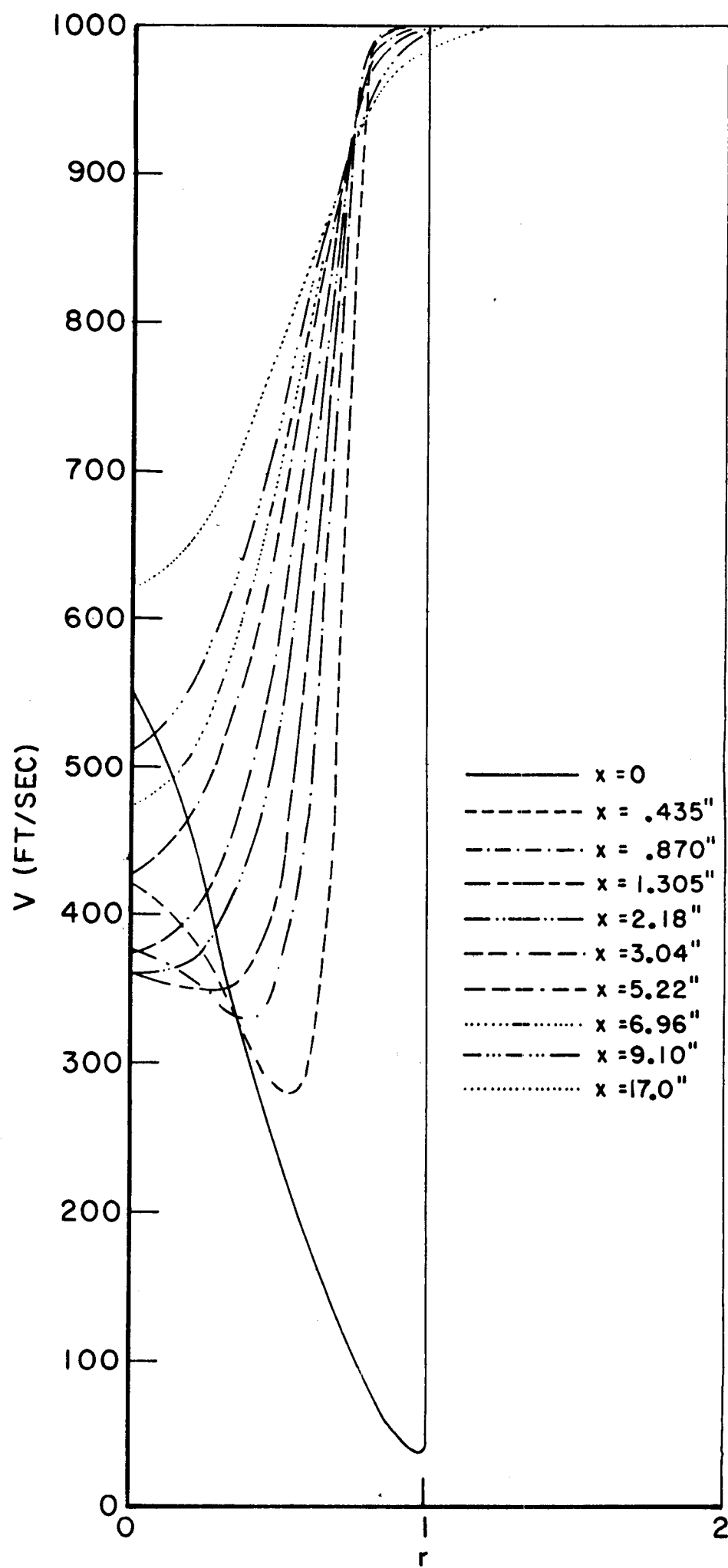


THEORETICAL COMPOSITION FIELD FOR
COAXIAL HELIUM VELOCITY = 550 FT/SEC



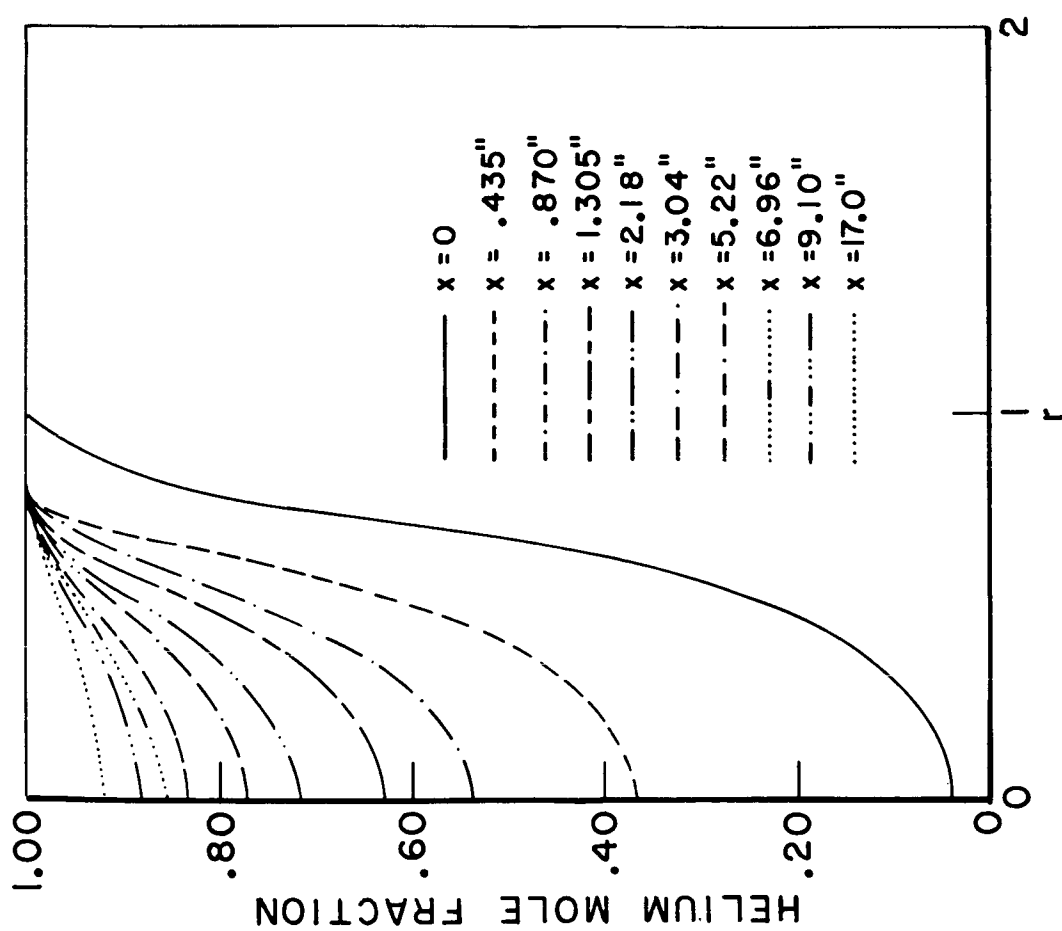
THEORETICAL TEMPERATURE FIELD FOR
COAXIAL HELIUM VELOCITY = 1000 FT/SEC

FIGURE 29

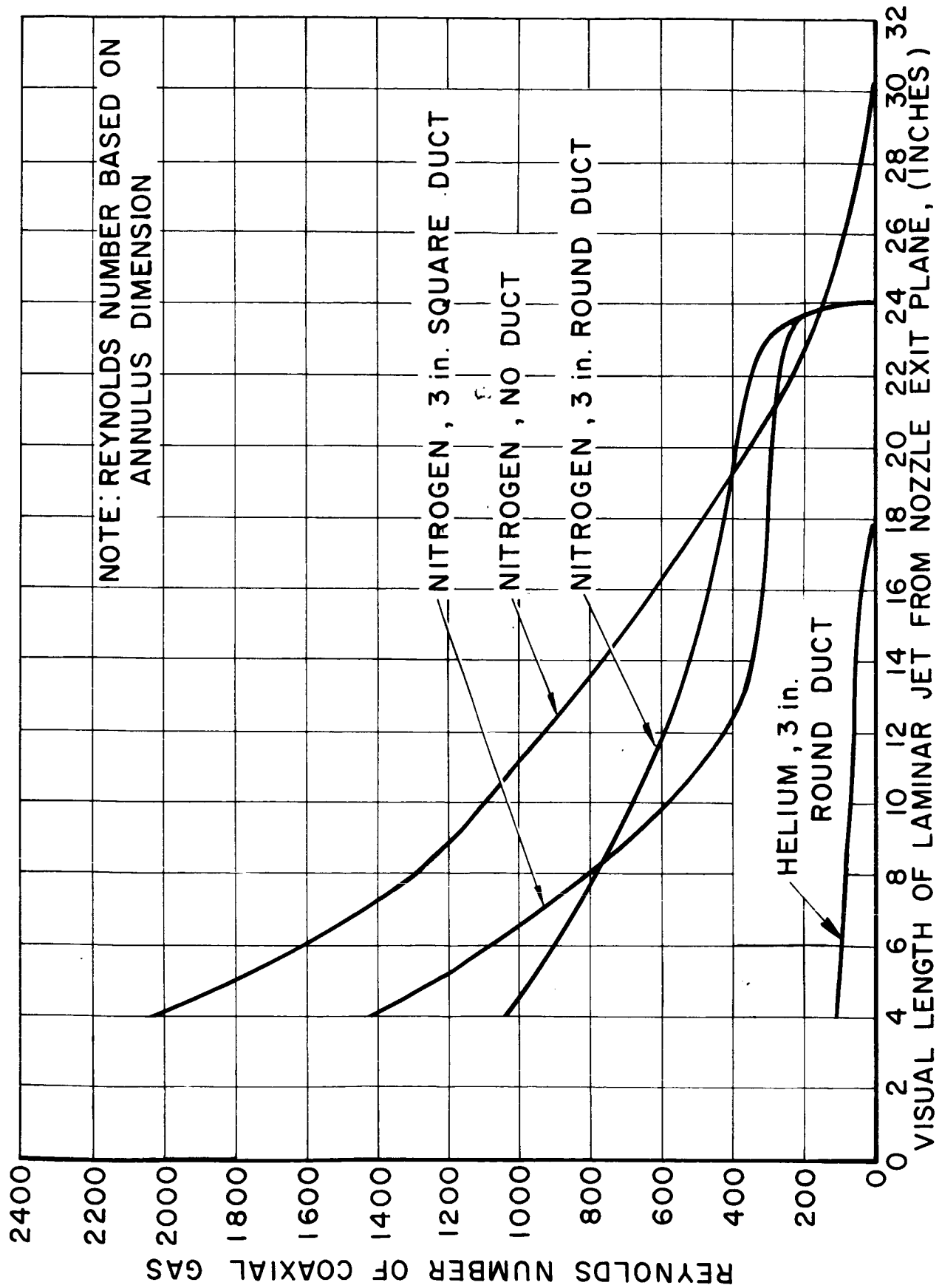


THEORETICAL VELOCITY FIELD FOR
COAXIAL HELIUM VELOCITY = 1000 FT/SEC

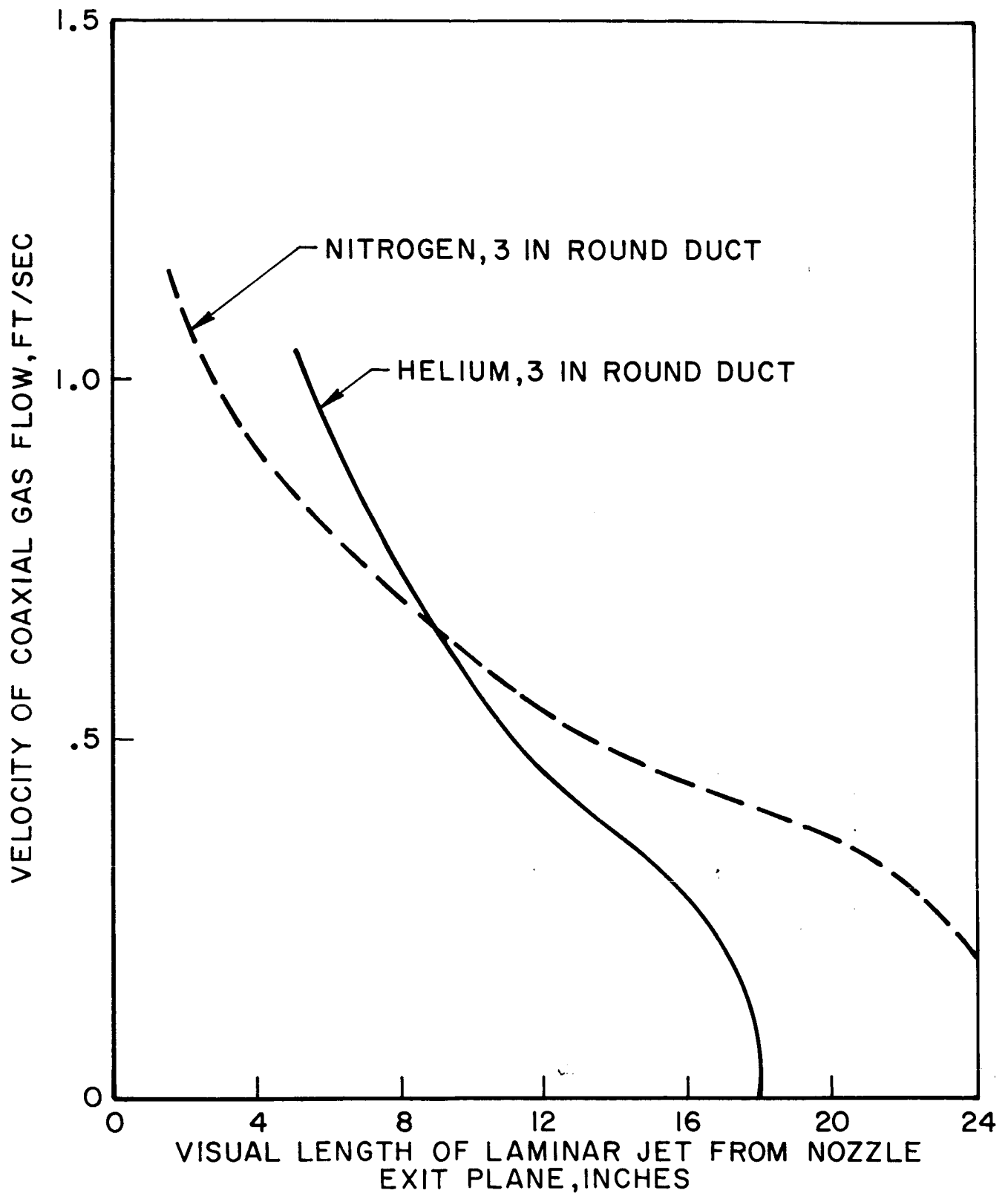
FIGURE 30



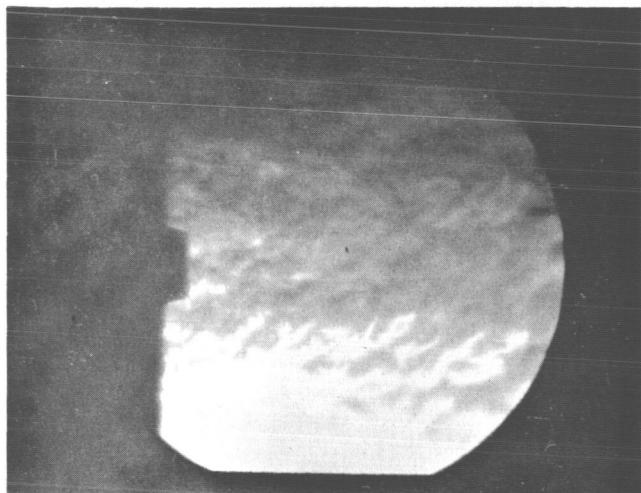
THEORETICAL COMPOSITION FIELD FOR
COAXIAL HELIUM VELOCITY = 1000 FT/SEC



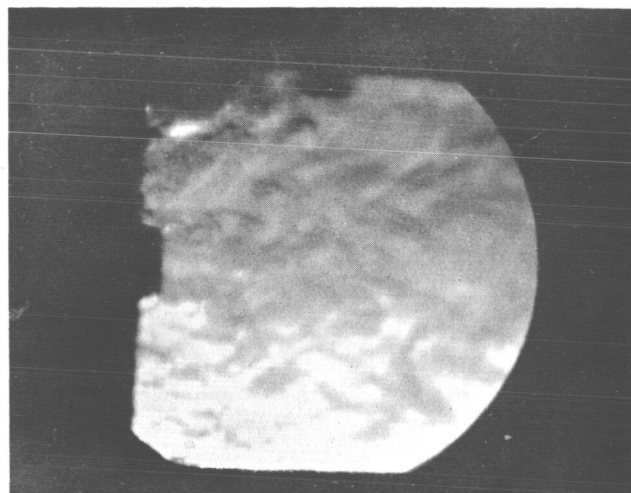
VISUAL LENGTH OF LAMINAR ARCJET VERSUS COAXIAL-FLOW REYNOLDS NUMBER



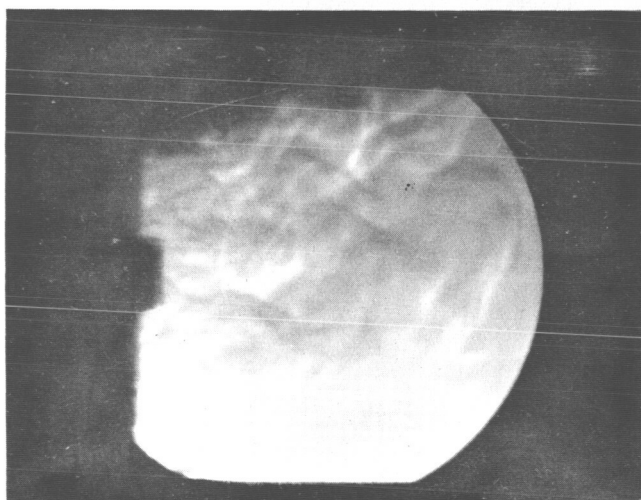
VISUAL LENGTH OF LAMINAR ARCJET
VERSUS COAXIAL-FLOW VELOCITY



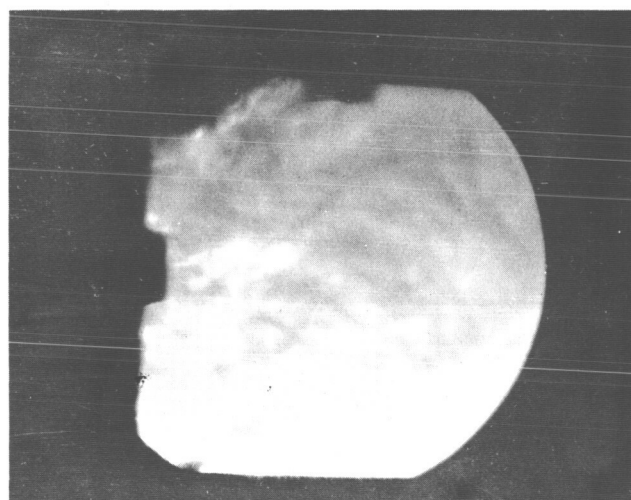
NO INJECTION PLATES



COARSE PERFORATED PLATE



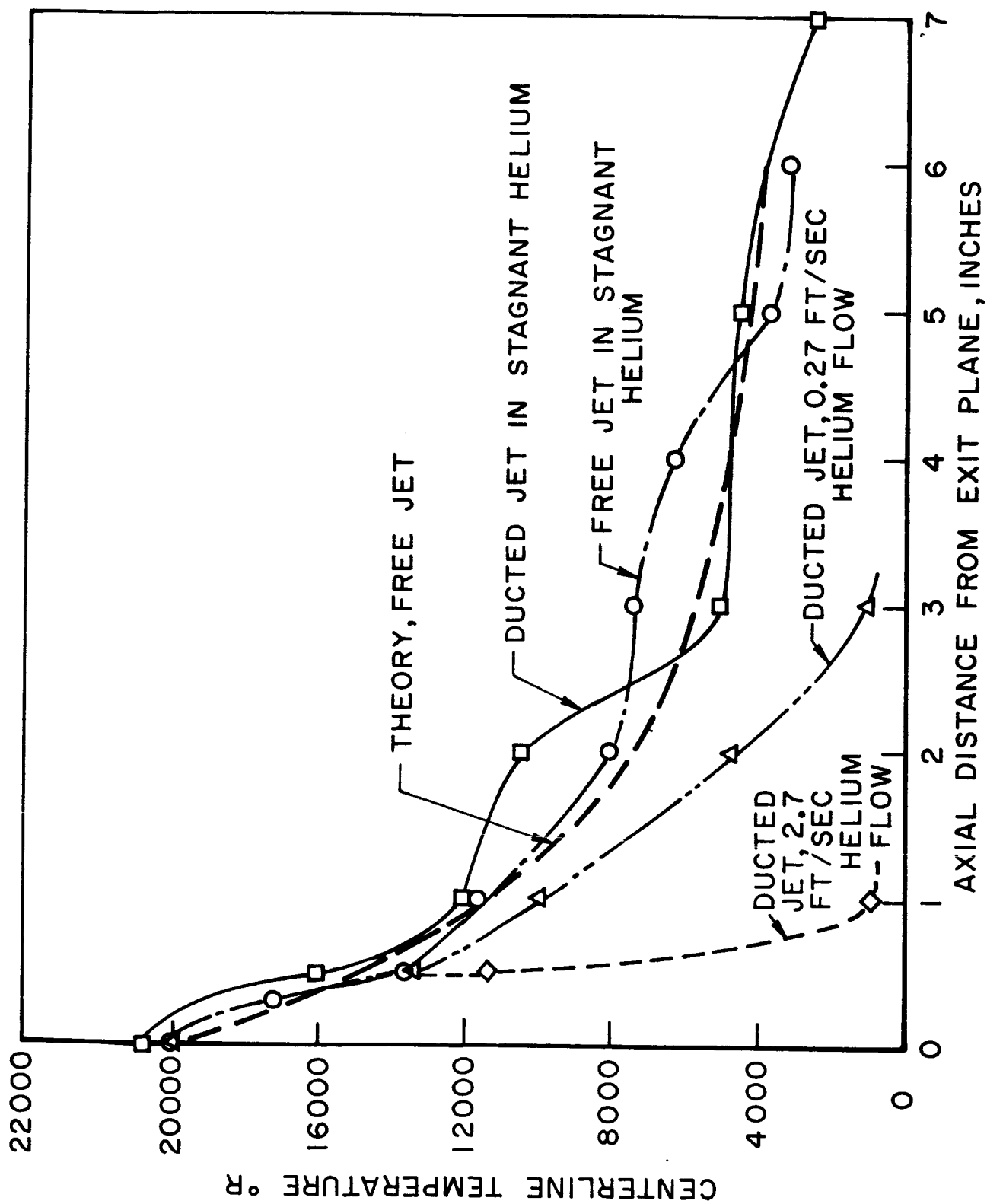
**COARSE AND MEDIUM
PERFORATED PLATES**



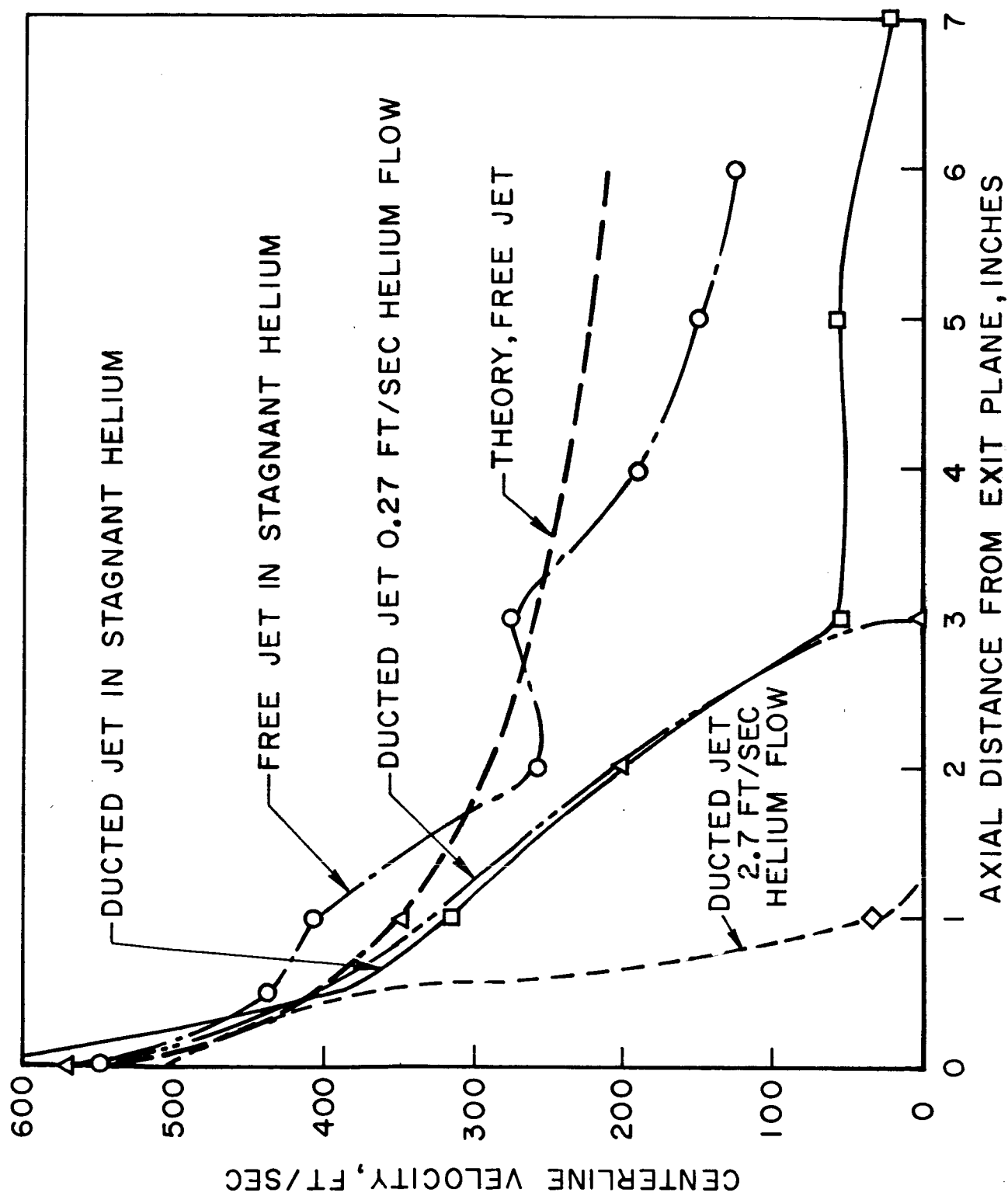
**COARSE AND MEDIUM
PERFORATED PLATES
AND 100 MESH SCREEN**

**SCHLIEREN PHOTOGRAPHS SHOWING SCALE OF TURBULANCE
IN COAXIAL HELIUM FLOW
(HELIUM VELOCITY 0.6 FT/SEC)**

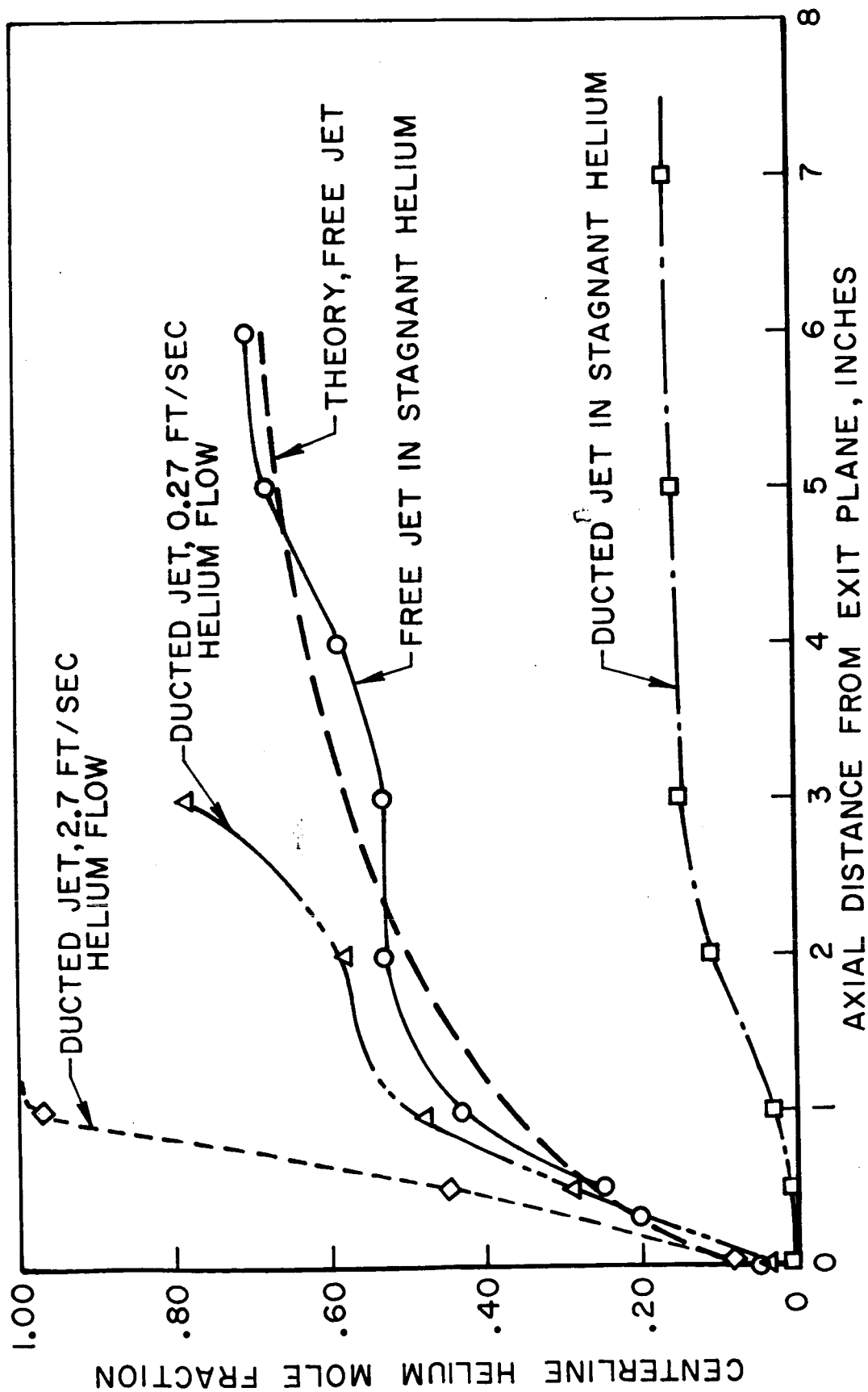
FIGURE 34



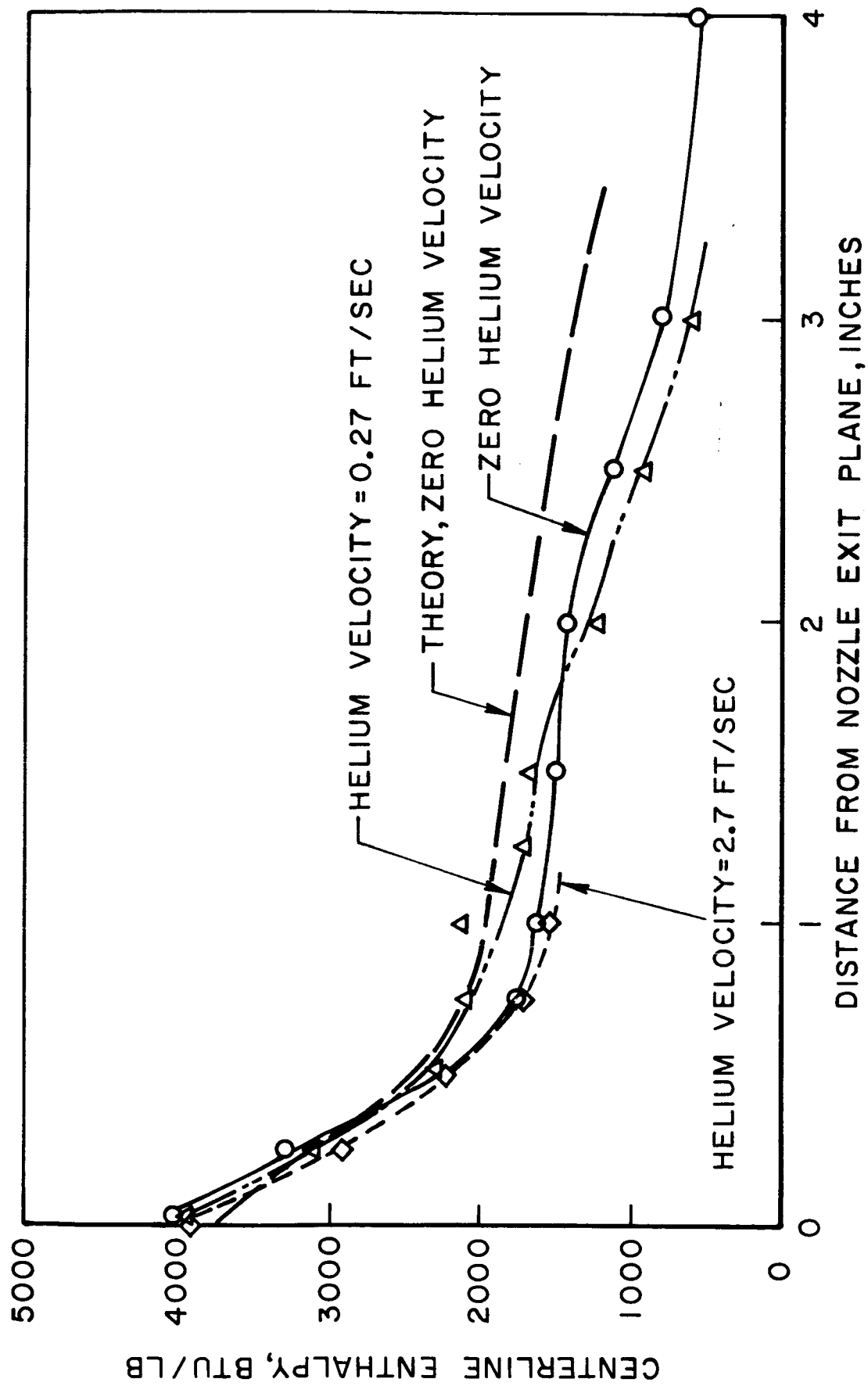
CENTERLINE TEMPERATURES VERSUS AXIAL POSITION



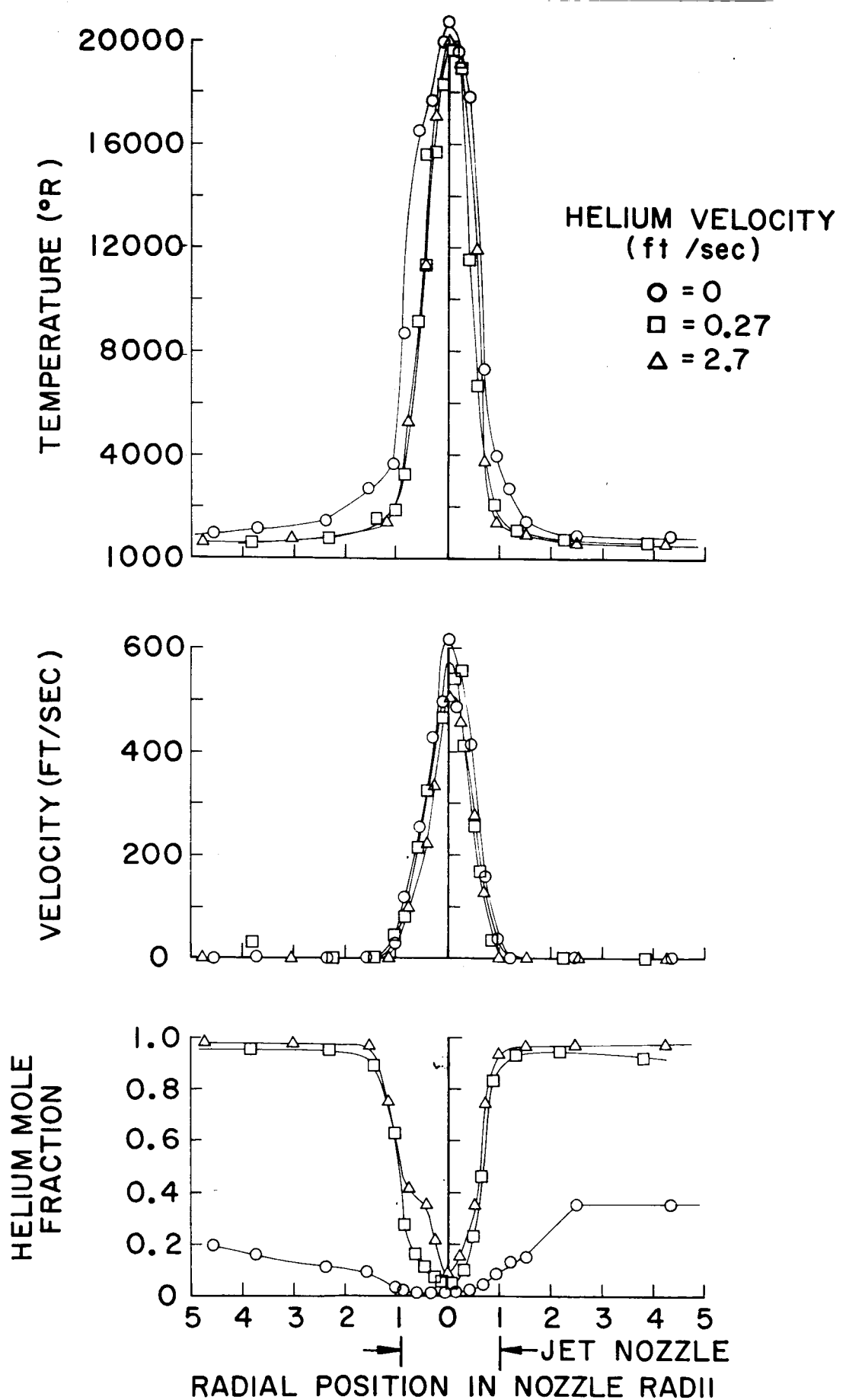
CENTERLINE VELOCITIES VERSUS AXIAL POSITION



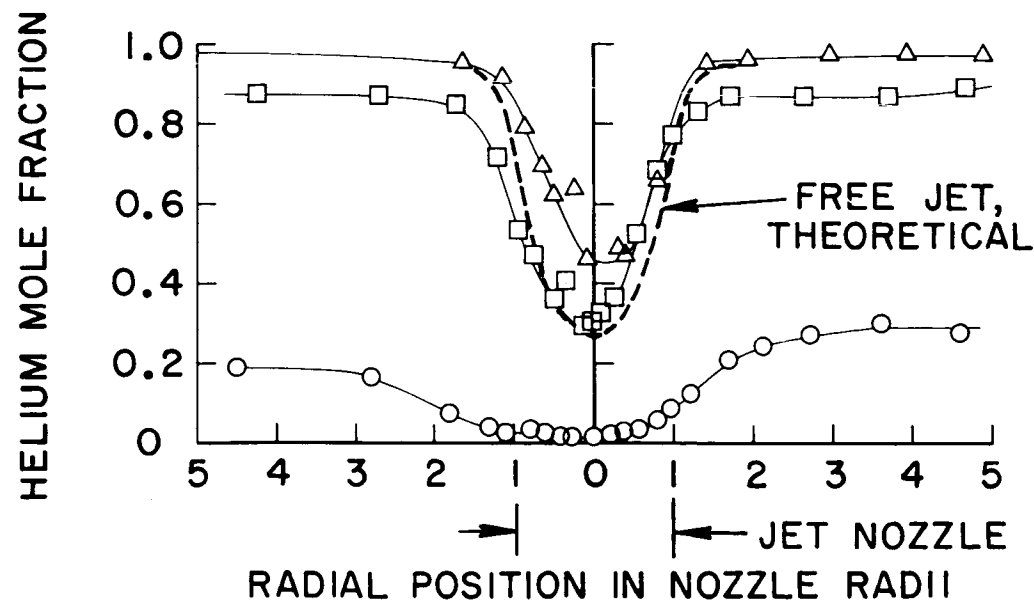
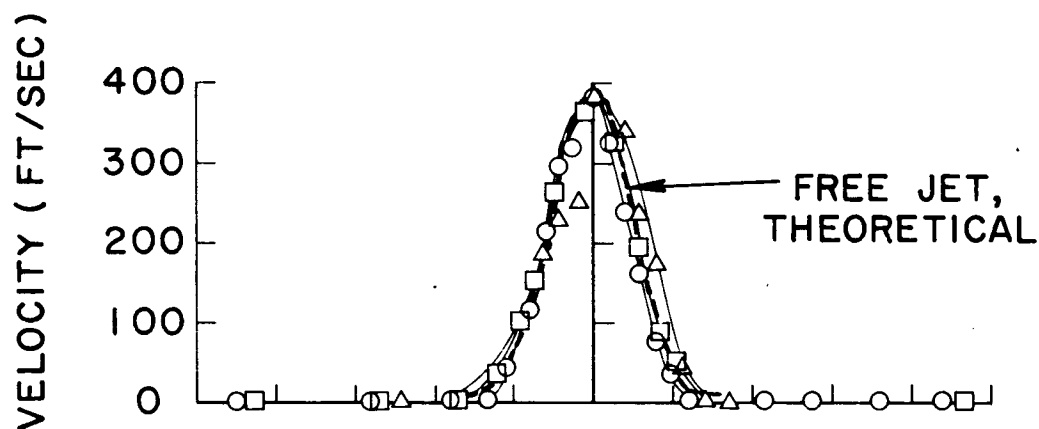
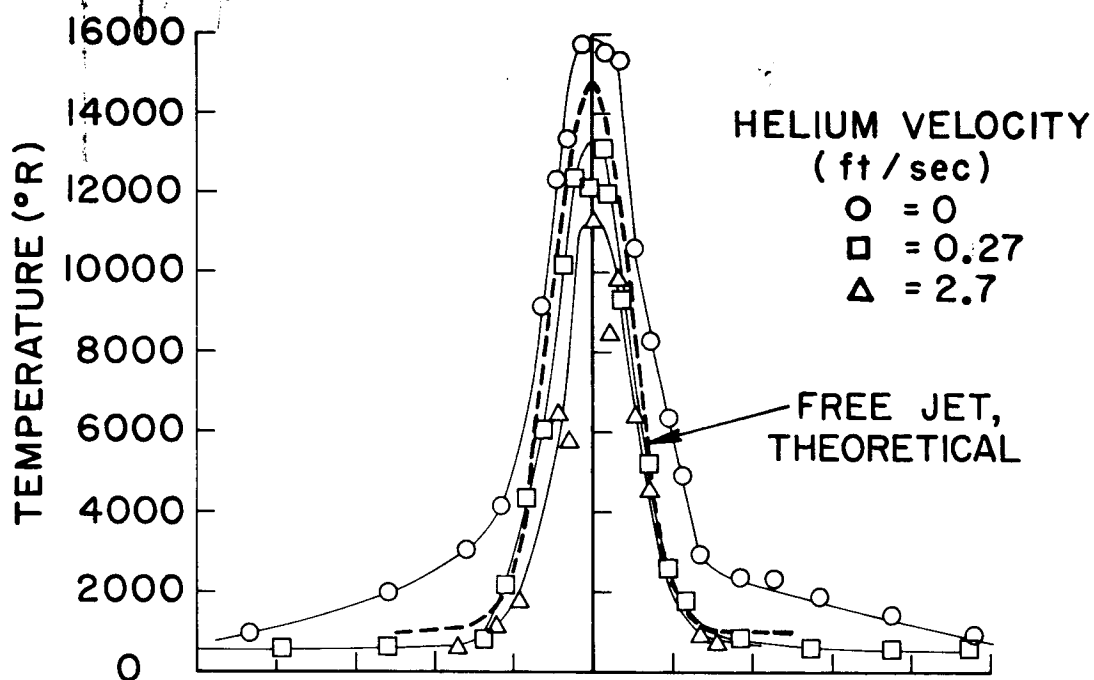
CENTERLINE HELIUM CONCENTRATION VERSUS AXIAL POSITION



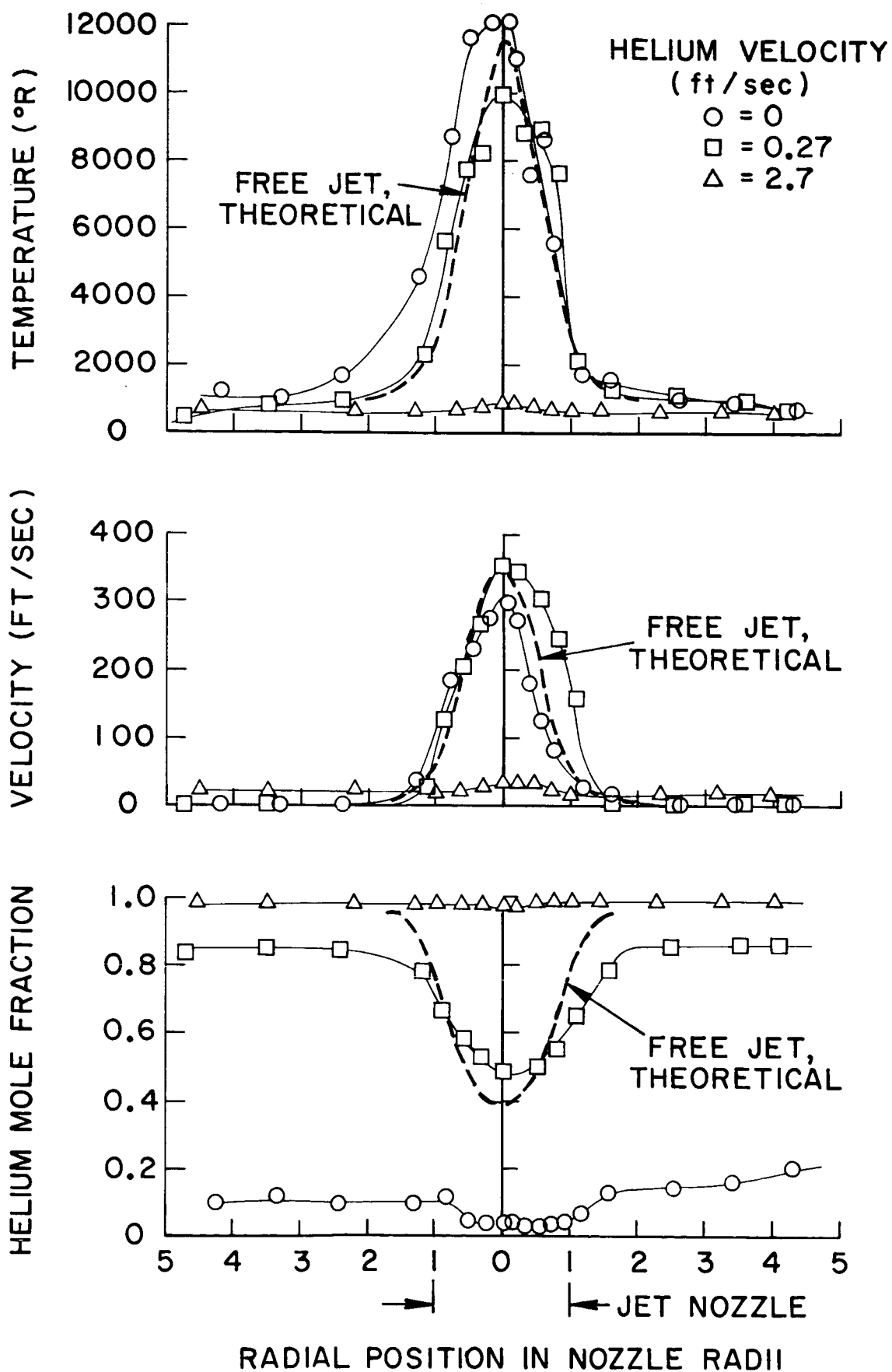
CENTERLINE ENTHALPY VERSUS AXIAL POSITION



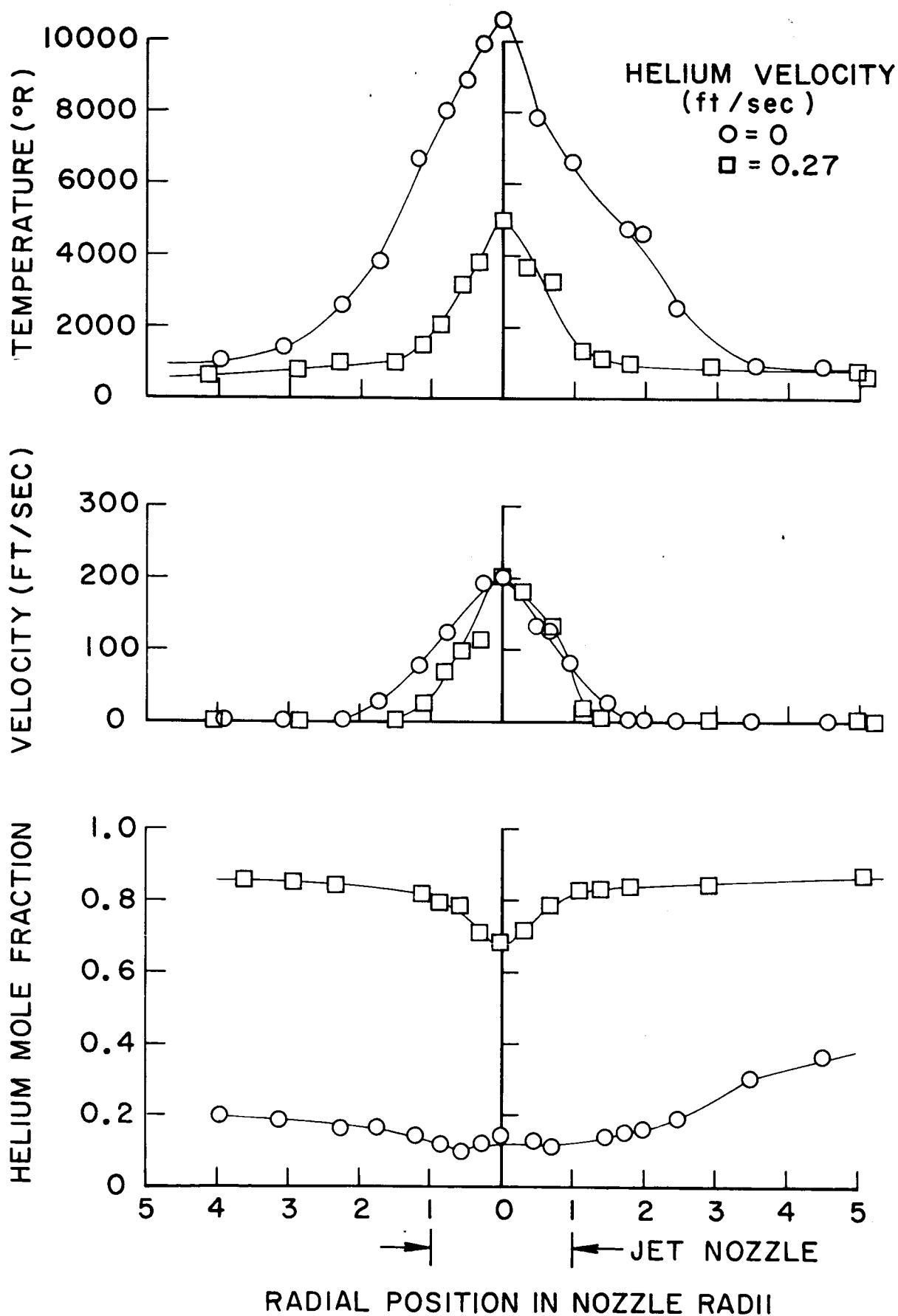
TEMPERATURE, VELOCITY AND COMPOSITION
PROFILES AT NOZZLE EXIT PLANE



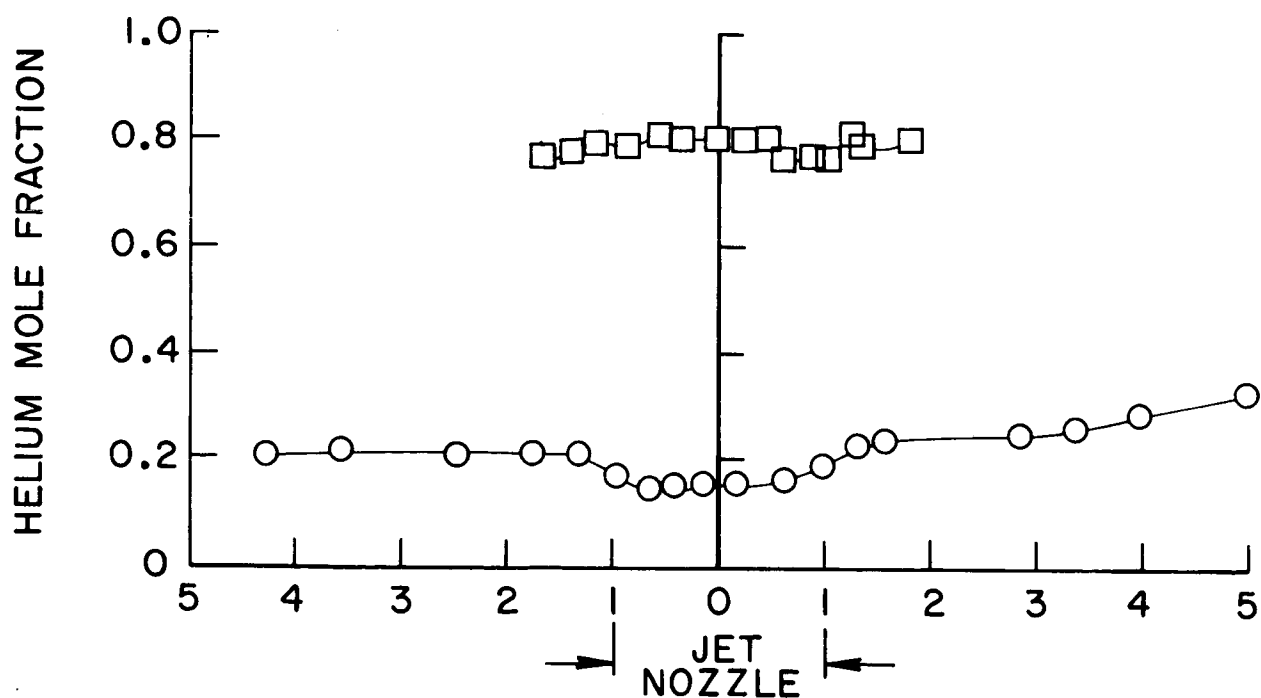
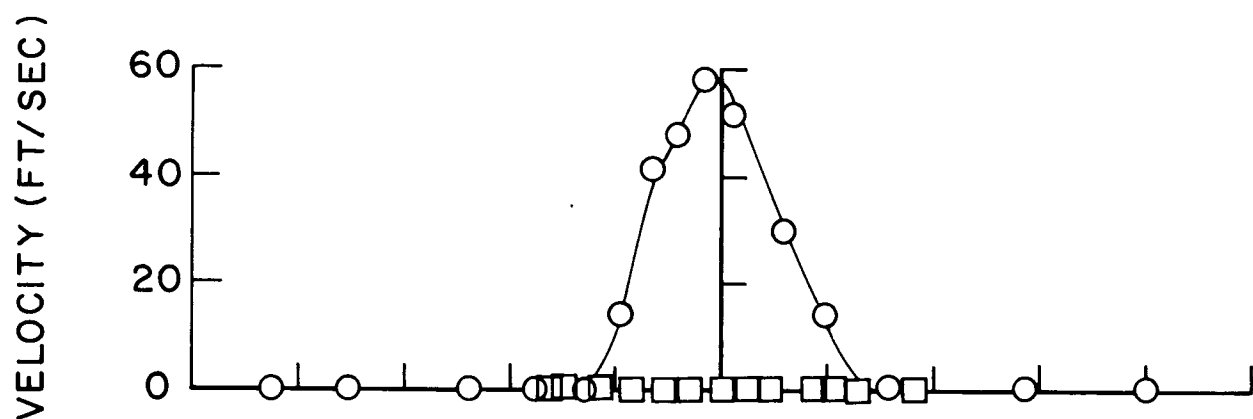
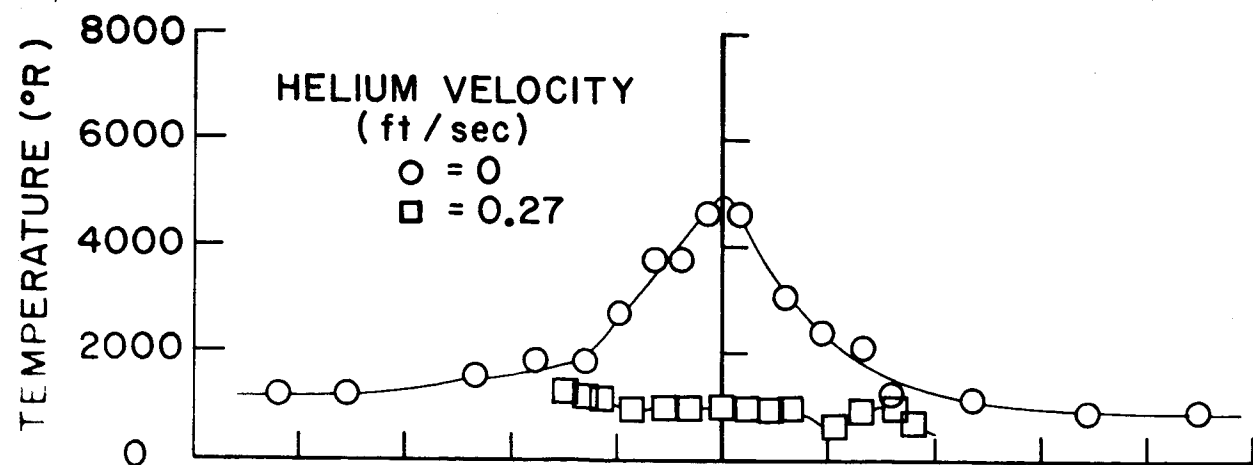
TEMPERATURE, VELOCITY AND COMPOSITION PROFILES
AT 1/2 INCH DOWNSTREAM FROM NOZZLE EXIT PLANE



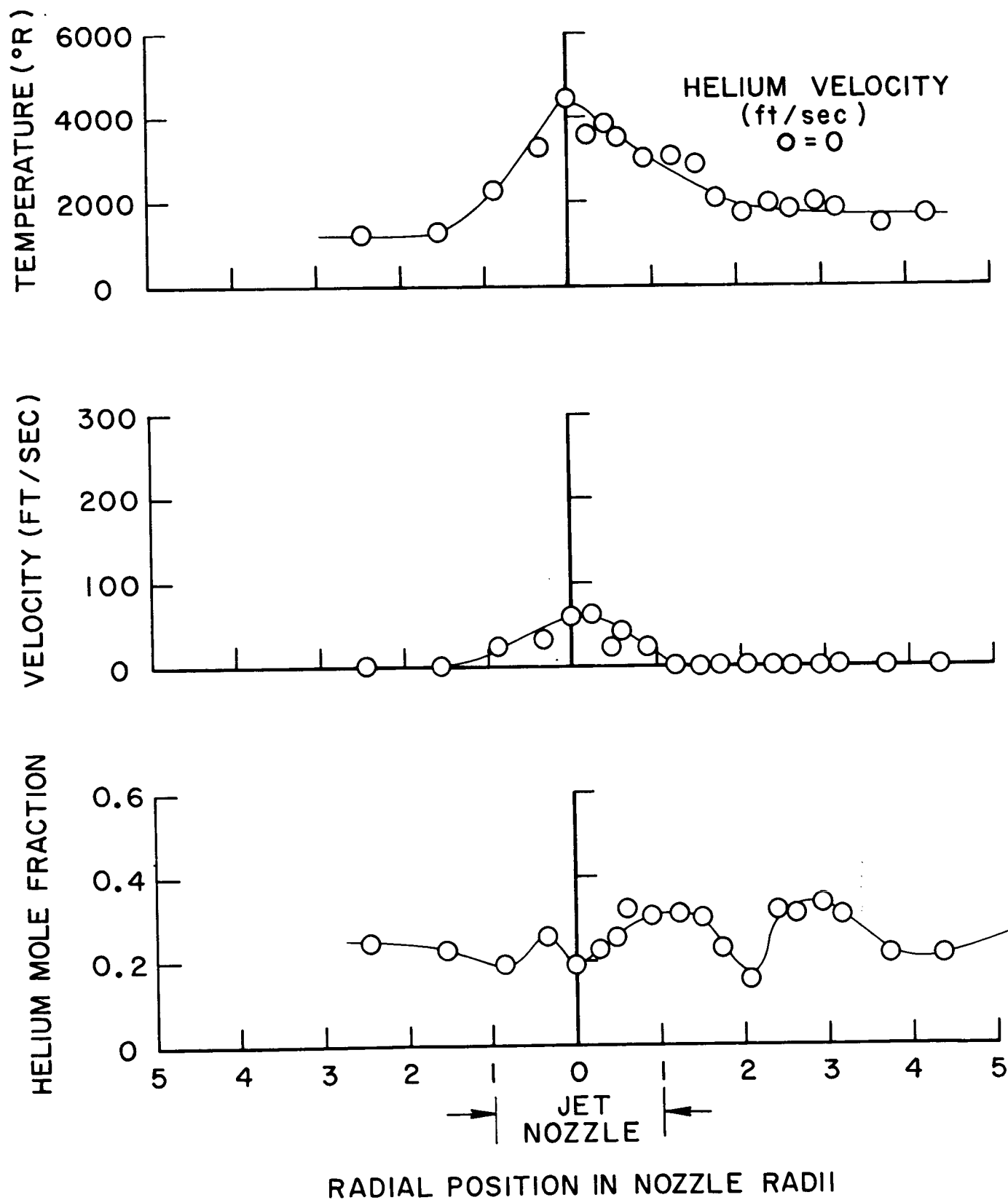
TEMPERATURE, VELOCITY AND COMPOSITION PROFILES
AT 1 INCH DOWNSTREAM FROM NOZZLE EXIT PLANE



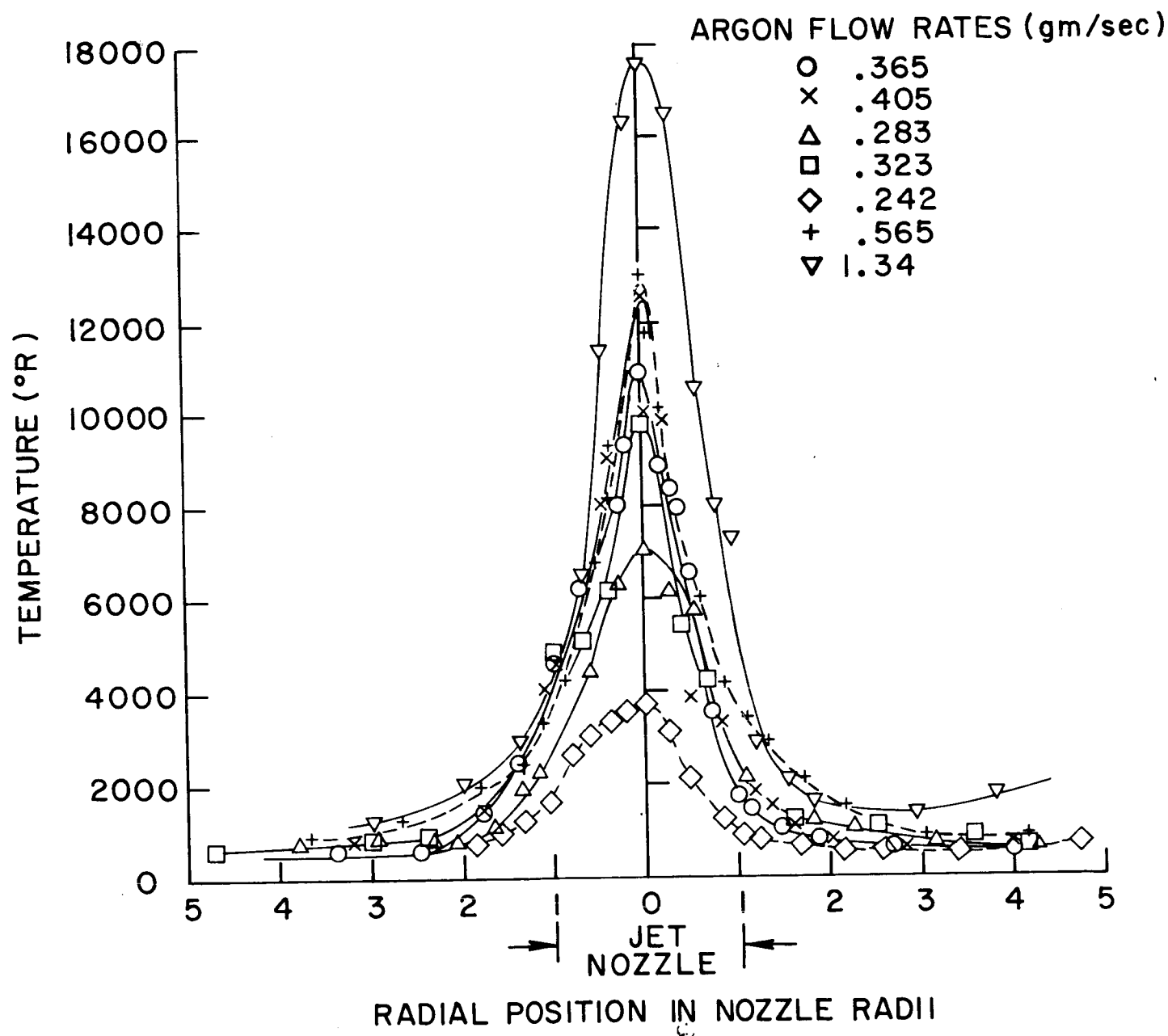
TEMPERATURE, VELOCITY AND COMPOSITION PROFILES
AT 2 INCHES DOWNSTREAM FROM NOZZLE EXIT PLANE



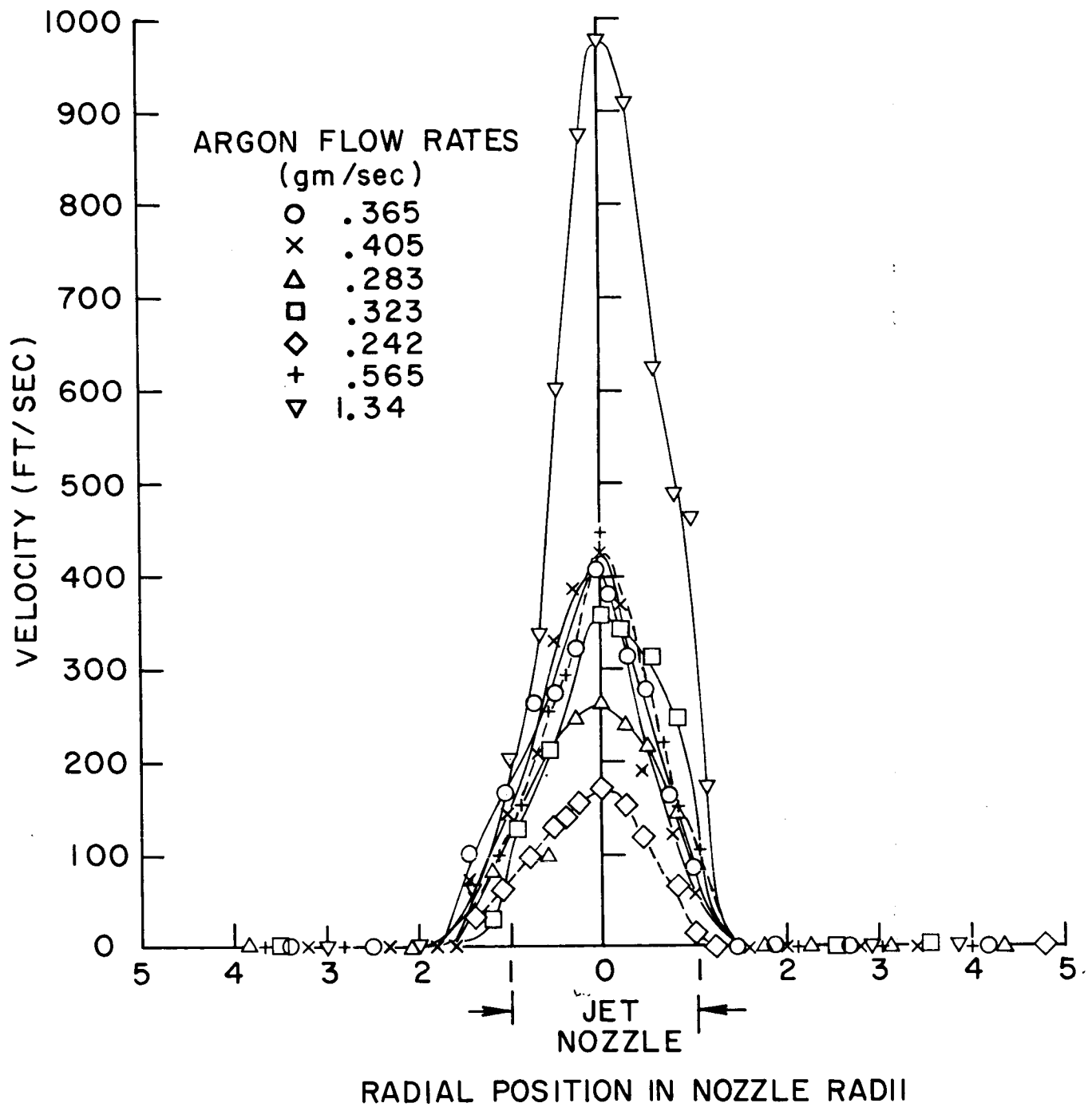
TEMPERATURE, VELOCITY AND COMPOSITION PROFILES
AT 3 INCHES DOWNSTREAM FROM NOZZLE EXIT PLANE



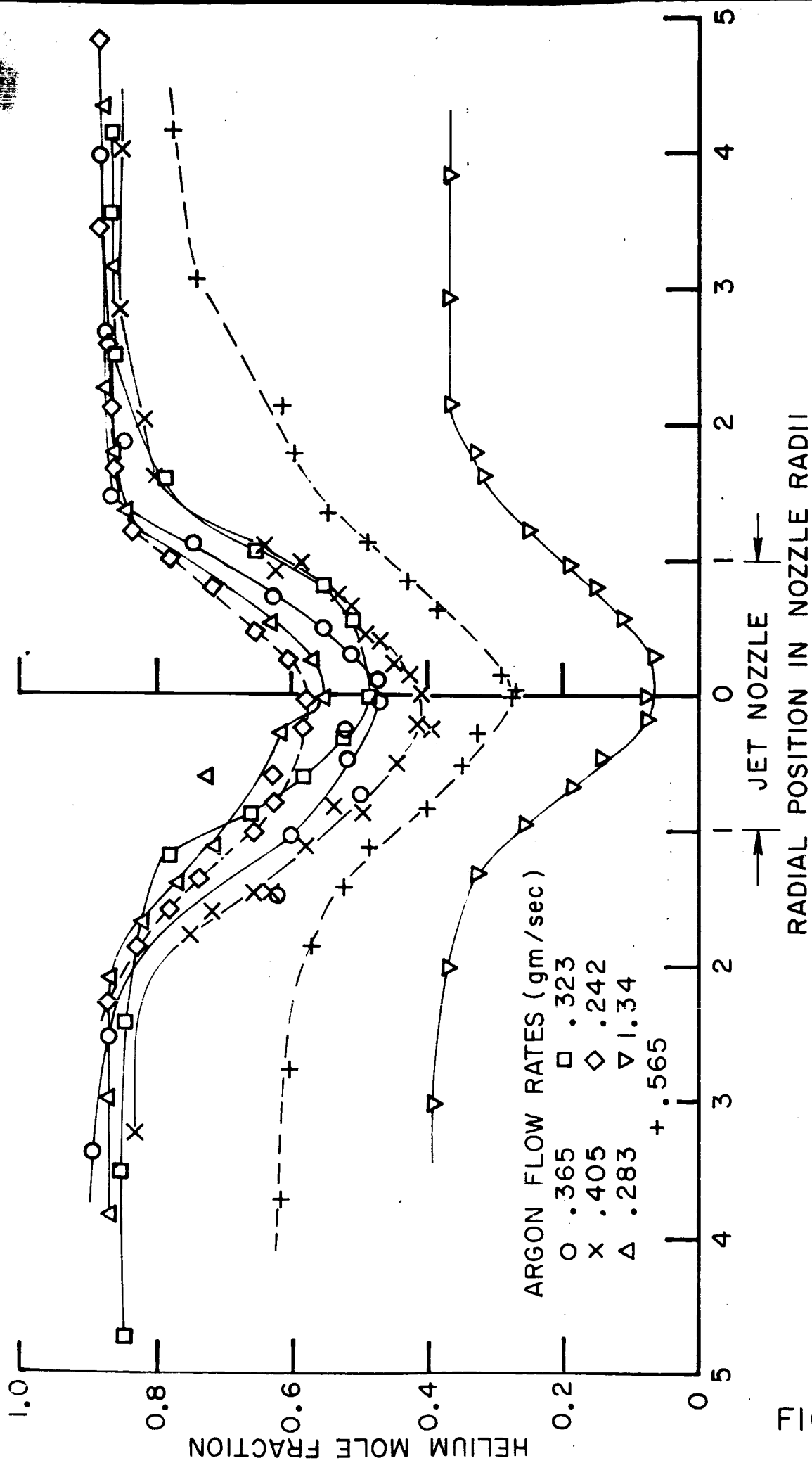
TEMPERATURE, VELOCITY AND COMPOSITION PROFILES
AT 5 INCHES DOWNSTREAM FROM NOZZLE EXIT PLANE



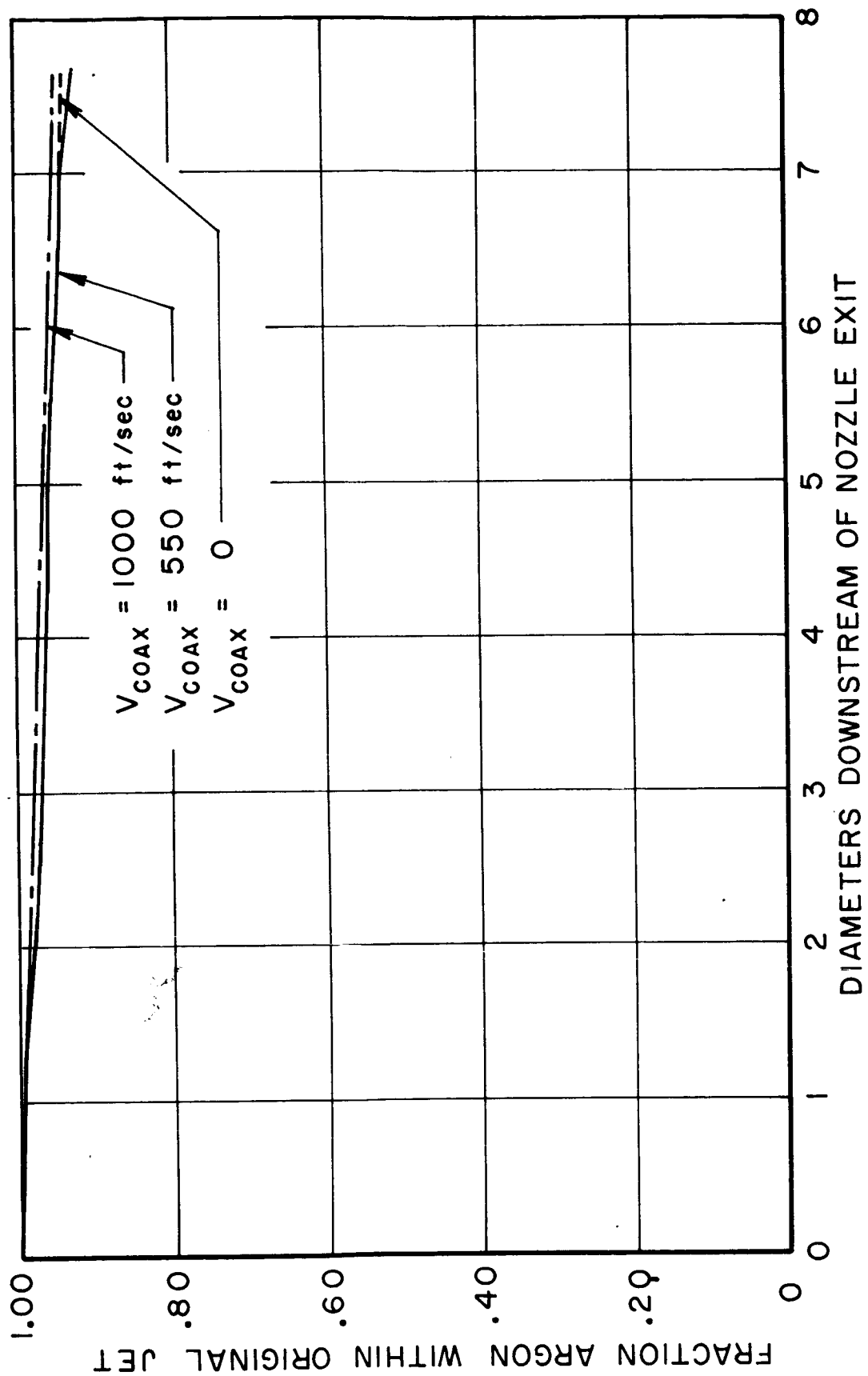
TEMPERATURE PROFILE AT ONE INCH DOWNSTREAM
FROM NOZZLE EXIT PLANE FOR VARIABLE ARGON FLOW
(HELIUM VELOCITY = 0.27 FT/SEC)



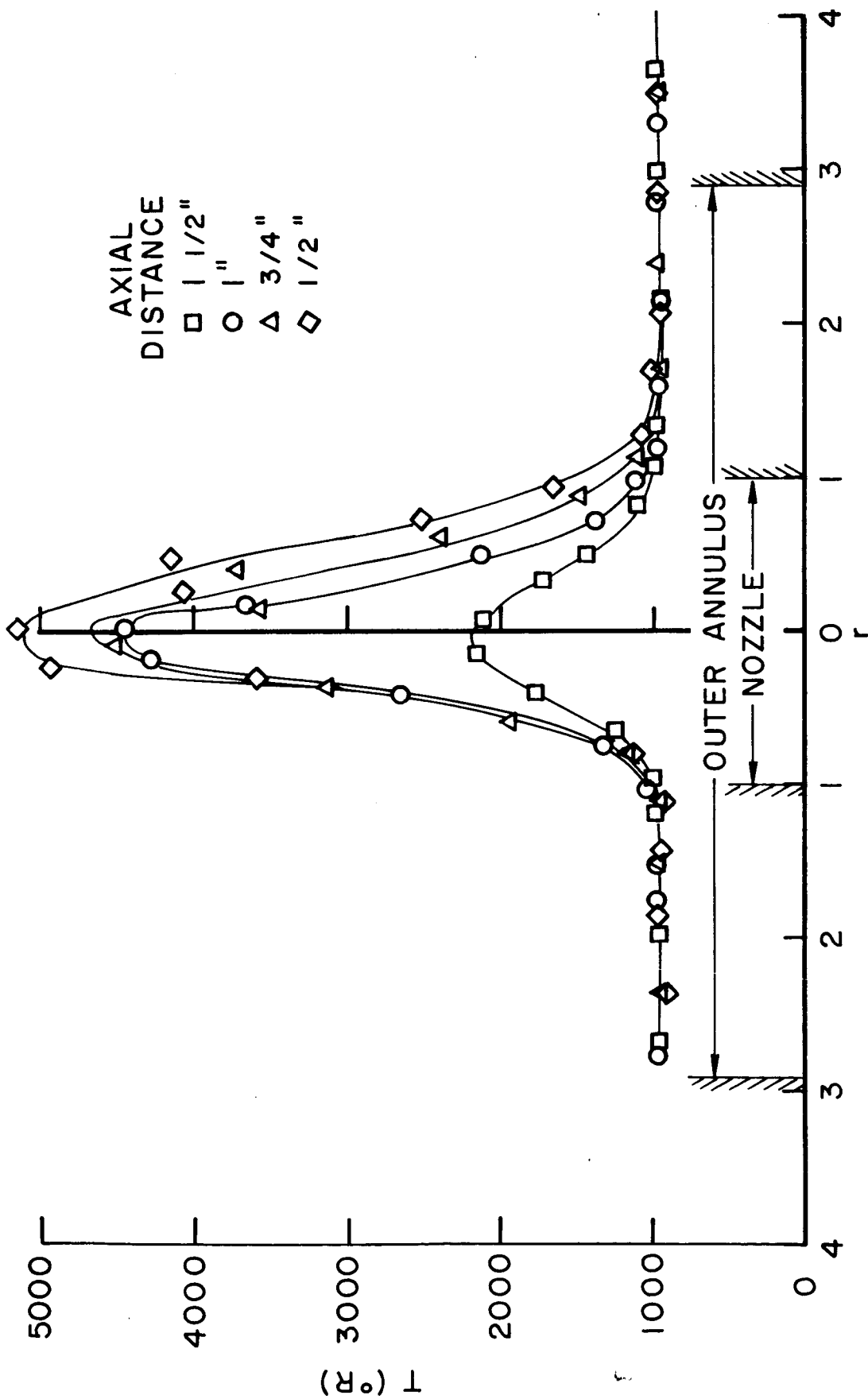
VELOCITY PROFILE AT ONE INCH DOWNSTREAM
FROM NOZZLE EXIT PLANE FOR VARIABLE ARGON FLOW
(HELIUM VELOCITY = 0.27 FT/SEC)



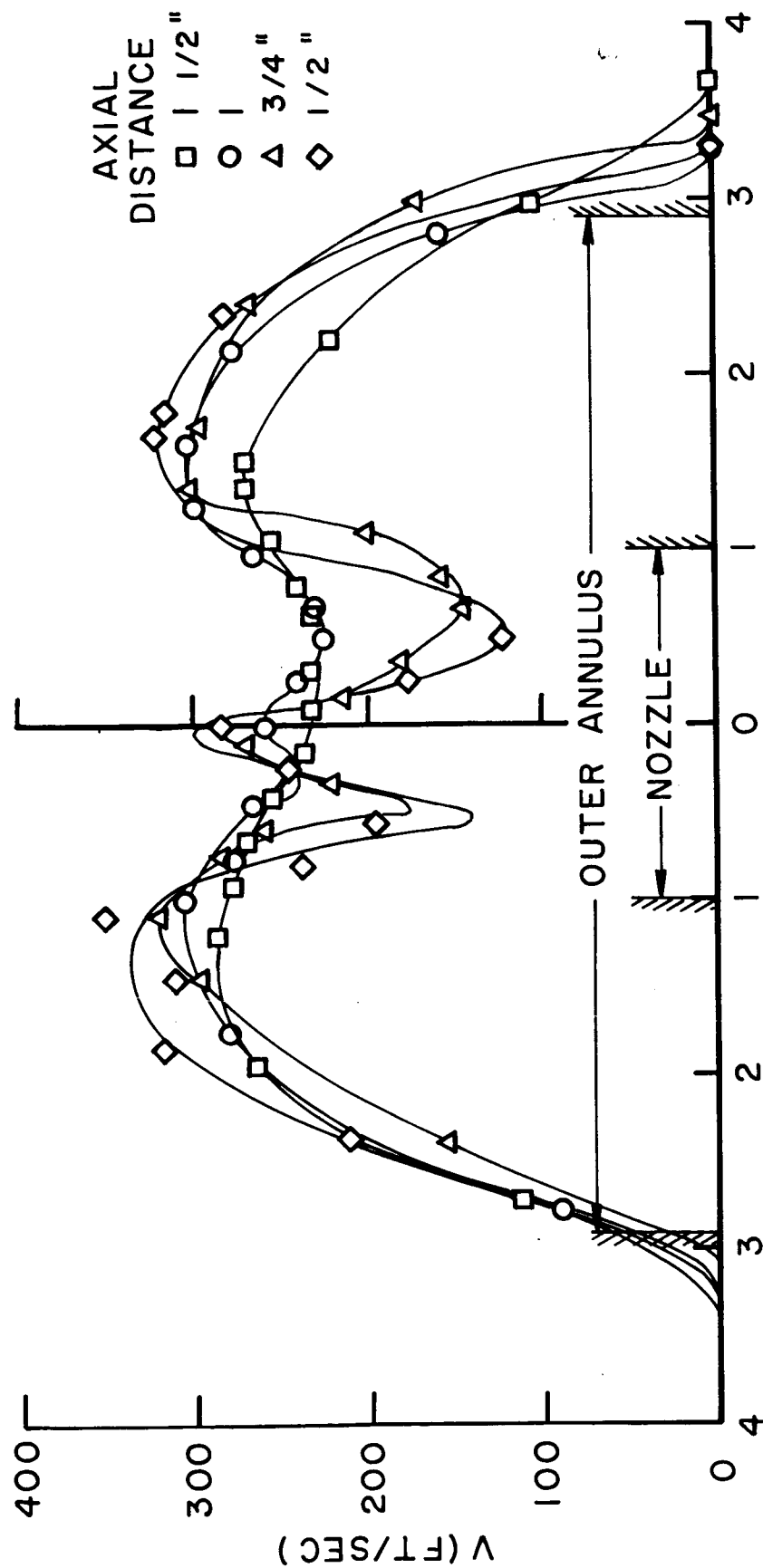
COMPOSITION PROFILE AT ONE INCH DOWNSTREAM
FROM NOZZLE EXIT PLANE FOR VARIABLE ARGON FLOW
(HELIUM VELOCITY = 0.27 FT/SEC)



THEORETICAL ARGON MASS WITHIN ORIGINAL JET AREA



EXPERIMENTAL TEMPERATURE PROFILE COAXIAL
NITROGEN VELOCITY = 200 FT/SEC



EXPERIMENTAL VELOCITY PROFILE COAXIAL
NITROGEN VELOCITY = 200 FT/SEC

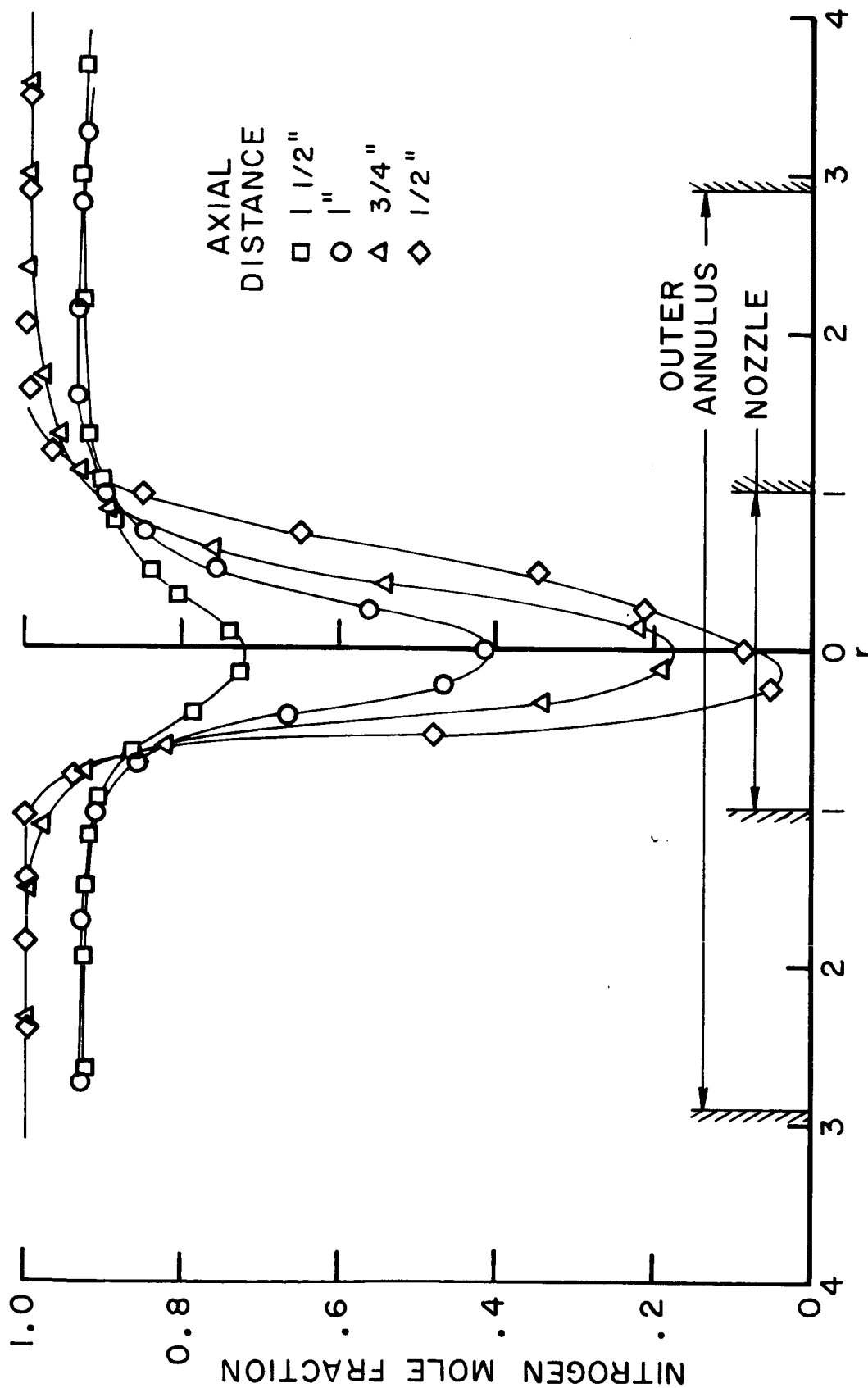
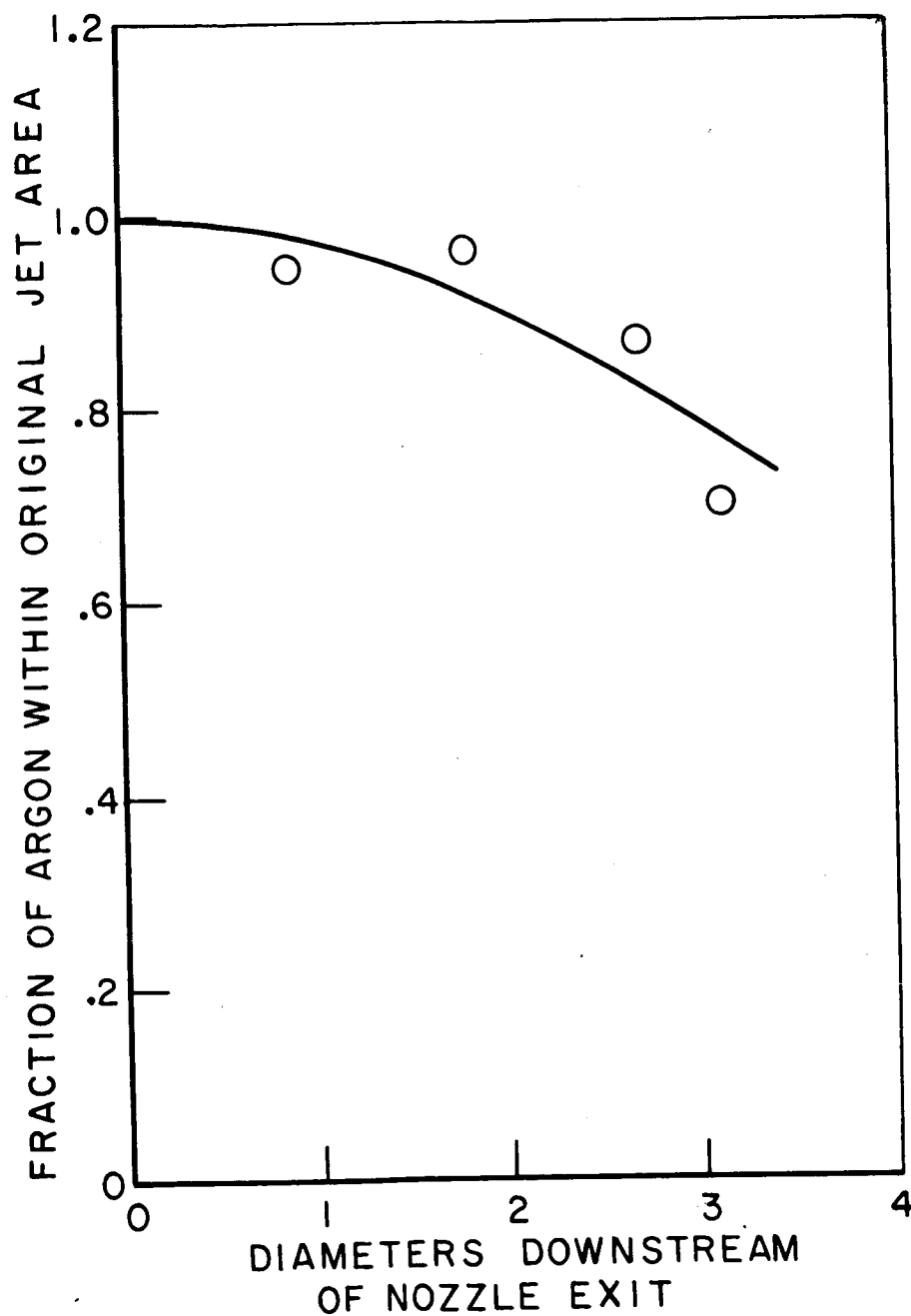


FIGURE 51

EXPERIMENTAL NITROGEN MOLE FRACTION COAXIAL
NITROGEN VELOCITY = 200 FT/SEC



EXPERIMENTAL ARGON MASS WITHIN
ORIGINAL JET AREA COAXIAL
NITROGEN VELOCITY = 200 FT/SEC